RADIO SPECTRAL LINE STUDIES OF THE INTERSTELLAR MEDIUM IN THE GALACTIC PLANE

By

ANDREW WILKIN SEACORD, II

A DISSERTATION PRESENTED TO THE GRADUATE COUNCIL OF
THE UNIVERSITY OF FLORIDA
IN PARTIAL FULFILLMENT OF THE REQUIREMENTS FOR THE
DEGREE OF DOCTOR OF PHILOSOPHY

UNIVERSITY OF FLORIDA

1975

To My Parents

With Gratitude

Louise DeLano Peck Seacord

and

Wilkin Henry Seacord

ACKNOWLEDGEMENTS

I wish to express my appreciation to Dr. Stephen Gottesman who introduced me to the intriguing problem of the galactic ridge and who has provided many comments and suggestions during the course of my study of it. His encouragement and cooperation during the final stages of this project are greatly appreciated.

The spectra observed as a part of this study were obtained with the 43 meter telescope at the National Radio Astronomy Observatory in Green Bank, West Virginia. I appreciate the opportunity to have used these facilities. I am grateful to the NRAO staff, particularly the operators and engineers, whose support made the observations successful.

I also wish to thank the other members of my doctoral committee whose comments and suggestions have been most helpful. Actually, many people within the Department of Physics and Astronomy deserve a word of thanks for their general support, for providing travel funds, and for making computer time available to me.

Finally, I owe many words of gratitude to my wife, Penny, who has been patient with me and often provided me

with much-needed words of encouragement and to my daughter, Becky, who has provided many interesting moments during the course of my work here.

TABLE OF CONTENTS

Abstract of Dissertation Presented to the Graduate Council of the University of Florida in Partial Fulfillment of the Requirements for the Degree of Doctor of Philosophy

RADIO SPECTRAL LINE STUDIES OF THE INTERSTELLAR MEDIUM IN THE GALACTIC PLANE

By

Andrew Wilkin Seacord, II

August, 1975

Chairman: Stephen T. Gottesman
Major Department: Astronomy

This study develops a model for the source of radio recombination line emission from the galactic plane. The model is based mainly on recombination line spectra observed in the direction of the supernova remnant 3C391. The H157α recombination line was observed and used with the H92α spectrum observed by Cesarsky and Cesarsky (1973) to obtain a model consistent with both spectra. Other criteria—such as the 80 MHz optical depth, the contribution to the thermal continuum temperature, and ionization rates—were also considered.

Four models were studied: a cold region illuminated by 3C391; an isolated cold region; a group of hot, dense H II regions; and a low density H II nebula. Of these, the best model is a small ($\sim$85 pc diameter) H II region with a temperature of 7500° K and an average electron density of 10^{-3} cm^{-3}.

The H157α spectrum in the direction of the pulsar 1858+03 was also observed. It was found that it is probable that one of the recombination line nebulae lies along the line of sight to the pulsar. In this case the pulsar would be at a distance of 2.6 kpc in order for its dispersion measure to agree with the measured value of 402 pc cm^{-3}.

The large scale distribution of the H II nebulae was also studied. The results of available radio recombination line spectra surveys from the galactic plane suggest that they exist within an annular region, which extends from 4 to about 8.7 kpc from the galactic center.

CHAPTER I

INTRODUCTION

The Galactic Ridge

As a radio telescope is scanned across the plane of the Milky Way at some galactic longitude,[1] it is seen to be a source of radio emission. For radio frequencies of 100 MHz or greater, the intensity increases as the galactic equator is approached and peaks at the equator itself. Scans through the galactic plane made at several different frequencies reveal that the emission has two components, thermal and nonthermal. At frequencies below a few GHz, the emission is predominantly nonthermal with a spectral index between -2.7 and -3.0 (Westerhout, 1958; Matthews, Pedlar and Davies, 1973). At 85 MHz the radiation is almost completely nonthermal and the intensity

---

[1] In this work, the revised galactic latitude, b^{II}, and longitude, l^{II}, as adopted by the IAU (Blaauw *et al.*, 1960) will be used throughout. The superscript II, however, will be dropped from the notation.

distribution across the galactic plane has a total half-intensity width of about 5° at longitude greater than 12° from either side of the galactic center (Hill, Slee, and Mills, 1958). As the frequency increases, the overall intensity decreases and the width of the emission becomes smaller, approaching a thin ridge at centimeter wavelengths. At 1390 MHz the half-intensity width is generally about 1°.5. The thickness of the nonthermal emission region increases somewhat near the galactic center. This thin continuum emission region surrounding the galactic equator has been named the "galactic ridge."

The galactic ridge has been recently mapped with an antenna resolution of 11 arc minutes at frequencies of 1414, 2695, and 5000 MHz by Altenhoff et al. (1970). Matthews, Pedlar, and Davies (1973) have used these maps to obtain the latitude distribution of the continuum intensities at three longitudes where no resolved sources are present. They plotted the distribution with the intensity scale at each of the frequencies adjusted so that, if the emission were entirely nonthermal, the three distribution curves would be congruent. The plots are congruent at latitudes greater than about 0°.5, but inside this range, the intensity increases markedly with frequency due to thermal emission. These curves illustrate the two components of the galactic ridge continuum emission.

It is known that hydrogen is concentrated within a thin region around the galactic equator (cf. Westerhout, 1958; Baker and Burton, 1975). The thermal emission comes from the free-free process between electrons and protons from ionized hydrogen.

At frequencies below about 30 MHz, a scan cutting through the ridge shows an intensity profile with two peaks, one on each side of the equator, The decrease of intensity along the equator results from absorption of the strong nonthermal emission by the free-free process within the thermal emission region. The map by Shain, Komesaroff, and Higgins (1961) at 19.7 MHz shows the absorption lane prominently.

The galactic ridge took on an interesting aspect when Gottesman and Gordon (1970) observed low intensity H157α radio recombination line spectra in two directions in which the Altenhoff et al. (1970) maps show no resolved sources. Gordon, Brown, and Gottesman (1972) found that at a longitude of 33°, the recombination line emission is limited to a latitude of less than 0.°5 above the equator. In the region toward the galactic center, recombination line emission has been observed at a latitude of $-0.^{\circ}62$ (Lockman and Gordon, 1973). Previous to Gottesman and Gordon's observations, radio recombination lines had only been observed from known galactic H II regions. They have not been detected from the interstellar medium in the solar neighborhood.

A number of workers have studied the galactic ridge in order to determine the nature of the radio recombination line sources and how they relate to the thermal continuum and 21 cm spectral line emission. The analysis of Cesarsky and Cesarsky (1971, 1973b) and Lockman and Gordon (1973) find that the electron temperature of the radio recombination line emission regions is close to 20 °K. Other workers derive temperatures ranging from 10^3 to 10^4 °K (Gottesman and Gordon, 1970; Gordon and Gottesman, 1971; Matthews, Pedlar, and Davies, 1973; Jackson and Kerr, 1971; Chaisson, 1974a; and Downes and Wilson, 1974). Very recently two papers have appeared, which conclude that these recombination lines originate from low density H II regions (Jackson and Kerr, 1975; Pankonin, 1975).

Objective, Method, and Scope of This Study

The problem to which this study is directed is that of determining the type of region responsible for the recombination line emission in the galactic ridge. The first step will be to observe recombination line emission from regions in the ridge in which there are no H II regions visible on the Altenhoff *et al.* (1970) maps and from which other data have previously been obtained. The recombination line spectrum will provide one piece of datum, the power contained in the spectral line. However, there are several

parameters which define the type of region: electron temperature, electron, neutral hydrogen, ionized hydrogen number densities, size of region, and distribution of the region, or regions, within the galactic ridge. The latter may imply a relation between recombination line emission and other phenomena such as low frequency radio absorption and galactic structure.

Since the observations made as a part of this study can only supply one bit of information, the identity of the recombination line source can be obtained only after other observations are utilized. Even so, there are still more parameters whose values are to be found than there are observed quantities. For that reason, the values of some parameters must be chosen at the onset of model computation. A type of model is hypothesized and theory or the conclusions from previous observation suggest what these values are. The second step will be to obtain, from one region in the ridge, a model solution which is consistent between two similar data. The ideal case for this is the region toward the supernova remnant 3C391 from which Cesarsky and Cesarsky (1973b) have observed an H92α recombination line spectrum. This region has undergone a considerable amount of scrutiny, particularly by those who have attempted to measure the 80 MHz optical depth (Caswell et al., 1971; Dulk and Slee, 1972; Goss, 1972).

The third step in the process will be to assume that this model applies in the mean sense to the entire ridge and use the remaining data obtained for this study to check the model. The method is to calculate a parameter which depends on the model, to see if it agrees with what is observed. Finally, recombination line surveys will be combined in such a way as to examine the large scale structure of the recombination line ridge.

The theoretical basis of this study will be developed in Chapter II. All equations used in the analysis will be derived and approximations and assumptions will be discussed. The third chapter will discuss theory behind the observing procedure. The method and conditions under which the observations were made and the display of the processed spectra will occupy Chapter IV. Chapters II, III, and IV provide a basis for the subsequent work.

Four types of regions on which to base the models will be selected. Three of them result from previous observation of 3C391, a summary of which begins Chapter V. The Hot Spot model is based on unpublished observation of Altenhoff et al. (1973). The remainder of Chapter V develops the four models. Chapter VI is involved with the selection of the most probable model and tests this by computing the distance to the pulsar 1858+03 and the 80 MHz optical depth expected in the direction of 3C396. Chapter VI ends with

an investigation of the large scale structure of ridge recombination line emission. The last chapter concludes the study by proposing future projects to study the galactic ridge.

CHAPTER II

INTERSTELLAR MEDIUM ASTROPHYSICS

Introduction

It is the purpose of this chapter to present a foundation on which this project is based, particularly the analysis of the spectra. The starting point is the equation of radiative transfer. The coefficients of absorption and emission are parameters of the solution to the transfer equation.

Since this study is based on radio spectral lines, the line absorption coefficient will be examined in detail. The line profile of a given element depends on the thermodynamic state, temperature, abundance, electron density, and motion of the gas creating the line.

The Transfer Equation and a General Solution of It

The transfer equation can be set up by considering the radiation passing through a region as shown in Figure II-1. The radiation entering this region has a frequency-dependent specific intensity, $I_0(\nu)$, which can be both thermal and nonthermal in origin. The line of sight enters

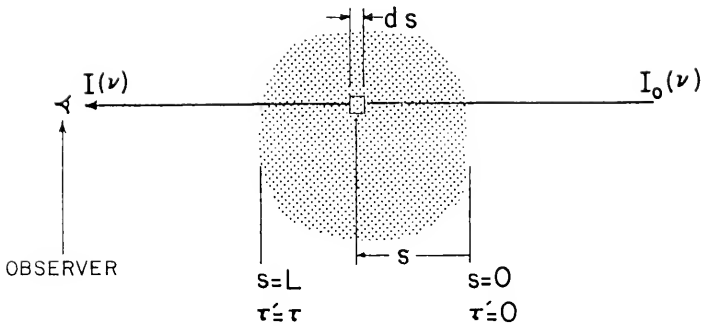

Figure II-1. Ray Path Geometry Through a Line-emitting Region. The region is shown shaded.

the region at a point where the path length, s, is zero. The total path length through the region is L. At the near boundary, where s = L, the specific intensity is $I(\nu)$. The change in specific intensity along a differential path length ds in a homogeneous medium is

$$dI(\nu) = -\kappa_L(\nu)\, I(\nu,s)\, ds - \kappa_T(\nu)\, I(\nu,s)\, ds + j_L(\nu)\, ds + j_T(\nu)\, ds + j_N(\nu)\, ds. \qquad \text{II-1}$$

The nonthermal emission coefficient is $j_N(\nu)$. In the interstellar medium the nonthermal absorption processes are not important. The thermal process, which will generate or absorb radiation, is the free-free process; it will be discussed later. The coefficients of thermal continuum emission and absorption are $j_T(\nu,s)$ and $\kappa_T(\nu,s)$ respectively. The applicable coefficients for spectral lines are denoted by the subscript L.

Let $j(\nu) = j_T(\nu) + j_L(\nu)$ and $\kappa(\nu) = \kappa_T(\nu) + \kappa_L(\nu)$, then at any point,

$I(\nu) = I_T(\nu) + I_N(\nu) + I_L(\nu) = I_C(\nu) + I_L(\nu)$. Equation II-1 then becomes

$$\frac{dI(\nu)}{d\tau} = -I(\nu) + \frac{j(\nu)}{\kappa(\nu)} + \frac{j_N}{\kappa(\nu)}. \qquad \text{II-2}$$

The optical depth, τ, is defined by

$$\tau(\nu) \equiv \int_0^L \kappa(\nu)\, ds = \tau_C(\nu) + \tau_L(\nu).$$

The thermal source function, $S(\nu)$, is defined by

$$S(\nu) \equiv \frac{j(\nu)}{\kappa(\nu)} = \frac{j_L(\nu) + j_T(\nu)}{\kappa_L(\nu) + \kappa_T(\nu)} . \qquad \text{II-3}$$

Since there is no nonthermal absorption coefficient and the thermal and nonthermal processes are independent, there is no nonthermal source function.

A general solution to the transfer equation can be obtained by multiplying Equation II-2 by the integrating factor $\exp(-\tau)$ and integrating along the path length to get

$$I(\nu) = I_o(\nu)\, e^{-\tau} + \langle S(\nu)\rangle\, (1-e^{-\tau}) + \frac{\langle j_N(\nu)\rangle}{\langle \kappa(\nu)\rangle}\, (1-e^{-\tau}).$$

The brackets, $\langle\ \rangle$, denote the average over the path length. The intensity of the nonthermal emission generated within the line-emitting region is $I_N = \langle j_N \rangle L$ and $\langle \kappa \rangle L = \tau$; so, the general solution is

$$I(\nu) = I_o\, e^{-\tau} + \langle S(\nu)\rangle\, (1-e^{-\tau}) + \frac{I_N}{\tau}\, (1-e^{-\tau}). \qquad \text{II-4}$$

Nonthermal emission decreases in intensity with increasing frequency, in general.

In order to derive a solution for a specific region, the source function—which depends on the thermodynamic state of the region—must be found. It is important, therefore, to consider the conditions for thermodynamic equilibrium. This is the subject of the next section.

Thermodynamic Equilibrium

To be in thermodynamic equilibrium (TE), a gas must have the following properties.

1. The temperature and pressure throughout the region are constant and are equal to that of its surroundings; hence, there will be no flow of energy or mass through it.
2. The gas will radiate as a black body at that temperature.
3. Detailed balancing must exist; that is, for each process occurring in the gas, its inverse must also occur by an equal amount (e.g. ionization and recombination).
4. The velocities of the gas particles have a Maxwellian distribution.
5. The population of any excited state of an atom, ion, or molecule is determined by the Boltzmann equation.

6. The relative population of any level of ionization of a species to that of the neutral species is given by the ionization (Saha) equation.

The observed spectral line intensity depends on how well these conditions are met. Radio recombination line observations of a variety of regions indicate that the interstellar medium is generally not in local thermodynamic equilibrium (LTE); that is, the conditions of TE are not met even on a small (local) scale (Hjellming and Davies, 1970; Andrews, Hjellming, and Churchwell, 1971; Gordon, 1971; Brown and Balick, 1973). If LTE does not exist, the transfer equation parameters must be modified to account for this. In the following work, a superscript asterisk denotes an LTE quantity. The second condition of LTE dictates that $S^*(\nu) = B(\nu,T)$, the Planck function for a temperature T. For radio frequencies, this simplifies to

$$B(\nu,T) \simeq \frac{2kT}{c^2}\,\nu^2 \quad . \qquad \text{II-5}$$

In the case of non-LTE, a correction parameter is defined such that

$$S(\nu) = A(\nu)\, S^*(\nu) = A(\nu)\, B(\nu,T). \qquad \text{II-6}$$

In any steady-state situation (LTE or non-LTE), the total per-unit volume emission and absorption must balance. Only in LTE do emission and absorption balance at each frequency so that, by Kirchhoff's Law, $j(\nu) = \kappa(\nu)\ B(\nu,T)$.

The Thermal Continuum

Thermal emission and absorption are the result of an encounter between a free electron and a positively-charged ion after which the electron remains free (cf. Mitchell and Zemansky, 1934, p. 154). From a classical point of view, an electron moves in the field of an ion (e.g. H^+), is accelerated and absorbs a wave or is decelerated and emits a wave. As shown in Figure II-2, the trajectory of an electron with a given velocity is altered by an amount determined by the impact parameter, ρ. For radio frequencies, ρ is large enough that the entire trajectory can be approximated by a straight line.

Oster (1961) has derived an expression for the thermal absorption coefficient, which includes a quantum mechanical correction applicable for temperatures in excess of 5.5×10^5 °K. The derivation of $\kappa(\nu)$ was obtained by considering emission from a single electron with specified velocity and impact parameter. Then $j_T(\nu)$ was found for an ensemble by integrating first over a suitable

range of ρ and then over a Maxwellian velocity distribution. Then, $\kappa_T(\nu) = j_T(\nu)/B(\nu,T)$ and, for hydrogen,

$$\kappa_T(\nu) = 3.014 \times 10^{-2}\ T_o^{-1.5}\ \nu^{-2}\ \ln(4.955\times10^{-2}\ T_o^{-2.5}\ \nu^{-1})\ N_e \sum_i Z_i^2\ N_i\ . \qquad \text{II-7}$$

The numerical constants are functions of fundamental constants as shown in the Appendix, Equation A-1. The summation is over all ionic species present. Z_i is the effective charge number ($Z_{H+} = 1$) and N_i is the number denisty for the i^{th} species.

Altenhoff et al. (1960) have derived an approximate expression for $\kappa_T(\nu)$, which is

$$\kappa_T(\nu) = 8.235 \times 10^{-2}\ T_e^{-1.35}\ \nu^{-2.1}\ N_e \sum_i Z_i^2\ N_i. \qquad \text{II-8}$$

To bring this approximation into agreement with Oster's more exact formulation, it is multiplied by a correction factor $a(T_e,\nu)$. Using it, the optical depth then becomes

$$\tau_T(\nu) = \int_0^L (\nu)\ ds = 8.235 \times 10^{-2}\ a(T_e,\nu)\ T_e^{-1.35}\ \nu^{-2.1}\ E_T\ . \qquad \text{II-9}$$

E_T is the continuum emission measure defined by

$$E_T \equiv \int_o^L (N_e \sum_i Z_i^2 N_i)\, ds. \qquad \text{II-10}$$

The emission measure is expressed in units of pc cm^{-6}.

The factor $a(T_e,\nu)$ has been tabulated by Mezger and Henderson (1967) for the ranges $100 \leq \nu \leq 10^5$ MHz and $3 \times 10^3 \leq T_e \leq 15 \times 10^3$°K. For these ranges, $a(T_e,\nu)$ varies between 0.7680 and 0.9971.

The emission measure is often given by

$$E_T = \int_o^L N_e^2\, ds. \qquad \text{II-11}$$

The effect of heavy elements on the size of E_T depends on the fractional ionization of hydrogen; $x \equiv N_e/N_H$. The atomic species with an ionization potential less than that of hydrogen (13.6 eV) may be totally ionized. If $x \lesssim 10^{-3}$, the contribution of these elements to the electron pool will be an appreciable fraction of the total unless their abundances are less than those adopted by Spitzer (1968, p. 122). The most abundant contributor to the electron pool, other than hydrogen, is carbon which has an abundance $N_C \simeq 4 \times 10^{-4}\, N_H$.

The continuum emission spectrum from a region of the interstellar medium can provide some information about the conditions there. Consider Equation II-3 for the continuum; that is, $I_L = 0$. Let $I_o = I_N = 0$ and,

assuming LTE, $S(\nu) = B(\nu,T)$. Then, using Equation II-5,

$$I(\nu) = \frac{2kT}{c^2}\,\nu^2\,(1-e^{-\tau_T}). \qquad \text{II-12}$$

When the frequency is high enough that the gas is optically thin, $\tau_T << 1$, and

$$I(\nu) = \frac{2kT}{c^2}\,\nu^2\,\tau_T.$$

Since, by Equation II-8, $\tau_T \propto \nu^{-2.1}$, $I(\nu) \propto \nu^{-0.1}$ and the spectrum is nearly flat. For low frequencies such that the gas is optically thick, $\tau_T \gtrsim 1.5$ and $I(\nu) \propto \nu^2$. The turnover frequency, ν_T, is that for which $\tau_T = 1$, although sometimes the value of 1.5 is used. Setting τ_T equal to one in Equation II-8 and solving for ν_T gives

$$\nu_T = 1.893 \times 10^2\, a(T_e,\nu)^{-2.1}\, E_T^{-2.1}\, T^{-0.643}. \qquad \text{II-13}$$

If in some region for which ν_T can be measured, either E_T or T is already known, the other parameter can be found. One independent source of information is the integrated radio recombination line power. Radio recombination lines will be considered in the next section.

Radio Recombination Lines

Radio recombination lines arise from transitions between levels with large principal quantum numbers; $n \gtrsim 40$. They result from the capture (recombination) of an electron by an ion into an upper level. The nomenclature for such a transition is Xn(Δn) where X designates the recombining species; n is the principal quantum number for the transition which is specified by α for $\Delta n = 1$, β for $\Delta n = 2$, etc. The predominant element from which recombination lines are observed is hydrogen; however, radio recombination lines of helium, carbon, and possibly heavier elements have been observed (Gordon, 1974; Chaisson, 1973; Pedlar and Hart, 1974).

The emission frequency, ν_{mn}, for the transition between the m^{th} and n^{th} levels ($m > n$) is given by the Rydberg formula (cf. Shore and Menzel, 1968, p. 13)

$$\nu_{mn} = c\, R_x\, Z_x^2 \left(\frac{1}{n^2} - \frac{1}{m^2}\right) \simeq 2c\, R_x\, Z_x^2\, \frac{\Delta n}{n^3} \,. \qquad \text{II-14}$$

R_x is the Rydberg constant for the species X and Z_x is its effective charge number. Radio recombination line frequencies for hydrogen and helium have been tabulated by Lilley and Palmer (1968).

The recombination line strength depends on the number of atoms in the region which are excited to the

upper level of the transition. Since the gas may not be in LTE, it is necessary to calculate the LTE populations and the departure parameters, which indicate the degree to which the gas is out of LTE. These matters will be discussed in the following subsections.

Thermodynamic Temperatures and Level Populations

Radio recombination line emission regions contain excited neutral atoms, ions, and electrons. The number densities (in units of cm^{-3}) for hydrogen are N_{H0}, N_{H+}, and N_e respectively. N_H is the total hydrogen density. In LTE there is an equilibrium situation where recombinations are balanced by ionizations. What is desired is a statistical relation between the kinetic temperature of the gas, N_{H+}, N_e, and N_n, the number density of atoms in the n^{th} level of excitation.

For a gas in LTE, the population number density of ions in the n^{th} excited level and the i^{th} ionization state is given by the Boltzmann equation (cf. Aller, 1963, p. 112):

$$N^*_{ni} = N^*_{oi} \frac{g_n}{g_o} \exp(-\chi_{in}/kT_{ex}). \qquad \text{II-15}$$

This equation is based on the condition that the assembly has a Maxwellian velocity distribution. In

Equation II-15, N^*_{oi} is the LTE population of the ground state; g_n and g_o are the statistical weights of the excited and ground states respectively; χ_{in} is the excitation energy within the i^{th} state of ionization; and T_{ex} is the excitation temperature. The statistical weights are the number of sublevels in the n^{th} level; $g = (2J + 1)$. J represents the total angular momentum—spin plus orbital—of the level. Under the conditions of LTE, the excitation temperature, T_{ex}, is equal to the kinetic temperature of the gas.

The radio recombination lines, which have been observed involve highly excited neutral atoms, for example H I, He I, and C I. So, the desired population is N^*_{no} expressed in terms of the electron density and the respective number of the singly ionized species. For the species X,

$$N^*_n(X) = 4.143 \times 10^{-16} N^*_i(X) N_e T_{ex}^{-1.5} \frac{g_n}{2u_1(T)} \exp(-\varepsilon_{in}(X)/k T_{ex}). \qquad \text{II-16}$$

The details of the derivation of this equation are given in the Appendix; it results from placing the values of the fundamental constants into Equation A-5. The partition function, $u_1(T)$, is given by Equation A-2. $\varepsilon_{in}(X)$ is the threshold energy which is (Equation A-6)

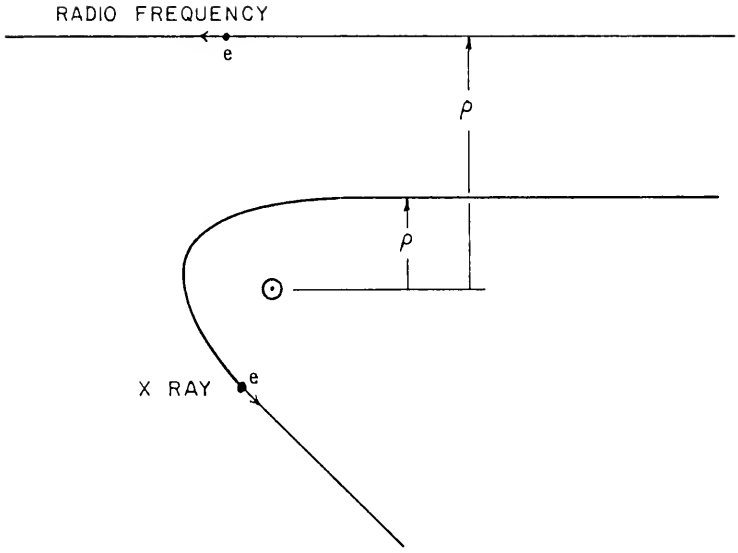

Figure II-2. The Free-Free Process. The electron, e, approaches the central ion. The impact parameter, ρ, is shown for two cases.

$$\varepsilon_{1n}(x) = -(\chi_1 - \chi_{1n}) = 157900 \quad (Z_{x1}^2/n^2) \text{ k.} \qquad \text{II-17}$$

The kinetic energy of a particle with mass M is

$$\varepsilon_K = 1/2M\ v^2 = 3/2\ k\ T_K.$$

If the gas has more than one constituent, each with a different mass, the kinetic temperature of each constituent will be the same although, because of the different masses, the RMS velocity of each constituent will be different. The RMS velocity of the component with mass M is

$$\langle v^2 \rangle 1/2 = \left(\frac{3k\ T_K}{M}\right)1/2 . \qquad \text{II-18}$$

If the gas particle velocity distribution should suddenly become non-Maxwellian, collisions involving a deflection of 90° will thermalize them to an equilibrium temperature unless the system is thermodynamically unstable (Spitzer, 1968, p. 90). In a situation where there is a nonequipartition of energy, the electrons will have the largest kinetic temperature because of their low mass. The energies of the electrons and ions will equalize first because of the long-range interactions between them. Following this, there will be elastic collisions between the ions and neutral atoms. Collisions between electrons and atoms are not

as an effective means of equalizing the kinetic energies as are collisions between ions and the electrons (Spitzer, 1968, p. 140).

Population and Depopulation Mechanisms of High n-Levels

The high n-levels are populated and depopulated by several mechanisms which are discussed by Brockelhurst (1970), Dupree and Goldberg (1970) and McDaniel (1964, p. 588). The parameters, such as cross-sections, probabilities, and coefficients are discussed in general by these authors as well as by Spitzer (1968), Kaplan and Pikelner (1970), and by the workers listed in Table II-1 who have calculated high n-level populations. The mechanisms involved are as follows.

1. Electron recombination followed by a cascade.
2. Dielectric recombination (in atoms with more than one electron).
3. Excitation and de-excitation induced by electron collisions.
4. Collisional ionization followed by three-body recombination leaving an excited atom X': $H + e \rightarrow X^+ + e + e$ and $X^+ + e + e \rightarrow X' + e$.
5. Stimulated and spontaneous emission.

6. Fine structure excitation; i.e. redistribution of angular momentum with a level: $n\ell \rightarrow n\ell'$.

Excitation to high n-levels from the ground level by radiative excitation is not important in H II regions (Dyson, 1969; Dupree and Goldberg, 1970).

To account for the effects of a departure from LTE with respect to level populations, the departure coefficient, b_n, is employed;

$$b_n \equiv N_n/N_n^* \quad . \qquad \text{II-19}$$

The departure coefficient is a function of the electron temperature and density and the intensity of the radiation field. When b_n is calculated for a type of region, the radiation temperature is chosen on the basis of specific environmental conditions of the region and b_n is tabulated or plotted as a function of n for specific values of T_e and N_e. For example, Dupree (1972a) has done this for departure coefficients in a cool region. The coefficients were first calculated for an isolated region where $I_o(\nu) = 0$ and then the effects of an adjacent 10^4 °K H II region on the b_n values were demonstrated.

Statistical equilibrium requires that there are as many transitions into a level as there are transitions out of it. The equation of statistical equilibrium for

the n^{th} level is of the form (Seaton, 1964; Dupree, 1972a, b)

$$N_n\left[\sum_{j=n_o}^{n-1} A_{n,j} + \sum_{j=n-p'}^{n-1} C_{n,j} + \sum_{j=n+1}^{n+p'} C_{n,i} + \left(\sum_{m=n+1}^{\infty} B_{n,m} + \sum_{j=1}^{n-n_o} B_{n,n-j}\right)\right] I(\nu)$$

$$= \sum_{p=1} \left(N_{n-p}\, C_{n-p,n} + N_{n+p}\, C_{n+p,n}\right) + \left(\sum_{m=n+1}^{\infty} N_m\, B_{m,n}\right.$$

$$\left. + \sum_{j=n_o}^{n-1} N_j\, B_{j,n}\right) I(\nu) + \sum_{j=n+1}^{m'} N_j\, A_{j,n} + N_e\, N_i\, (\alpha_n^r + \alpha_n^d + C_{i,n}).$$

II-20

The symbols used in Equation II-20, which have not yet been defined, are as follows:

$A_{m,n}$ = Einstein spontaneous emission probability, $m > n$;

$B_{n,m}$ = Einstein absorption probability, $m > n$;

$B_{m,n}$ = Einstein stimulated emission probability, $m > n$;

$C_{j,k}$ = collision probability for a transition between the j^{th} and k^{th} levels;

$C_{n,i}$ = collisional ionization probablity from level n;

$C_{i,n}$ = three-body recombination probability;

α_n^r = rate of radiative recombination into level n;

α_n^d = rate of dielectronic recombination into level n (= 0 for hydrogen);

m' = the maximum level considered in cascades from higher levels;

p' = the maximum p for bound collisional transitions, $p = |\Delta n|$;

n_o = the lowest level of the atom considered for the computation;

and N_i = the ion number density.

Collisional Transition Probabilities and Cross-sections

In order to compute the departure coefficients, means of simplifying Equation II-20, limiting the number of equations or limiting the range of the summations should be considered. At some level n = m', the electron is close enough to the continuum that the collisional ionization probability, $C_{n,i}$, is much greater than the probability for a spontaneous transition to lower levels, $A_{m,n}$. The levels beyond the m' cut-off level are in thermodynamic equilibrium and, $b_n = 1$ for $n > m'$.

Sejnowski and Hjellming (1969) find that inclusion of collisional transitions of $p = |\Delta n| > 1$ will lower the value of b_n by only a few percent from that considering only transitions of p = 1. Consequently, many workers limit their calculations to p' = 1.

Collisions involving a change of ℓ- state within a level, $n,\ell \rightarrow n, \ell \pm 1$, occur frequently. In cold hydrogen gas with $N_e \geq 10^{-3}$ cm^{-3}, fine structure collisions by protons as well as electrons, occur more frequently within levels for which $n \geq 100$ than do radiative processes (Pengelly and Seaton, 1964). Because of this, all n^2 ℓ-states are equally populated. Also, at low temperatures, fine structure excitation by electron collisions provide the main cooling mechanism of the gas (Dalgarno and McCray, 1972). By this process, electron kinetic energy is converted to low frequency radiation which leaves the gas, thus removing energy from the thermal pool.

The total population of level n is divided into ℓ-states according to

$$N_{n,\ell} = \frac{(2\ell + 1)}{n^2} N_n$$

(Dupree, 1969). The total population is $N_n = \sum_{\ell} N_{n,\ell}$. For hydrogen, the levels are degenerate and $b_{n,\ell} = b_n$; b_n is independent of ℓ.

The collisional transition rates, $C_{j,k}$ for $k = j \pm p$, depend on cross-sections $Q_{j,k}$ by

$$C_{j,k} = N_e \ <v \ Q_{j,k} \ (v)>. \qquad \text{II-21}$$

The average is obtained by integrating over a Maxwellian velocity distribution.

The bound-bound cross-sections have been computed by means of one of three approximations or methods: binary encounter method, impact parameter method, and a method based on the correspondence principle. The binary encounter method uses a classical approximation, which is valid for electron-atom collisions if the time of interaction between the incident and bound electrons is short compared to the orbital period of the bound electron and the collision takes place in a region smaller than the size of the atom. This time is sufficiently short when the energy transferred between the two electrons is large. With this condition, the energy transferred is assumed to be equivalent to that transferred between two free electrons. Because of this requirement, the binary encounter method gives best results for ionizing collisions; the results are poor for $p \simeq 1$. In calculating cross-sections, Brockelhurst (1970) uses the binary encounter method for $p > 6$. The application of the theory involved is discussed at length by Burgess and Percival (1968).

The impact parameter method for electron-atom collisions uses the assumption that the incident electron follows a straight-line trajectory past the target atom with an impact parameter ρ (cf. Figure II-2). Seaton

(1962) computes the collision cross-section for a bound transition $(n,\ell \rightarrow n', \ell')$ for both weak and strong coupling. For weak coupling,

$$Q_{j,k} = \int_{\rho_o}^{\infty} P_{kj}(\rho)\ 2\pi\rho\ d\rho,$$

where $j = n,\ell$, $k = n', \ell'$, and ρ_o is the cut-off value of ρ, which is approximately equal to the smaller of the two atomic radii of the j and k states. $P_{kj}(\rho)$ is the transition probability as a function of impact parameter.

For strong coupling, Seaton (1962) defines ρ_1 such that $P_{kj}(\rho_1) = 1/2$. For $\rho<\rho_1$, P_{kj} oscillates about a mean value of 1/2 so that in this range, $Q_{j,k} = 1/2\pi\rho_i^2$. For a transition of $p = 1$, most of $Q_{j,k}$ comes from $\rho>\rho_1$, and

$$Q_{j,k} = 1/2\pi\rho_1^2 + \int_{\rho_1}^{\infty} P_{kj}(\rho)\ 2\pi\rho\ d\rho.$$

Seaton (1962) calculates the cross-sections for the weak- and strong-coupled cases and accepts the smaller of the two values. $P_{kj}(\rho)$ is calculated with the symmetrized, time-dependent perturbation theory. Brockelhurst (1970) claims that the impact parameter method will not work for $p > 1$. He assumes the case of strong coupling and

finds that most of Q comes from $\rho < \rho_1$ for which the perturbation theory is not valid.

The classical method only works for large p; the semi-classical impact parameter method is valid only for $p \simeq 1$. The correspondence principle method can be used to obtain cross-sections for intermediate transitions. All variations of the correspondence principle state that for large scale systems, where the uncertainty is much larger than Planck's constant, h, the result of a quantum mechanical approach is identical to that using a classical approach. Percival and Richards (1970a) show that the Bohr correspondence principle can be applied to the energy transfer of a collisional excitation for the case of a weak interaction and if the quantum and classical first-order perturbation theories are both valid. Also, the collisional probability must be much larger than that of a radiative transition, a condition which is satisfied for $n \gtrsim 100$. With the the Bohr principle for collisions, the mean net energy transferred during the collision is equivalent to the energy transferred from independent Fourier components of order +p and -p of the classical atomic orbital motion. $P_{jk}(\rho)$ is computed from these Fourier components.

For the case of a strong interaction, Percival and Richards (1970b) show that the Heisenberg correspondence principle relates the quantum mechnical matrix elements

with the Fourier components of classical atomic orbital motion. The results for H II regions are published in a separate paper (Percival and Richards, 1970c).

For collisional ionization, either the binary encounter method (Burgess and Percival, 1968) or the classical Thompson theory (Dyson, 1969; Seaton, 1964) can be used to obtain the collision rates. From the Thompson theory

$$C_{n,i} = 3.46 \times 10^{-15} \; n^2 \; N_e \; T^{-1/2}.$$

The inverse of collisional ionization is three-body recombination. Using the equation of detailed balancing

$$N_n^* \; C_{n,i} = N_i^* \; N_e \; C_{i,n}.$$

Radiative and Dielectronic Recombination Coefficients

The radiative recombination coefficient for capture into level n is represented by α_n^r. The partial recombination coefficient, $\alpha_{(k)}$, is that for captures into all levels above and including the k^{th}; $n \geq k$. It is given by $\alpha_{(k)} = \sum_{j=k}^{\infty} \alpha_j$. Usually k = 2. The total recombination coefficient , $\alpha_{(1)}$, includes radiative captures into the ground level. Seaton (1959) has derived formulations for $\alpha_{(1)}$ and $\alpha_{(2)}$ using a symptotic expansion

of the Kramers-Gaunt factor. With a notation similar to that of Spitzer (1968, p. 117),

$$\alpha_{(k)} = 2.065 \times 10^{-11} Z^2 T^{-1/2} \xi_k (T_K). \qquad \text{II-22}$$

The function $\xi_k(T)$ involves the asymptotic expansion. Spitzer (1968, p. 117) has tabulated ξ_1 and ξ_2. They are plotted as Figure II-3.

Dielectronic recombination occurs in atoms, which have two excitable electrons. This process is very important in establishing the high level populations of carbon atoms and is, in fact, responsible for these levels being over populated with respect to the LTE populations. It takes place in two steps, the first of which is a capture of an electron into a high level, n. The energy, rather than being radiated, is transferred to a bound electron, which rises to an excited level; $n' << n$. This is an unstable condition and the second step is to dispose of the energy of the lower excited level by means of a downward transition to a stable level. The energy difference is either radiated—leaving the atom with a single, highly excited level—or it is transferred to the highly excited electron which leaves the atom by autoionization, a process called the Auger effect (McDaniel, 1964, p. 590; Shore and Menzel, 1968, p. 93). The radiative process dominates (Dupree, 1969). The dielectronic

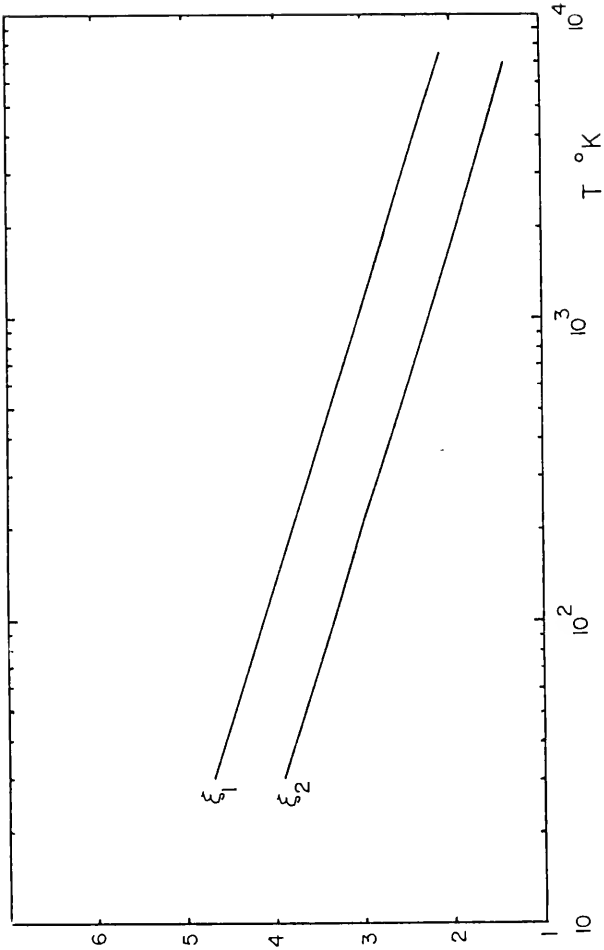

Figure II-3. ζ Functions for Calculating the Radiative Recombination Coefficient. ζ_1 is for the total recombination coefficient. These functions are tabulated by Spitzer (1968, p. 117).

recombination mechanism is more effective at populating highly excited states than is the radiative recombination mechanism; i.e., $\alpha_n^d > \alpha_n^r$, at least for $T_e \sim 10^4$ °K and $N_e > 1\ cm^{-3}$ (Dupree, 1969).

Departure Parameters, b_n and δ_{mn}

It will be shown later that the spectral line strengths depend not only on the departure coefficient, b_n, but—since the transition involves two b_n's—it also depends on the derivative of b_n with respect to n. For that reason, when b_n is computed, a parameter related to the derivative is also computed;

$$\delta_{mn} \equiv \frac{b_m - b_n}{b_m} \quad , \qquad \text{II-23}$$

where $m > n$.

Departure parameters have been published by several workers. Information about this work is summarized in Table II-1. The first column gives the reference to the work. The parameters calculated by Dupree (1969) and Hoang-Binh and Walmsley (1974) are for carbon. The second and third columns give the range of n over which the parameters are tabulated or plotted. Columns 4, 5 and 6 give the range parameters used in the calculations: n_o, m', and p' (cf. Equation II-20). The seventh column indicates the method by which the collision cross-sections

Table II-1

Reference	n_{min}	N_{max}	n_o	m'	p'	Collision Model*	Range of T_e [°K] and N_e [cm^{-3}]
Dyson (1969)	80	300	2	400	4	IP(1)	$5 \times 10^3 \leq T_e \leq 2 \times 10^4$ $10 \leq N_e \leq 10^5$
Sejnowski & Hjellming (1969)	20	240	2	240	20	IP(2)	$5 \times 10^3 \leq T_e \leq 10^4$ $10 \leq N_e \leq 10^4$
Brockelhurst (1970)	40	300	2	>500	75	(3)	$2.5 \times 10^3 \leq T_e \leq 2 \times 10^4$ $10 \leq N_e \leq 10^5$
Dupree (1972a)	50	250	10	600	1	BE(4)	$20 \leq T_e \leq 1000$ $0 \leq N_e < 10^3$
Dupree (1969) (Carbon)	20	300	2	600	1	IP(5)	$T_e = 10^4$ and 2×10^4 $1 \leq N_e \leq 10^4$
Hoang-Binh & Walmsley (1974) (Carbon)	80	250	?	500	1	BE CP(6)	$T_e = 10$ and 100 $1 \leq N_e \leq 10^3$

*The collisional approximations are BE = Binary Encounter, IP = Impact Parameter, CP = Correspondence Principle. The references to the cross sections are as follows:

(1) Seaton (1962) (2) Seaton (1962) and Saraph (1964) (3) Brockelhurst (1970): IP for p = 1; CP for $2 \leq p \leq 6$; and BE for p 6 including ionization (4) Flannery (1970) (5) Saraph (1964) (6) Banks et al. (1973): BE for small p; CP for large p.

were calculated. The reference to the source of the cross-sections is given in the parentheses following the designation. Since the departure parameters are functions of the electron temperature and density, the last column of the table gives the range of these quantities for which the parameters were computed.

All, except Hoang-Binh and Walmsley (1974), do not consider incident radiation in the calculations. Dupree (1972) does, however, show the effect of an adjacent H II region on a line-emitting region with a temperature of 20 °K. The radiation field from the H II region increases b_n slightly for $n \gtrsim 80$.

The physical significance of departure from LTE can be illustrated by showing the relation which n, T_e, and N_e have on b_n and δ_{mn}. This is done with Figure II-4 in which are drawn curves for $T_e = 10^4$ and 7.5×10^3 °K computed by Sejnowski and Hjellming (1969) and curves for $T_e = 100$ °K computed by Dupree (1972a). For each temperature, there are separate curves for $N_e = 10^3$ and 10 cm^{-3}.

As n decreases, collisions become less important in determining level populations. For small n, radiative processes dominate and the curves show an asymptotic behavior. The heavy portion of the 10^4 and 7.5×10^3 °K curves in Figure II-4 is the radiative asymptote. Depopulation by stimulated emission is much less frequent

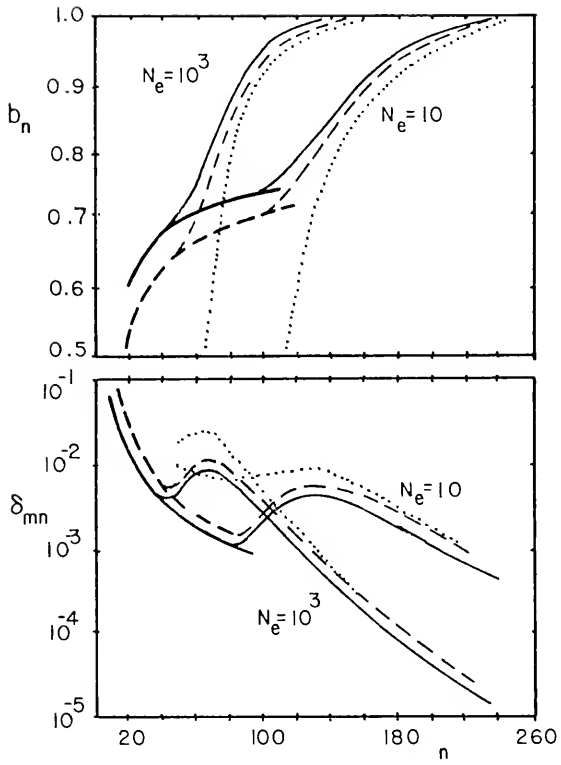

Figure II-4. Departure Parameters for Hydrogen as a Function of n, T_e, and N_e. The curves with a solid line are for $T_e = 10^{4}$°K and with a dashed line are for $T_e = 7.5 \times 10^{3}$°K (Sejnowski and Hjellming, 1969). The dotted curve is for T_e = 100°K from Dupree (1972a).

than by spontaneous emission (Gordon, 1974), except when an intense radiation field is present.

As N_e decreases, collisions become less frequent and the radiative asymptote extends to larger n. Then, for hydrogen, there is a decrease in the rate of collisional excitation of lower n-levels which causes a decrease in level population with respect to the LTE values as n decreases. In the case of carbon, however, dielectronic recombination is efficient enough in populating upper levels that the population will exceed the LTE values for $n \gtrsim 20$ and $N_e \lesssim 10^3$ cm^{-3}. In any case, the populations approach their LTE values as $n \to \infty$ (Dupree, 1969).

It should be noted that for hydrogen, b_n and δ_{mn} are both positive in the radio regime. For any two levels m and n, where $m > n$, b_m is closer to one than is b_n. In that sense, the upper level is "overpopulated" with respect to the lower level. If the slope of the b_n curve is large enough, there is an enhancement of the line intensity over that obtained from a region in LTE even though the level population is less than its LTE value. This occurs because of stimulated emission induced by an exterior source or the region's own thermal radiation field. An examination of the radio recombination line absorption coefficient and non-LTE solutions of the transfer equation will show how this happens.

Radio Recombination Line Absorption Coefficient

The rate, $R(\nu)$ at which a bound-bound absorption takes place between enrgy levels n and m ($m > n$) is equal to the product of the number of absorbers, N_n, the Einstein absorption probability, B_{nm}, and the energy flux, $I(\nu)\, d\Omega/4\pi$. The degree of absorption is modulated by the spectral line profile function, $\phi_L(\nu)$. Then

$$R(\nu) = N_n\, \phi_L(\nu)\, B_{nm}\, I(\nu)\, \frac{d\Omega}{4\pi} .$$

The energy per photon is $h\nu_{nm}$. The absorption coefficient, $\kappa_L'(\nu)$, is defined such that the energy absorbed along an increment of path length ds is

$$d\varepsilon_A = -\kappa_L'(\nu)\ \ I(\nu)\, d\Omega = -N_n\, \phi_L(\nu)\, B_{nm}\, I(\nu)\, h\nu_{nm}\, \frac{d\Omega}{4\pi}\ ds.$$

However, energy may be emitted by stimulated emission of the amount

$$d\varepsilon_I = j_I(\nu)\, d\Omega = N_M\, \psi_L(\nu)\, B_{mn}\, I(\nu)\, h\nu_{mn}\, \frac{d\Omega}{4\pi}\, ds,$$

and by spontaneous emission by the amount

$$d\varepsilon_S = j_S(\nu)\, d\Omega = N_m\, \psi_L(\nu)\, A_{mn}\, h\nu_{mn}\, \frac{d\Omega}{4\pi}\, ds.$$

$\psi_{mn}(\nu)$ is the emission line profile, which is usually identical to the absorption profile. Inserting $d\varepsilon_A$, $d\varepsilon_I$, and $d\varepsilon_S$ in the transfer equation (Equation II-2) gives

$$\frac{dI(\nu)}{ds} = N_m \psi_L(\nu) A_{mn} \frac{h\nu}{4\pi} - [N_n \phi_L(\nu) B_{nm} - N_m \psi_L(\nu) B_{mn}] \frac{h\nu}{4\pi} I(\nu).$$

Let $\phi_L(\nu) = \psi_L(\nu)$ and define a total absorption coefficient, $\kappa_L(\nu)$, by

$$\kappa_L(\nu) = (N_n B_{nm} - N_m B_{mn}) \phi_L(\nu) \frac{h\nu}{4\pi}$$

$$= \frac{h\nu}{4\pi} \phi(\nu) B_{nm} (1 - \frac{B_{mn}}{B_{nm}} \frac{N_m}{N_n}).$$

Using $g_n B_{nm} = g_m B_{mn}$ (Mihalas, 1970, p. 83), the Boltzmann equation, and the departure coefficients, the absorption coefficient becomes

$$\kappa_L(\nu) = \frac{h\nu}{4\pi} \phi_L(\nu) B_{nm} b_n N_n^* [1 - \frac{b_m}{b_n} \exp(-h\nu/k T_{ex})]. \qquad \text{II-24}$$

For LTE, $b_m = b_n = 1$ and the LTE absorption coefficient is

$$\kappa_L^*(\nu) = \frac{h\nu}{4\pi} \phi_L(\nu) B_{nm} N_n^* [1 - \exp(-h\nu/k T_{ex})]. \qquad \text{II-25}$$

The Einstein probability can be written in terms of the oscillator strength, f_{nm};

$$B_{nm} = \frac{4\pi^2 e^2}{h\nu\ Mc}\ f_{nm}\ . \qquad \text{II-26}$$

In the above equation, e is the electron's charge; M is its mass. Oscillator strengths for hydrogen radio recombination lines have been computed by Goldwire (1968) and Menzel (1969).

Substituting Equation II-26 into Equation II-25 and assuming that $h\nu << kT_{ex}$, the absorption equation becomes

$$\kappa_L^*(\nu) = \frac{h\ \nu_{mn}\ \pi\ e^2}{M\ c\ k\ T_{ex}}\ \phi(\nu)\ N_n^*\ f_{nm}.$$

N_n^* can be obtained from the Saha-Boltzmann equation (Equation A-5) and ν_{mn} can be obtained from an approximation to the Rydberg equation; $\nu_{mn} \simeq 2c\ R_H\ Z^2\ \Delta n/n^3$. Using these and the appropriate constants (R_H = 1.097 x 10^5, Z = 1, u(T) = 1, and $g_n = 2n^2$), the LTE absorption coefficient becomes

$$\kappa_L^*(\nu) = 1.071 \times 10^7\ \phi(\nu)\ \frac{\Delta n}{n}\ f_{nm}\ N_i\ N_e\ T_e^{-2.5}\ \exp(\varepsilon_n/k\ T_{ex}) \qquad \text{II-27}$$

where $\varepsilon_n/k = 157890/n^2$. The LTE optical depth is

$$\tau_L^*(\nu) = 1.071 \times 10^7 \, \phi(\nu) \, \frac{\Delta n}{n} \, f_{nm} \, T_e^{-2.5} \, \exp(\varepsilon_n / k \, T_{ex}) \, E_L . \qquad \text{II-28}$$

E_L is the line emission measure defined by

$$E_L \equiv \int_0^L N_i \, N_e \, ds$$

and N_i is the number density of the recombining ion.

Following the notation of Dupree and Goldberg (1970), β_{mn} is defined by

$$\beta_{mn} \equiv [1 - \frac{b_m}{b_n} \exp(-h\nu/k \, T_{ex})] \, / \, [1 - \exp(-h\nu/k \, T_{ex})]. \qquad \text{II-29}$$

Then $\kappa_L(\nu) = b_n \, \beta_{mn} \, \kappa_L^*(\nu)$ and $\tau_L(\nu) = b_n \, \beta_{mn} \, \tau_L^*(\nu)$.

In most cases for radio recombination lines, $h\nu / k \, T_{ex}$ is small enough that the exponentials involving them are equal to $1 - h\nu/k \, T_{ex}$. Then,

$$\beta_{mn} \simeq \frac{k \, T_{ex}}{h\nu} \left[1 - \frac{b_m}{b_n} \left(\frac{h\nu}{k \, T_{ex}} \right) \right] = \frac{b_m}{b_n} \left[1 - \frac{k \, T_{ex}}{h\nu} \left(\frac{b_m - b_n}{b_m} \right) \right].$$

Using δ_{mn}, which was defined in Equation II-23,

$$\beta_{mn} \simeq \left(\frac{1}{1 - \delta_{mn}} \right) \left(1 - \frac{k \, T_{ex}}{h\nu} \, \delta_{mn} \right). \qquad \text{II-30}$$

If $\Delta b = b_m - b_n$ is small, $\Delta b \rightarrow db$ and

$$\delta_{mn} = \frac{db}{b_m} \simeq \frac{d(\ln b)}{dn}\Big|_{m=n} \cdot \Delta n \ ,$$

which is a notation often used.

Gordon (1971) and Hjellming and Gordon (1971) define a different β than that defined in Equation II-29;

$$\beta'_{mn} \equiv (1 - \frac{k T_{ex}}{h\nu} \delta_{mn}) \simeq 1 - \frac{k T_{ex}}{h\nu} \cdot \frac{d \ln b}{dn} \Delta n.$$

This is given for reference only since the definition of β_{mn} in Equation II-29 will be used in the present work.

Line Profiles

There are three line profile functions, which are relevant to radio recombination line analysis. They are the Gaussian, Lorentzian, and the convolution of these two, the Voigt function. The Gaussian function arises from the Doppler shift resulting from thermal, turbulent, expansion, and contraction motions of the line emitter relative to the observer. A Lorentzian profile for a radio recombination line results from pressure broadening. Natural broadening, or radiation damping, also produces a Lorentzian profile, but this is such a small effect that it is impossible to detect in the observed line profiles. If pressure broadening occurs, the effect would be blended with the Doppler broadening and a Voigt profile would result.

Doppler broadening. Mainly, thermal broadening will be considered. The thermal motion of particles in a gas with a kinetic temperature T_K has a Maxwellian velocity distribution; so, the number of particles, out of a total of N, which have a radial velocity between v and v + dv is

$$d\,N(v) = \frac{N}{v_o\sqrt{\pi}} \exp[-(v-v_c)^2/v_o^2]\,dv.$$

In this equation, v_o is the most probable velocity and v_c is the velocity of the ensemble as a unit. $v_o = (2k\,T_K/M)^{1/2}$ where M is the mass of the particles. The intensity of the spectral line at a frequency ν_1 is proportional to the number of emitters Doppler-shifted to that frequency. The line profile is a Gaussian;

$$\phi(v) = \frac{1}{v_o\sqrt{\pi}} \exp[-(v-v_c)^2/v_o^2]\,dv. \qquad \text{II-31}$$

The profile function is a probability distribution;

$$\int_{-\infty}^{\infty} \phi(v)\,dv = 1.$$

The power spectrum is usually displayed in terms of antenna temperature as a function of velocity. Velocity is physically related to the emitter and the line half-power width is then invariant to the line rest

frequency. The peak line antenna temperature, $T'(c)$, is that for which $v = v_c$. The temperature profile is

$$T'(v) = T'(c) \exp[-(v-v_c)^2/v_o^2]. \qquad \text{II-32}$$

The integrated line power, which is the area under the profile, is

$$P = \int_{-\infty}^{\infty} T'(v)\, dv = T'(c)\, v_o \sqrt{\pi}. \qquad \text{II-33}$$

Since v_o is not known, it is desired to substitute it with a measurable quantity. When the line power drops to one half of its peak intensity, $v = v_1$ and

$$T'(v_1) = 1/2 \frac{P}{v_o \sqrt{\pi}} = \frac{P}{v_o \sqrt{\pi}} \exp[-(v_1-v_c)^2/v_o^2].$$

The Doppler half-width is defined by $\Delta v_D = 2(v_1-v_c)$; then

$$\Delta v_D = 2v_o \sqrt{\ln 2} = \left(\frac{8k\, T_D}{M} \ln 2\right)^{1/2}. \qquad \text{II-34}$$

T_D is the Doppler temperature which is the effective temperature of the gas if the line width were the result of thermal motion only.

The integrated line power in units of °K km/s is

$$P(°K\ km/s) = \left(\frac{\pi}{4 \ln 2}\right)^{1/2} T'(c)\Delta v_D.$$

However, P is usually given in units of °K kHz; so,

$$P(°K\ kHz) = \left(\frac{\pi}{4\ \ln\ 2}\right)^{1/2} \left(\frac{\nu_o}{c}\right) T'(c)\ \Delta v_D$$

$$= 1.0645\ \left(\frac{\nu_o}{c}\right) T'(c)\ \Delta v_D. \qquad \text{II-35}$$

In Equation II-35, ν_o is the rest frequency measured in kHz; the velocity of light, c, and the Doppler width are both measured in km/s. Likewise, the integrated optical depth, τ_L, is

$$\tau_L = \int \tau_L(\nu)\ d\nu = 1.0645\ \tau(v_c)\left(\frac{\nu_o}{c}\right) \Delta v_D. \qquad \text{II-36}$$

The Doppler temperature is given by

$$T_D = \frac{M}{8k\ \ln\ 2}\ (\Delta v_D)^2\ . \qquad \text{II-37}$$

Doppler broadening includes the effects of thermal motion by an amount Δv_T, turbulence of a scale smaller than the antenna beam (Δv_{turb}), and expansion or contraction of the emitting region (Δv_x). These velocity components combine to give a total Doppler width of

$$\Delta v_D = (\Delta v_T^2 + \Delta v_{turb}^2 + \Delta v_x^2)^{1/2}. \qquad \text{II-38}$$

Pressure broadening and the Voigt profile. When the electron density is high enough that the time between collisions is shorter than the life-time of the excited atomic level, the energy distribution of the radiative transition is altered. The wavetrain is abruptly terminated by the passing electron. The line profile emitted by the assembly of atoms is a Lorentz function (Kuhn, 1962, p. 392). Peach (1972) has shown, however, that the profile is not an exact Lorentz function, but it is close enough for an accuracy of about 10 percent. The main effect of the Lorentzian is to redistribute the emitted energy to the wings of the line. Griem (1967) has shown that proton-atom collisions are not important.

Brockelhurst and Seaton (1972) have determined that the pressure broadened half-power width for a $m \rightarrow n$ transition is

$$\Delta\nu_p = 9.4 \left(\frac{n}{100}\right)^{4.4} \left(\frac{10^4}{T_e}\right)^{0.1} N_e.$$

Pressure broadening will occur in addition to Doppler broadening. If the gas has an electron temperature T_e and a Doppler temperature T_D (Equation II-37), the ratio of pressure to Doppler broadening is, by Brockelhurst and Seaton (1972),

$$\frac{\Delta\nu_P}{\Delta\nu_D} = 0.142 \left(\frac{n}{100}\right)^{7.4} \left(\frac{N_e}{10^4}\right) \left(\frac{2\times10^4}{T_D}\right)^{1/2} \left(\frac{10^4}{T_e}\right)^{0.1} . \qquad \text{II-39}$$

To obtain appreciable pressure broadening of radio recombination lines, $T_D \gtrsim 2 \times 10^4$, and $T_e \gtrsim 10^4$, and $N_e > 10^4$. So far, the only possible radio recombination line sources known to have such parameters are dense knots in emission nebulae such as M42, W51, and W3 (Hjellming and Davies, 1970) or dense H II regions associated with type I OH masers (Habing et al., 1974). No pressure broadening has been seen, however (Gordon, 1974).

When Doppler and pressure broadening occur together, the resulting profile is the convolution of a Lorentz with a Gaussian which is a Voigt profile, $\phi_V(\nu)$. The convolution integral cannot be evaluated exactly. So, the function is expressed in the form

$$\phi_V(\nu) = \frac{1}{\Delta\nu_D \sqrt{\pi}} H(a,\omega). \qquad \text{II-40}$$

where $H(a,\omega)$ is the Voigt function

$$H(a,\omega) \equiv \frac{a}{\pi} \int_{-\infty}^{\infty} \frac{e^{-y^2}}{(\omega-y)^2+a^2}\, dy$$

and

$$\omega \equiv \frac{\nu - \nu_c}{\sigma} , \quad y \equiv \frac{\nu}{\sigma} , \text{ and } a \equiv \frac{\Delta\nu_p}{\sigma} .$$

The frequency dispersion, σ, is given by $\sigma = \nu_D \, 2(\ln 2)^{-1/2} = \nu_D \left(\frac{\nu_o}{c}\right) (\ln 2)^{-1/2}$. Posener (1959) has tabulated the Voigt function for values of astronomical interest.

Non-LTE Solutions of the Transfer Equation and Line Enhancement

Two solutions of the transfer equation will be developed here for use in the analysis of the spectra. They will be derived starting with Equation II-4. Since the frequency of the spectral line is high, the Rayleigh-Jeans approximation to the Planck function can be used to convert specific intensity to brightness temperature. From Equation II-4, the brightness temperature is

$$T_B(\nu) = T_L(\nu) + T_C(\nu) = A(\nu)\, T_e\, (1-e^{-\tau}) + \frac{T_N}{\tau} (1-e^{-\tau})\, T_o e^{-\tau} \,, \qquad \text{II-41}$$

where $\tau = \tau_L(\nu) + \tau_T(\nu)$.

Since, from Equation II-6, $A(\nu) = S(\nu)/B(\nu,T_e)$ and $j_L(\nu) = b_m \kappa_L^* B(\nu,T_e)$,

$$A(\nu) = \frac{\kappa_T + b_m \kappa_L^*}{\kappa_T + b_n \beta_{mn} \kappa_L^*} = \frac{1 + b_m (\kappa_L^*/\kappa_T)}{1 + b_n \beta_{mn} (\kappa_L^*/\kappa_T)} \,. \qquad \text{II-42}$$

Optically thin H I region adjacent to a strong source of radiation. Assuming that $\kappa_L >> \kappa_T$ at the line

center (i.e. at $\nu = \nu_c$),

$$A(\nu) \simeq \frac{b_m \left(\kappa_L^*/\kappa_T\right)}{b_n \beta_{mn} \left(\kappa_L^*/\kappa_T\right)} = \frac{b_m}{b_n \beta_{mn}} .$$

Since the region is optically thin, Equation II-41 reduces to

$$T_B(\nu) = \frac{b_m}{b_n \beta_{mn}} T_e \left(\tau_T + \tau_L\right) + T_N + T_o \left(1 - \tau_T - \tau_L\right).$$

When the frequency is off the line (i.e. $\nu >> \nu_c$) only the continuum is observed;

$$T_B(\nu) = T_C(\nu) = \frac{b_m}{b_n \beta_{mn}} T_e \tau_T + T_N + T_o(1-\tau_T).$$

Subtracting this equation from the preceding one gives only the line;

$$T_L(\nu) = T_B(\nu) - T_C(\nu) = \frac{b_m}{b_n \beta_{mn}} T_e \tau_L - T_o \tau_L.$$

Since $\tau_L = b_n \beta_{mn} \tau_L^*$,

$$T_L(\nu) = \tau_L^*(\nu) \left(b_m T_e - b_n \beta_{mn} T_o\right). \qquad \text{II-43}$$

This is the line brightness temperature from an optically

thin H I region for which $\kappa_L >> \kappa_T$. The second term in Equation II-43 will produce line enhancement if β_{mn} is negative. To convert the brightness temperature to antenna temperature, the right side of the equation must be multiplied by the beam dilution factor, ρ_B, and the main antenna beam efficiency, η_B. These are defined by $\rho_B \equiv \Omega_S/\Omega_M$ and $\eta_B \equiv \Omega_M/\Omega_A$, where Ω_S is the solid angle of the line-emitting region; Ω_M is the solid angle of the antenna main beam; and Ω_A is the total solid angle of the antenna beam. The antenna temperatures are denoted with a prime; so, Equation II-43 becomes

$$T_L'(\nu) = \rho_B \eta_B \tau_K^*(\nu) (b_m T_e - b_n \beta_{mn} T_o). \qquad \text{II-44}$$

Isolated region. This solution of the transfer equation will be for the case of an isolated emitting region for which the incident radiation is weak and can be ignored. Then $T_o = T_N = 0$ and Equation II-41 reduces to

$$T_B(\nu) = A(\nu) T_e [1-e^{-(\tau_L+\tau_T)}].$$

Off the line, $A(\nu)$ will be unity; so, the continuum temperature is

$$T_C(\nu) = T_e(1-e^{-\tau_T}).$$

Taking $A(\nu)$ from Equation II-42 and converting $T_B(\nu)$ to antenna temperature, $T_L(\nu) = T_B(\nu) - T_C(\nu)$ and

$$T_L'(\nu) = \rho_B \eta_B T_e \left\{ \frac{\tau_T + b_m \tau_L^*}{\tau_T + b_n \beta_{nm} \tau_L^*} \left[1-e^{-(\tau_L+\tau_T)}\right] - (1-e^{-\tau_T}) \right\}. \qquad \text{II-45}$$

Line enhancement. Equations II-44 and -45 will be used for the analysis of this study's observations. The equations indicate how non-LTE conditions affect the radio recombination line temperature. For LTE $b_n = b_m = \beta_{mn} = 1$; $\delta_{mn} = 0$; and Equation II-44 becomes $T_L(\nu) = \tau_L^* (T_e - T_o)$.

Figure II-4 shows that as N_e decreases, collisions become less frequent; so, the level populations and b_n decreases. As the departure from LTE increases, δ_{mn} becomes larger. When $\delta_{mn} > (h\nu/kT)$, β_{mn} is negative and amplification of the line takes place. This process is often referred to as the "partial maser" process. The populations of the transition levels are not actually inverted as is apparently true for, say, H_2O masers (Sullivan, 1973).

The line enhancement can be seen from Equations II-44 and -45 in which $\tau_L = b_n \beta_{mn} \tau_L^*$ is negative. Usually, $\tau_L^* << \tau_T$ because the path length involved with τ_T is much larger than that involved in

τ_L^*. Also, b_m is always positive. Therefore, if $\left| b_n \beta_{mn} \tau_L^*/\tau_T \right| < 1$, $A(\nu)$ increases and the total absorption, $\tau_L + \tau_T$, decreases.

The line enhancement will be lessened somewhat because $b_m < 1$. However, for a decrease in electron density from 10^3 to 10 cm^{-3}, δ_{mn} increases by more than a factor of ten while b_m decreases by about 14 percent. The net result is a substantial increase in line power.

Equation II-44 also indicates the possibility that the recombination lines may be seen in absorption against a strong radio source if the relative magnitudes of b_n and δ_{mn} are such to make β_{mn} positive. However even for the case of a dense H II region ($E_L \sim 10^7$ pc cm^{-6}) seen through a tenuous H II region, Brockelhurst and Seaton (1972) have shown graphically that absorption cannot be greater than 8 percent. So far, radio recombination lines have not been seen in absorption.

The Radiation Field

The radiation field intensity entering a recombination line-emission region, and used in Equation II-20 to determine the level populations, is computed from $I_o(\nu) = W(\nu)\ B(\nu,T)$. Usually the radiation source is a nearby nebula whose blackbody temperature is 10^4 °K. The dilution factor, $W(\nu)$, is a product of three factors;

$$W(\nu) = W_G \; W_A(\nu) \; A(\nu). \qquad \text{II-46}$$

$W_A(\nu)$ represents absorption of the radiation by the intervening medium between the source and the line emission region. If τ is the intervening optical depth, $W_A(\nu) = e^{-\tau}$. If the nebula is adjacent to the line-emission region, $W_A(\nu) = 1$.

$A(\nu)$ represents the departure of the radiation source from a blackbody. It is defined in Equation II-6.

The geometrical dilution factor, W_G, can be found as follows. Consider a radiation source which is roughly spherical in shape with a diameter d_s and located at a distance r_R from the line-emitter. The geometry is shown in Figure II-5a. The line-emitting region sees the radiation source as a disc of angular diameter and filling a solid angle $\Omega_R = \pi \theta_R^2/4$. Then

$$W_G = \frac{\pi d_s^2/4}{4 \pi r_R^2} = \frac{d_s^2}{16 r_R^2} = \frac{\Omega_R}{4\pi} . \qquad \text{II-47}$$

If the two regions are contiguous, $r_R \simeq 1/2 \; d_s$ and $W_G = 1/4$. If, however, the radiation source is much larger than is the line emitter, Figure II-5b applies and $W_G = 1/2$. Finally, if the source of radiation surrounds the line emitter or if the line is emitted by a dense H II region, $W_G = 1$.

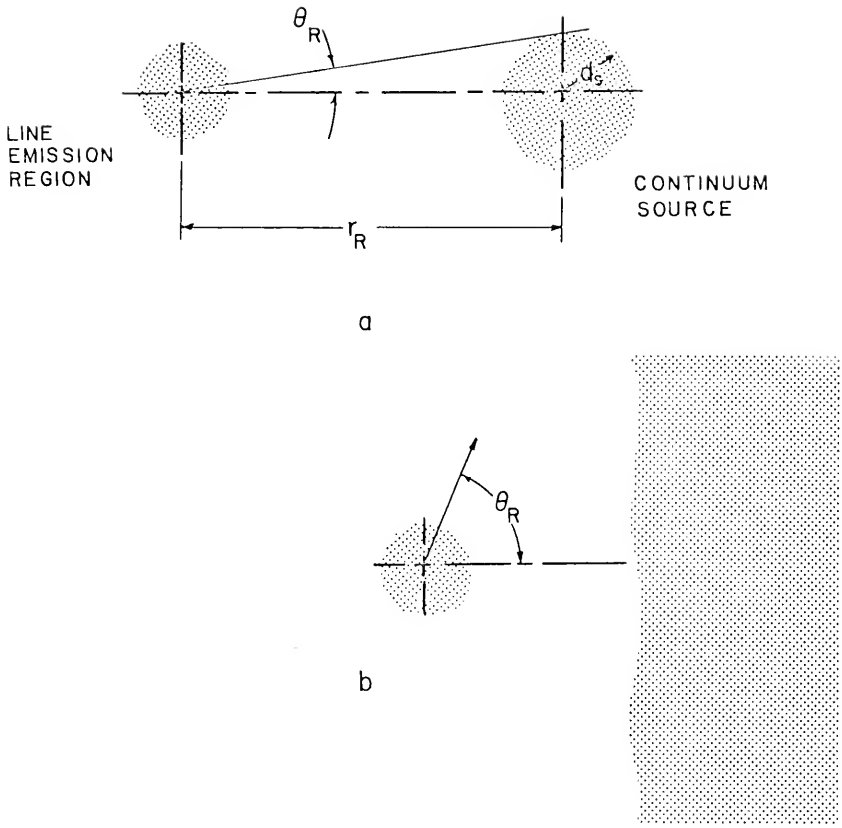

Figure II-5. Determination of the Geometrical Dilution Factor, W_G. Part a shows the line emitting region and the continuum source to be about the same size and $r_R > d_s$. Part b shows the line emitting region adjacent to a large continuum source.

A numerical example will illustrate the case where $r_R > d_s/2$. Consider the radiation of temperature T_R entering a small line emitting region located 100 pc from an H II region, such as NGC 7000 (the North American Nebula), for which $T_e \simeq 10^4$ °K and r_s = 25 pc (Kaplan and Pikelner, 1970, p. 152). For this case $A(\nu) = 1$. Assume that $W_A(\nu) = 1$ also. Then, using Equation II-47, it is found that T_R = 131 °K. This indicates that, unless the line-emitting region is directly adjacent to a large H II region, the line-emitting region can be considered as being isolated. In the case where the line emitter is itself an H II region ($T_e = 10^4$ °K), Dyson (1969) shows that the effect of the free-free continuum on the departure parameters is very small. Dupree (1972) and Hoang-Binh and Walmsey (1974) demonstrate the effect of a large H II region adjacent to the line-emitting region.

Ionization Rates

Knowing the radiative recombination coefficient, $\alpha(T)$, the required rate of ionization per atom of species X, ζ_X, can be determined from the condition of detailed balance. For hydrogen,

$$N_H \zeta_H = N_e N_{H^+} \alpha(T). \qquad \text{II-48}$$

The radiative recombination coefficient may be obtained from Equation II-22. Habing (1970) has a formula for computing ζ_H which uses the assumption that $\alpha(T) \propto T^{-0.65}$;

$$\zeta_H = 1.27 \times 10^{-15} \nu_T^{2.1} T^{-0.3} \tau_T(\nu_T) / \int \tau_{21}(v)\, dv. \qquad \text{II-49}$$

In this formula, $\tau_T(\nu_T)$ is the continuum optical depth at a frequency ν_T and $\tau_{21}(v)$ is the 21 cm line optical depth discussed in the next section.

Ionization rates can be calculated theoretically from a given source of ionization such as low energy cosmic rays (Dalgarno and McCray, 1972) and OB stars. These rates can be compared to the ionization rate required by a model for a line emitting region.

As an example the ionization rate within the Stromgren sphere surrounding an OB star will be considered. Let S_u be the total number of ultraviolet photons with energy greater than $h\nu_L$ emitted from the central star. ν_L is the frequency of the Lyman limit. Also let r_S be the Stromgren radius which is the radial distance from the star at which the ionizing radiation flux is zero. Then

$$S_u = \frac{4}{3} \pi r_S^3 N_e N_{H^+} \alpha(T)$$

(Spitzer, 1968, p. 116). From Equation II-48, $\alpha(T) = N_H \zeta_H / N_e N_{H^+}$ and the ionization rate of an OB star is

$$\zeta_H = \frac{3S_u}{4 \pi r_S^3 N_H} \quad . \qquad \text{II-50}$$

The ultraviolet flux, S_u, from stars of spectral class O5 through B1 are tabulated by Spitzer (1968, p. 117).

The 21 cm Hydrogen Line

The well known 21 cm hydrogen line is emitted by a magnetic dipole transition between the hyperfine levels of the ground state. This is the result of the difference of energy levels between the proton and electron spins being parallel (upper state, F = 1) and antiparallel (lower state, F = 0). The frequency of the transition is 1420.405 MHz. The upper state is metastable; the spontaneous emission probability is $A_{10} = 2.85 \times 10^{-15}$ sec^{-1} (Kaplan and Pikelner, 1970, p. 410). Usually the metastable state is depopulated by collisional excitation more frequently than it is by the 21 cm radiative transition. The F = 1 state is populated by atom-atom collisions (Kaplan and Pikelner, 1970, p. 420).

Designating the lower and upper states by 0 and 1 respectively, the absorption coefficient is

$$\kappa_{10}(\nu) = \frac{h\nu_{10}}{4\pi} \phi(\nu) \left[N_0 B_{01} - N_1 B_{10}\right].$$

The parameters are analagous to those of the recombination line. Since collisions play an important part in populating the upper state, it will be assumed for the moment that the populations are LTE values as determined by the Boltzmann equation. The statistical weights of the states are $g_1 = 3$ and $g_0 = 1$. Then, since $g_0 B_{01} = g_1 B_{10}$ and $h\nu_{10}/kT \ll 1$,

$$\kappa_{10}(\nu) = \frac{h\nu_{10}}{4\pi} \phi(\nu) \frac{h\nu_{10}}{k T_s} N_0 B_{01}.$$

T_s is the excitation temperature which, for the 21 cm transition, is called the spin temperature because the transition results from a change of electron spin orientation. The absorption coefficient is expressed in terms of the spontaneous emission coefficient, A_{10};

$$A_{10} = \frac{2h \nu_{10}^3}{c^2} B_{10}.$$

Then

$$\kappa_{10}(\nu) = \frac{3N_o h c^2}{8\pi k T_s \nu_{10}} A_{10} \phi(\nu). \qquad \text{II-51}$$

The absorption coefficient is used to obtain the neutral hydrogen column density along a line of sight.

For a cold gas, the total neutral hydrogen density, N_{H°, is $N_0 + N_1$. From the Boltzmann equation, the number density at some point s in the line of sight is

$$N_H(s) \simeq N_0(s)\,[1+3(1-h\nu_{10}/k\,T_s)] \simeq 4N_0(s),$$

since $h\nu_{10}/k \simeq 0.07$. Substituting in values for the constants and integrating over the line profile and along the line of sight gives

$$\iint_{\nu}\int_{0}^{L} \kappa_{10}(\nu,s)\,ds\,d\nu = \int \tau_{21}(\nu)\,d\nu = 2.58 \times 10^{-15} \int_0^L \frac{N_H(s)}{T_s}\,ds, \qquad \text{II-52}$$

where the path length, L, is in cm and ν_{10} is in Hz.

If the line profile is Gaussian with a half-power width ν_D and a peak optical depth τ_{21}, Equation II-36 can be used to obtain

$$\int_0^L \frac{N_H(s)}{T_s}\,ds = 4.126 \times 10^{14}\,\tau_{21}\,\Delta\nu_D\,. \qquad \text{II-53}$$

It may be necesary to determine whether or not the spin and gas kinetic temperatures are equal. Starting with the equation of detailed balance,

$$N_1 N_H C_{10}(T_K) + N_1 A_{10} + N_1 B_{10} I(\nu_{10},T_R)$$

$$= N_0 N_H C_{01}(T_K) + N_0 B_{01} I(\nu_{10},T_R).$$

$C_{01}(T_K)$ and $C_{10}(T_K)$ are the collisional excitation and de-excitation probabilities, respectively, whose formulation is given by Kaplan and Pikelner (1970, p. 420). Solving the detailed balance equation for T_s in terms of T_K and the radiation temperature, T_R, gives

$$T_s = \frac{557.3\ T_K^{0.5}\ N_H + T_R}{557.3\ T_K^{-0.5}\ N_H + 1} \quad . \qquad \text{II-54}$$

$T_s \simeq T_K$ if the hydrogen density is large enough that $557.3\ T_K^{0.5}\ N_H >> T_R$. For H I regions, $T_K > 64$ °K and $N_e > 1\ cm^{-3}$ is not unreasonable (Baker and Burton, 1975); so $557.3\ T_K^{0.5}\ N_H > 4.4 \times 10^3$ °K which is much larger than one would expect T_R to be. Therefore, unless $N_H << 1\ cm^{-3}$, $T_s = T_K$.

Absorption spectra of the 21 cm line have been obtained by three techniques. Hagen, Lilley, and McClain (1955) obtained absorption spectra in the direction of discrete sources by averaging the spectra from off-source beams and subtracting this from the on-source beam spectrum. The accuracy to which this method yields the true absorption spectrum depends on how uniform the hydrogen gas is over the grid of beams.

Radhakrishnan et al. (1972a) and Hughes, Thompson, and Colvin (1971) have observed absorption spectra in the direction of radio sources (e.g. 3C391) with two-element interferometers. The front-ends and synchronus detectors are switched in such a way that the system is insensitive to all but the absorption spectrum in the direction of the source.

A third method has been used to obtain absorption spectra in the direction of pulsars. Some of this work has been done by Gordon et al. (1969), Manchester et al. (1969), Gordon and Gordon (1970), Guelin et al. (1969), and Encrenaz and Guelin (1970). The pulsar is observed with a gated, spectral line receiver which alternately stores and integrates the spectrum with the pulsar on and with it off. At the end of the integration period, the pulsar-off spectrum is subtracted from the pulsar-on spectrum. The difference of the two is the absorption spectrum. The pulsar is a particularly useful beacon because its dispersion measure provides a value of the integrated electron density along the line of sight. Therefore, two pieces of information about the intervening interstellar medium are known.

Pulsar Dispersion Measure

The arrival time of the pulsed radio emission from pulsars is frequency dependent. The pulse travels at the

group velocity. The group index of refraction is a function of the electron density of the medium through which the pulse travels. The difference of arrival time, $t_1 - t_2$, of the respective frequencies ν_1 and ν_2 is, then, the integrated electron density along the path length L. This is the dispersion measure, DM, which is calculated from the equation (cf. Terzian, 1972)

$$DM \equiv \int_0^L N_e \, ds = 2.4 \times 10^{-4} \, (t_1 - t_2) \, (\nu_1^{-2} - \nu_2^{-2})^{-1}. \qquad \text{II-55}$$

From this equation, the unit of DM is pc cm^{-3}.

CHAPTER III

THE TELESCOPE SENSITIVITY AND THE OBSERVING SCHEME

The observations, which will be discussed in the next chapter, were made in such a way as to make the most efficient use of the telescope. This chapter will discuss the basis for the observational scheme. The important factor was the system sensitivity which is affected by the microwave frontend of the receiver and the one-bit autocorrelation spectrometer.

The general theory involved with the operation of a one-bit autocorrelation spectrometer for astronomical use was discussed in detail by Weinreb (1963). The operation of the instrument used for the observations is discussed in two reports. The IF filter system, which precedes the correlator and determines the width of the spectral window, is described by Mauzy (1968). The operation of the entire system, with emphasis on the digital autocorrelator, is described by Shalloway et al. (1968). A discussion of system sensitivity for the different methods of observing radio spectra is presented by Ball (1972).

System Sensitivity

The nominal system sensitivity is the RMS noise temperature, ΔT, given by

$$\Delta T = \frac{\gamma T_{sys}}{\sqrt{\Delta f \; t_i}} \quad . \qquad \text{III-1}$$

The parameters are as follows:

γ = a constant which depends on the system and the method of its operation;

T_{sys} = the system noise temperature;

Δf = the frequency resolution bandwith; and

t_i = the integration time.

T_{sys} is the combination of the noise temperatures received by the antenna as well as the power generated by the antenna-transmission line system and the receiver.

The total bandwith, B, observed by the spectrometer is divided up into N channels. Both B and N are selectable. Each channel has the effect of measuring the spectral power within a filter whose bandpass is of the form $(\sin \nu)/\nu$ having a half-power width of

$$\Delta f = 1.21 \frac{B}{N} \qquad \text{III-2}$$

(Shalloway et al., 1968). The spacing between channel centers is B/N.

The factor γ in Equation III-1 is greater than one and is the degradation of the system sensitivity due to the operation of the autocorrelator. It is a one-bit digital machine which computes the autocorrelation function, $\rho(n\Delta t)$, of the undetected IF power; $n\Delta t$ is the time delay at the n^{th} channel. The first step in obtaining the autocorrelation function is to clip the signal, a random Gaussian voltage, $v(t)$. The clipper generates a function, $y(t)$; $y(t) = +Y$ if $v(t) > 0$ and $y(t) = -Y$ if $v(t) < 0$. The function $y(t)$ is then sampled at a rate equal to $2B = 1/\Delta t$. The output of the sampler is fed into an N-bit shift register and N one-bit multipliers. The shift register is updated at the time intervals of Δt. The output of each of the multipliers updates a counter. At the end of the integration time, each counter contains the sum which represents one point of the autocorrelation function. The function is in the form of an array which is transferred to the on-line computer which computes the power spectrum by taking the Fourier transform of it.

The effect of using one-bit quantization is to increase ΔT above that which would result from a many-bit quantization (Weinreb, 1963, p. 32). This is accounted for in the constant γ of Equation III-1. This constant is actually a product of two factors; $\gamma = \alpha\beta$. The effect of one-bit quantization is that $\beta = 1.39$ (Weinreb,

1963, p. 49).[1] The value of the other factor depends on the weighting function used in computing the correlation function. A uniform weighting function was used for which $\alpha = 1.099$ (Weinreb, 1963, p. 22). Therefore, $\gamma = 1.528$ and Equation III-1 becomes

$$\Delta T = \frac{1.528\ T_{sys}}{\sqrt{\Delta f\ t_i}} \quad . \qquad \text{III-3}$$

The Observing Scheme

There are several observing schemes which can be used to observe spectral lines (cf. Ball, 1972). The observing scheme must provide a reference spectrum which is used to remove the effects of the receiver passband from the desired spectra.

The "Total Power" scheme can provide an efficient means of obtaining the reference spectrum. Before observing a source on the program, a spectrum is obtained while the antenna is pointed in a direction close to the program

---

[1] Burns and Yao (1969) have determined that the clipping factor, β, is a function of the sampling rate. For a sampling rate of $2B$, $\beta = \pi/2 = 1.571$. If this is correct, $\gamma = 1.726$ and the RMS noise of the data discussed in Chapter IV should be multiplied by a factor of 1.13. However, the data reduction routines continue to use $\beta = 1.39$ (Cram, 1973, p. 133).

source and where the spectral line is not detected. This spectrum is the receiver passband function. The nomenclature of the Total Power method is to designate the reference spectrum by "OFF" and a program spectrum by "ON." If the receiver passband remains unchanged while the OFF and ON spectra are observed, subtracting the OFF spectrum from the ON spectrum removes the effect of the passband from the desired spectrum. The efficiency of this observing scheme is realized if one OFF spectrum can be used with more than one ON spectrum if there are several sources in the observing program.

Let the observing time on an OFF source be t_F and that on an ON be t_N. If an OFF source is followed by n ON sources, each of which is observed for a time t_N, the total observing time, t_o, will be $t_o = t_F + n\, t_N$. The times t_F and t_N and the ratio n must be chosen so that the receiver passband remains unchanged during the time t_o. The most efficient use of observing time for a given number of program sources will be obtained if the ratio $a = t_F/t_N$ is chosen to minimize ΔT.

When an OFF spectrum with an RMS noise $(\Delta T)_F$ is subtracted from an ON spectrum with an RMS noise $(\Delta T)_N$ the RMS noise of the resulting spectrum will be

$$T = [(\Delta T)_N^2 + (\Delta T)_F^2]^{1/2} .$$

For spectral line observations, T_{sys} is not expected to change more than a few percent between the OFF and ON positions; then an average system temperature, T_{ave}, can be used to get

$$\Delta T = \frac{\gamma\ T_{ave}}{\sqrt{\Delta f}} \left(\frac{1}{t_N} + \frac{1}{t_F}\right)^{1/2} .$$

Referring to Equation III-1, the integration time is

$$t_i = \frac{t_N\ t_F}{t_N + t_F} . \qquad \text{III-4}$$

Since $t_F = a\ t_N$ and $t_o = (a + n)t_N$,

$$\Delta T = \frac{T_{ave}}{\sqrt{\Delta f\ t_o}} (a + 1 + n + n/a)^{1/2}$$

The value of a is determined when T is a minimum, for which

$$\frac{d(\Delta T)}{da} = 0.$$

Then $(1-n/a^2)(a+1+n+n/a)^{-1/2} = 0$. The only reasonable solution is $a = \sqrt{n}$. Therefore, the most efficient Total Power observing pattern exists for

$$t_F = \sqrt{n}\ t_N . \qquad \text{III-5}$$

CHAPTER IV

THE RADIO RECOMBINATION LINE OBSERVATIONS

Introduction

The H157α radio recombination line spectra for this study were obtained between 18 and 24 April, 1973 with the 43 meter radio telescope of the National Radio Astronomy Observatory (NRAO)[1] located in Green Bank, West Virginia. The rest frequency of the line is 1.683200 GHz. The H157α line was chosen for two reasons. It is conveniently located within the passband of the NRAO 18 cm cooled receiver which has good sensitivity and a reputation of being very stable. Also, the frequency of this line is such that the line strength is relatively strong. The total power observing scheme was used to obtain the spectra.

The sources used for the observations are the two supernova remnants (SNR) 3C391 and 3C396 and the pulsar 1858+03. These were chosen on the basis of the objectives discussed in Chapter I; they are located in the galactic

---

[1] NRAO is operated by Associated Universities, Inc. under contact with the National Science Foundation.

ridge and independent data from the intervening interstellar medium are available. A radio galaxy, 3C295 (Goldstein 1962), was also observed, but its galactic latitude is 61° and no radio recombination line was observed in its direction. The purpose of observing it was to demonstrate that the recombination lines came from the ridge gas and were not affected by instrumental effects.

Along with 3C391 and 3C396, a region adjacent to each of them was also observed. These will be referred to by the designation COMP. The COMP spectra were observed for two reasons. The primary reason was to be able to subtract out emission from the region immediately surrounding each of the SNR's and, thereby, make these observations compatible with those made with narrow beams. The second reason for obtaining the COMP spectra was to determine the angular scale over which the medium changes.

Table IV-1 lists the center position of each beam. The right ascension and declination (1950.0 epoch) and the galactic longitude and latitude are given for each of the regions studied. The OFF beams are the reference beams used for the Total Power observing scheme. Their selection and use will be discussed in the following section.

Figure IV-1 shows the continuum radiation environment of the regions observed. The continuum maps are adapted from the 1414 MHz maps of Altenhoff et al. (1970). The

Table IV-1

Antenna Beam Positions

Beam	$\alpha(1950)$	$\delta(1950)$	l^{II}	b^{II}
3C391	$18^h\ 46^m\ 47.^s8$	-0° 58' 48."0	31.°9	0.°0
COMP 3C391	$18^h\ 46^m\ 01.^s5$	-0° 53' 14."1	32.°1	-0.°2
3C396	$19^h\ 01^m\ 35.^s7$	+5° 22' 30."0	39.°2	-0.°3
COMP 3C396	$18^h\ 59^m\ 59.^s2$	+5° 16' 49."7	38.°9	0.°0
OFF[a]	$18^h\ 30^m\ 0.^s0$	+4° 30' 0."0	35.°0	+5.°0
1858+03	$18^h\ 58^m\ 40.^s0$	+3° 27' 2."0	37.°2	-0.°6
OFF[b]	$19^h\ 12^m\ 0.^s0$	+2° 00' 0.'0	37.°4	-4.°2

[a] the OFF beam for 3C391, 3C396, and their COMP beams

[b] the OFF beam for the pulsar, 1858+03

Figure IV-1. The Continuum Radiation Environment of the Program Regions. The size of the circles represents the antenna beam half-power width, 18 arc minutes. The 1414 GHz continuum maps are from Altenhoff *et al*. (1970). The counter is 1.74 °K of brightness temperature.

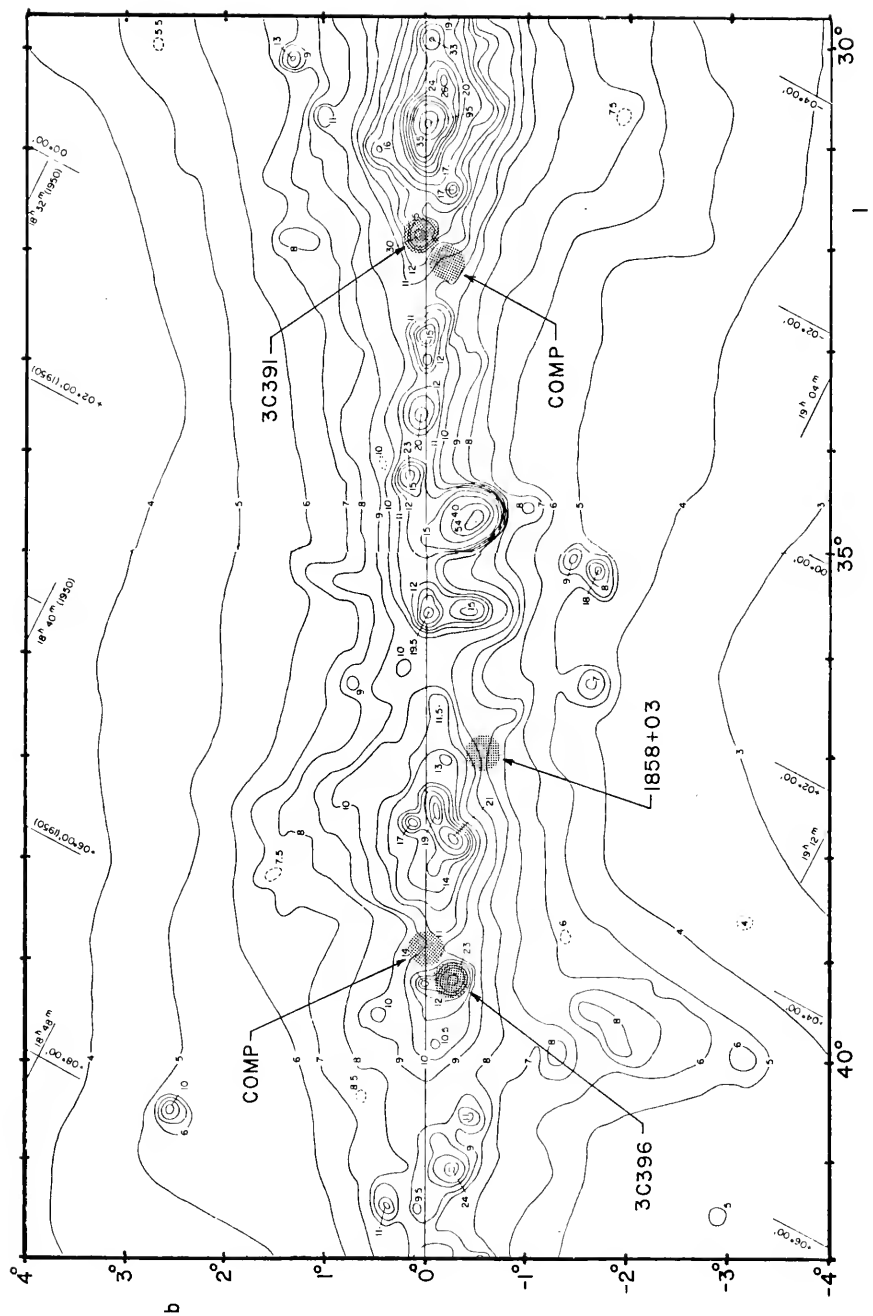
3C391
COMP
COMP
1858+03
3C396
b
l
30°
35°
40°
4°
3°
2°
1°
0°
-1°
-2°
-3°
-4°

size of the circle at each region is about equal to the half-power width of the antenna beam, 18 arc minutes at the H157α frequency.

Observing Scheme and Data Reduction

The receiver front-end was mounted at the prime focus of the 43 meter paraboloid. A scaler horn was located at the focal point of the reflector. The signals of linear orthogonal polarizations were separated behind the horn and fed into separate and identical receivers. The box containing the front-end equipment was rotated so that the E-plane of the horn was aligned normal to the celestial equater. Each receiver was load-switched and contained a two-stage parametric amplifier. The first stage of the parametric amplifier and the switched load were refrigerated.

The local oscillator frequency was generated by a frequency synthesizer followed by a 6x frequency multiplier. The intermediate frequency (IF) sent to the control room from the front-end box was 150 MHz. The synthesizer frequency was chosen to compensate for the Doppler effects of all motions of the telescope with respect to the recombination line emitter and so that the velocities of the spectra would be with respect to the local standard of rest (LSR). Since it was expected that the recombination line emission regions and galactic H I regions are

kinematically related, the 21 cm emission velocity longitude maps of Westerhout (1969) were consulted to determine the velocity offset needed to positon the anticipated H157α and C157α spectral features in the 2.5 MHz spectrometer passband. The velocity offset for the pulsar was +50 km/s. All other program regions involved an off set of -10 km/s. The synthesizer frequencies were calculated by the NRAO computer program DOPSET before any observations were made.

The 150 MHz IF from each receiver was monitored by a continuum reciever. The remaining signal was fed to the NRAO Model II autocorrelation spectrometer. The spectrometer creates 413 frequency channels which were divided into three sections. One section of 192 channels was connected to each of the front-end receivers. The remaining 29-channel section of the spectrometer was connected to one of the recievers to serve as a monitor. It was not used for the acquisition of the data.

Each section of the spectrometer had a passband of 2.5 MHz. This allowed a channel separation of 13.0 kHz. Each channel has a sin ν/ν profile with a half-power width of 15.8 kHz. At a frequency of 1.6832 Ghz, the velocity resolution of each channel was 2.82 km/s.

The operation of the spectrometer system is described by Shalloway et al. (1968) and the Total Power observing scheme is described in Chapter III. The autocorrelator

periodically transfers the autocorrelation function array into the on-line computer which performs the Fourier transform and loads the resulting spectrum array onto a seven-track magnetic tape. This array, along with source coordinates and control information, constitutes a record. The control information contains a number designation of the spectrum and whether it is a spectrum of a program (ON) source or a reference (OFF) source, The identity of its OFF spectrum is also specified.

Each source is observed for a length of time (t_F or t_N as used in Chapter III) during which a sequence of records is placed on the tape. This sequence of records is treated as a unit during off-line analysis and is called a "scan." At the beginning of the off-line processing, the records of each scan are averaged together and the spectrum of each scan is loaded on another magnetic tape. Then, for each ON spectrum, its OFF spectrum is located and the antenna temperature spectrum is computed from

$$T_L'(i) = \left(\frac{S(i) - R(i)}{R(i)}\right) T_{sys} ,$$

where S(i) and R(i) are the source (ON) and reference (OFF) spectra, respectively, as a function of the channel, i.

The system temperature, T_{sys}, is computed by the off-line computer on the basis of a calibration noise source whose power is periodically injected into each receiver.

The accuracy to which the system temperature is determined depends on how well the calibration temperature is known. During the observations the values determined during bench testing of the receiver were entered into the DDP-116 program. The calibration signal was injected into each receiver by a loop "antenna" placed in the waveguide at a point directly following the coupler which seperates the two polarizations. During the bench testing the horn was replaced by a termination. In spite of the careful matching of the termination to the system, its characteristics are somewhat different from those of the horn observing the sky. Consequently the amount of calibration noise power entering the system is not exactly the same in the two situations (Turner, 1973).

The calibration temperature discrepancy was corrected by daily calibrations using the radio source Virgo A whose continum spectrum is well known. Once a more accurate calibration temperature was known, a correction factor was later applied in the off-line processing. The continum flux of Virgo A at 1.6832 GHz is 182 Jy which was determined by plotting the fluxes published by Kellerman et al.(1969) and interpolating to this frequency. The continum receiver connected to the IF was used to measure the relative levls of Virgo A and the cold sky with and without the calibration signal. Table IV-2 shows the results of the daily calibration by which the system noise temperature,

T_{sys}, was also determined. The first calibration on 22 April gave unexplainable bad results; so, the calibration was repeated later. The spectra obtained in the meantime showed no indication of a problem. The values obtained during this bad calibration were not used to compute the averages from which the correction factors were computed.

Before the telescope was pointed toward any source, the receiver frontends were tuned so that the spectrometer passband was located in a portion of the reciever passband (25 MHz wide at the 3 db points) which was reasonably flat. The daily observing procedure began by peaking up on Virgo A in order to check the pointing accuracy of the telescope and obtain a correction factor for the calibration temperature. No problems with the pointing were found.

Before observing the first program region, a five-minute OFF scan followed by a five-minute ON scan of M17 was made to check the operation of the spectrometer. The OFF regions for this and the program regions were at least four degrees above or below the galactic plane where it was certain that the H157α line was not present. The H175α spectrum of M17, an emission nebula, is very strong. A five-minute scan gave adequate indication that the spectrometer was operating properly. The daily M17 spectra were compared to look for degradation of the system. None was noticed.

Table IV-2

Calibration and System Noise Temperatures

Date	$T_{sys\ B}$	$T_{cal\ A}$	$T_{sys\ B}$	$T_{cal\ B}$
April				
18	62.2	3.12	58.5	3.17
19	66.4	3.45	59.4	3.98
20	64.5	3.35	60.5	3.55
21	61.9	3.02	59.6	3.75
(22[a]	176.9	8.57	187.0	7.83)
22	60.4	3.21	58.0	3.21
23	84.5	4.40	84.4	3.59
Average	66.6	3.42	63.5	3.54
"Bench" values		3.23		3.63
Correction factor:		0.975		0.972

[a]These are the results of the bad calibration and are shown for reference only. They were not used to compute the averages.

Most of the observing program for 3C391, its COMP, 3C396, and its COMP was performed with the Total Power scheme using a sixty-minute cycle; a twenty-minute OFF scan was followed by a ten-minute scan on each of the four program regions in succession. The ratio of OFF-time to ON-time was determined on the basis of Equation III-5. To make the most efficient use of observing time, it is desirable to make the scans as long as possible so that the total time moving between regions is minimized. The maximum length of the cycle was limited by the length of time during which the receiver passband remained stable. During the observations it was found that the quotient spectra of the last few records of the sixty-minute cycle began to show a curvature of the baseline. This means that the receiver passband had changed enough since the OFF scan had been recorded that this OFF spectrum no longer represented the current passband well enough to produce a flat continuum on which the spectral features are enhanced. The curvature only affected the last few 3C396 COMP spectra; so, the cycle was maintained at sixty minutes.

The observations of these four regions continued until the RMS noise, expected after combining all scans of each region, was about 0.002°K. Most of the last two days were used to observe the pulsar and 3C295. Each was observed individually, usually with a fifty-minute cycle

consisting of a twenty-five minute OFF followed by a twenty-five minute ON. The 3C295 spectra showed no spectral features or abnormal baselines. Therefore, these data will not be discussed further in this study.

After each day's observations had been completed, the seven-track "telescope" tape was taken to Charlottesville, Virginia where an IBM 360/55 computer was used to average the records of each scan and load the resulting spectra on a nine-track "user" tape for further analysis. At the same time a summary of records and the quotient spectrum of each scan was printed. These tasks were performed by the first phase of the TPOWER data reduction program (Cram, 1973). The printout was sent to the observatory the next day. With these "quick-look" summaries, it was possible to determine which scans had problems which would make them unusable. On the basis of these reports some scans were deleted and reobserved on the last day of the program.

After all observations had been made, the final spectra were produced using the second phase of TPOWER, a system of routines controlled by a command language. It was during this process that the correction factor, determined from the daily noise tube calibration, was applied to adjust the antenna temperature scale. The scans were summed and weighted by the effective integrating time of each scan. Then the spectra of the two receivers were averaged together, thereby doubling the integrating time. The

resulting spectra were convolved with a five-channel "box-car" function and plotted. The plotted spectra were studied in order to estimate the structure of the baseline. Curvature of the baseline of each spectrum was removed with a TPOWER routine which first computes a specified order Chebyshev polynomial by means of a least squares fit to a specified portion of the baseline. The routine then subtracts the polynomial baseline from each spectrum and the spectra are then plotted in their final form.

A final task was performed in order to facilitate the analysis of the spectra. Gaussian functions were fitted to the spectral features. The TPOWER routine begins with initial estimates of the center channel and half-intensity width of each feature and, from that, determines a best-fit center, half-intensity width, and central intensity of the features.

The Spectra

The basic spectra for the program regions are shown in Figures IV-2, -3, and -4. Preceding the figures is Table IV-3 which lists the total effective integration time (t_i) and the order of the Chebyshev polynomial base line which was removed. The effective integration time was computed with Equation III-4. It includes the doubling obtained by averaging the spectra of the two receivers.

The RMS noise, listed in the third column, is computed from Equation III-3;

$$\Delta T = \frac{1.528\ T_{sys}}{\sqrt{\beta t_i}} .$$

T_{sys} is the average system temperature of both receivers and is 65.0 °K. The effective bandwidth, β, is five times the channel separation of 13.0 kHz because the spectra are displayed after being convolved with a five channel boxcar function. Table IV-3 also provides a table of contents which includes a list of the figure numbers for all spectra including those showing the Gaussian fits to the spectral features.

The lower portions of Figures IV-5 through 10 show the results of fitting Gaussin functions through the spectral features. The Gaussian functions of the individual features are added together and the combined function is plotted through the original spectrum. The upper portions of these figures show the plots of the residuals which are obtained by subtracting the combined Gaussian function from the spectrum.

The two possible features at -118.8 and 58.2 km/s on the COMP 3C396 spectrum are only about four times the RMS. Therefore, it was decided not to present Gaussian features fit to them.

The center velocity, half-power width, peak antenna temperature and integrated line power of each feature in the

Table IV-3

Parameters of the Spectra

Source	t_i [hours]	RMS Baseline Noise [°K][a]	Order of Baseline Removed	T_C' [°K]	Basic Spectra Figures[b] (Chapter IV)	Gaussian Fitting Components	Gaussian Fitting Figure (Chapter IV)
3C391	7.12	.0024	2	10.7	IV 2 A	2 3	IV 5 6
COMP 3C391	6.49	.0026	2	6.1	2 B	2 3	7 8
3C396	6.66	.0025	4	8.8	3 A	1	9
COMP 3C396	7.08	.0024	2	4.5	3 B	-	-
Pulsar 1858+03	7.10	.0024	2	3.7	4	2	10

[a] After smoothing with a 5-channel boxcar and averaging both receivers.

[b] The designation A refers to the upper portion of the figure, B to the lower portion.

spectra are listed in Table IV-4 which follows the spectra. Also listed for each parameter is its standard error (standard deviation of the mean) which, except for the standard error of the integrated line power, is computed by the Gaussian fitting routine. The standard deviation of the line power, s_p, is computed from the following equation (Parratt 1961, p. 117) with Equation II-35:

$$s_p = \left[\left(\frac{\partial P}{\partial T}\right)^2 s_T^2 + \left(\frac{\partial P}{\partial \Delta\nu}\right)^2 s_{\Delta\nu}^2\right]^{1/2}$$

$$= 1.0645 \left[(\Delta\nu)^2 s_T^2 + T^2 s_{\Delta\nu}^2\right]^{1/2}.$$

Here, s_T is the standard error of the peak line temperature and $s_{\Delta\nu}$ is the standard error of the line half-power width.

The discussion of the spectra will be a part of the analysis of the emitting region. Chapter V will present the analysis of the spectrum from the directions of 3C391 and its COMP beam. The model derived there will be applied to the analysis of the medium in the direction of 3C396, its COMP beam, and the pulsar 1858+03.

Figure IV-2. H157α Spectra from the Direction of 3C391 and Its COMP Beam. The velocity resolution is 11.6 km/s.

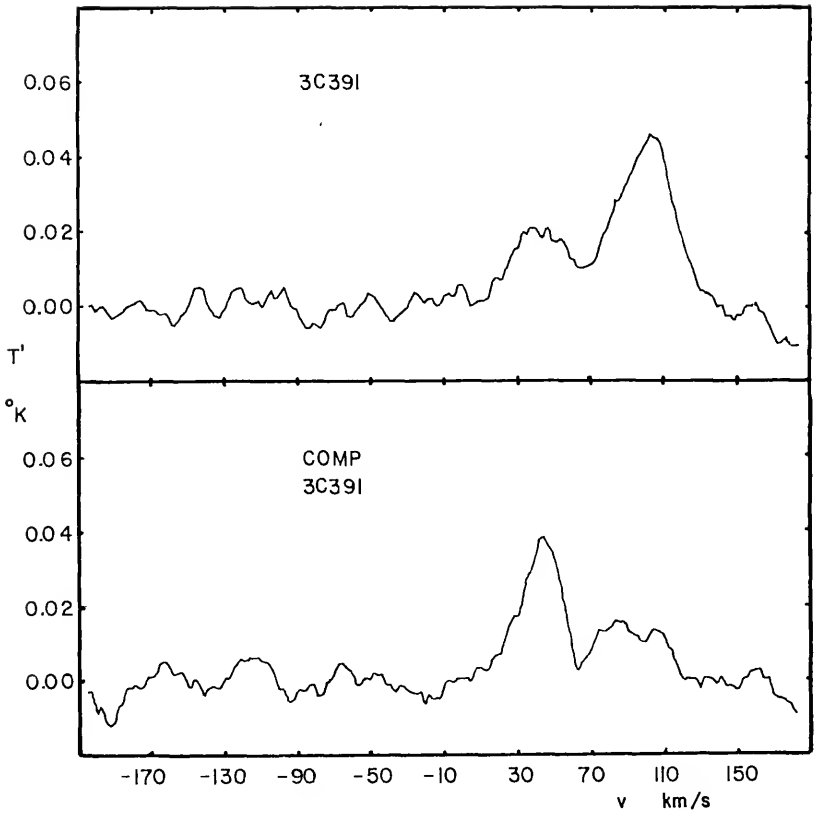
3C391
0.06
0.04
0.02
0.00
T'
°K
COMP
3C391
0.06
0.04
0.02
0.00
-170
-130
-90
-50
-10
30
70
110
150
v km/s

Figure IV-3. H157α Spectra from the Direction of 3C396 and Its COMP Beam. The velocity resolution is 11.6 km/s.

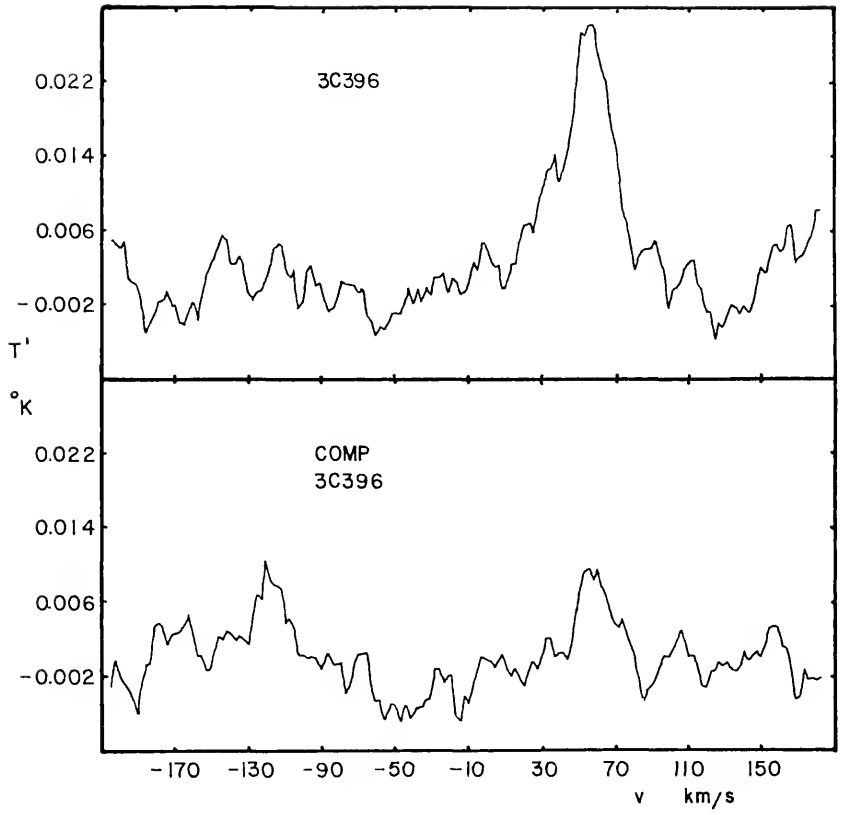
3C396
0.022
0.014
0.006
-0.002
T'
°K
COMP
3C396
0.022
0.014
0.006
-0.002
-170
-130
-90
-50
-10
30
70
110
150
v km/s

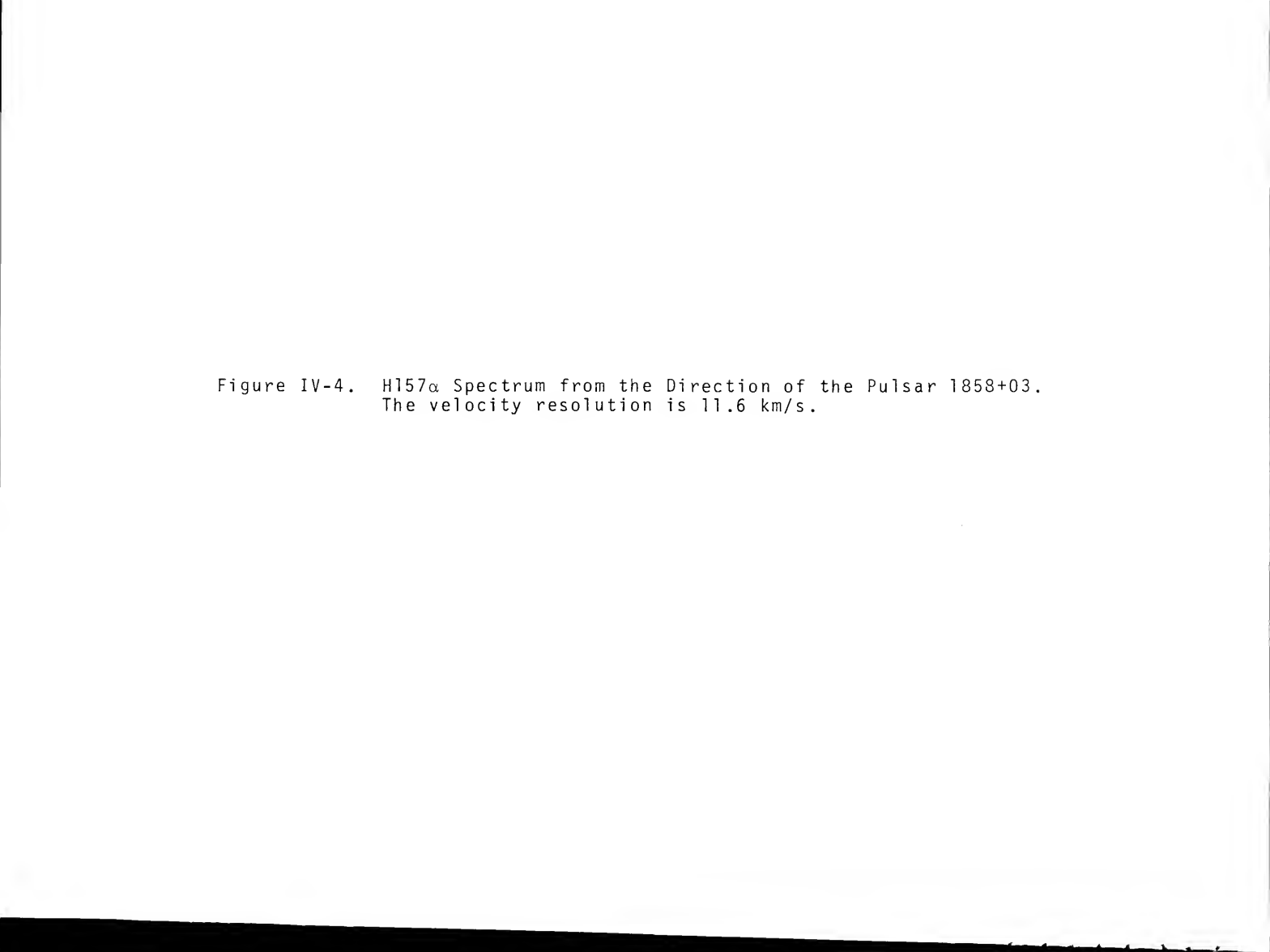

Figure IV-4. H157α Spectrum from the Direction of the Pulsar 1858+03. The velocity resolution is 11.6 km/s.

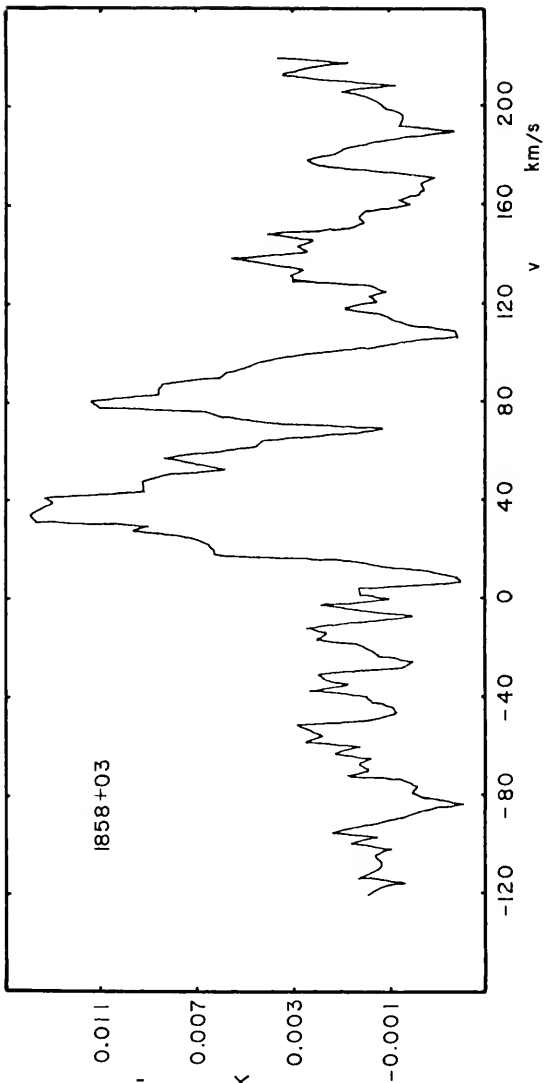
1858+03
0.011
0.007
0.003
-0.001
T'
°K
-120
-80
-40
0
40
80
120
160
200
v
km/s

Figure IV-5. Gaussian Profiles Fitted to the 3C391 Spectrum with a Single Gaussian Through the High-Velocity Feature. The lower curve is the fitted spectrum. The upper curve is that of the residuals.

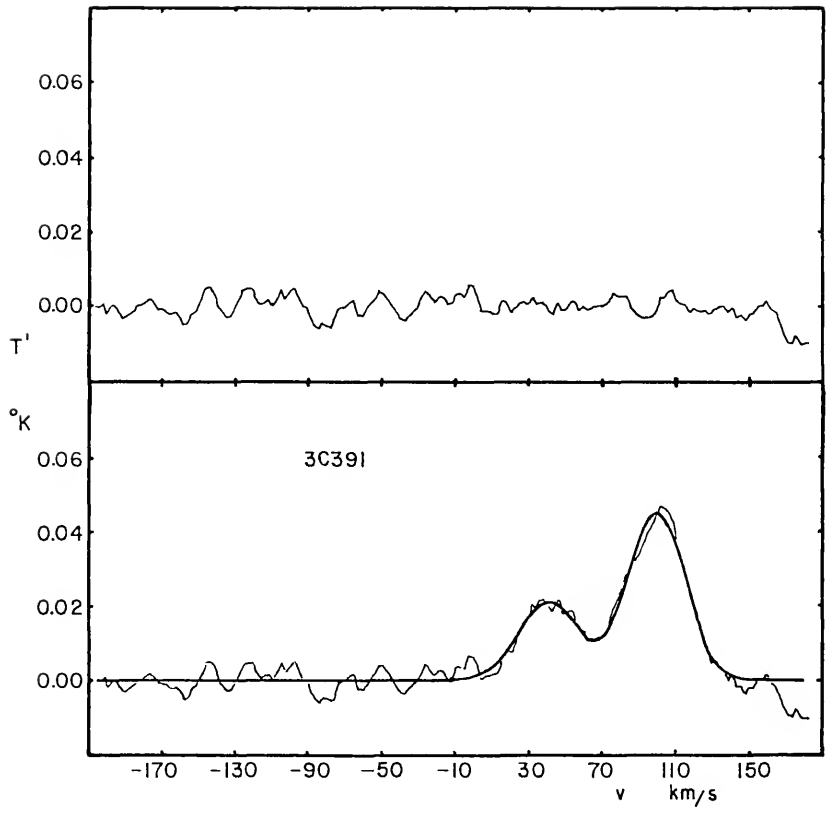
0.06
0.04
0.02
0.00
T'
°K
3C391
0.06
0.04
0.02
0.00
-170
-130
-90
-50
-10
30
70
110
150
v km/s

Figure IV-6. Gaussian Profiles Fitted to the 3C391 Spectrum with Two Gaussians Through the High-Velocity Feature. The lower curve is the fitted spectrum. The upper curve is that of the residuals.

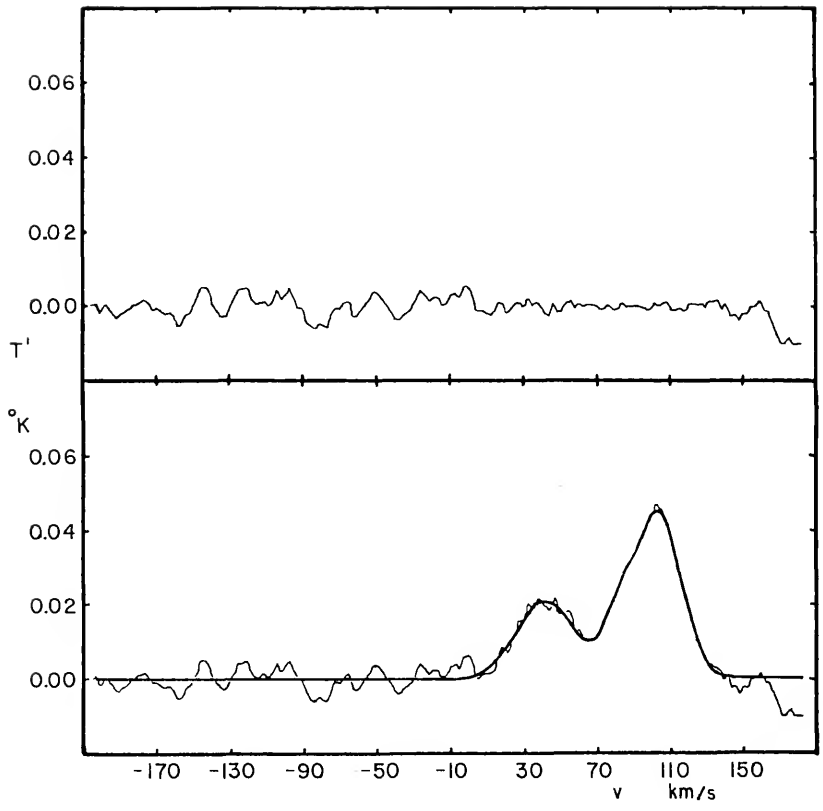
0.06
0.04
0.02
0.00
T'
°K
0.06
0.04
0.02
0.00
-170
-130
-90
-50
-10
30
70
110
150
v
km/s

Figure IV-7. Gaussian Profiles Fitted to the 3C391 COMP Spectrum with a Single Gaussian Through the High-Velocity Feature. The lower curve is the fitted spectrum. The lower curve is that of the residuals.

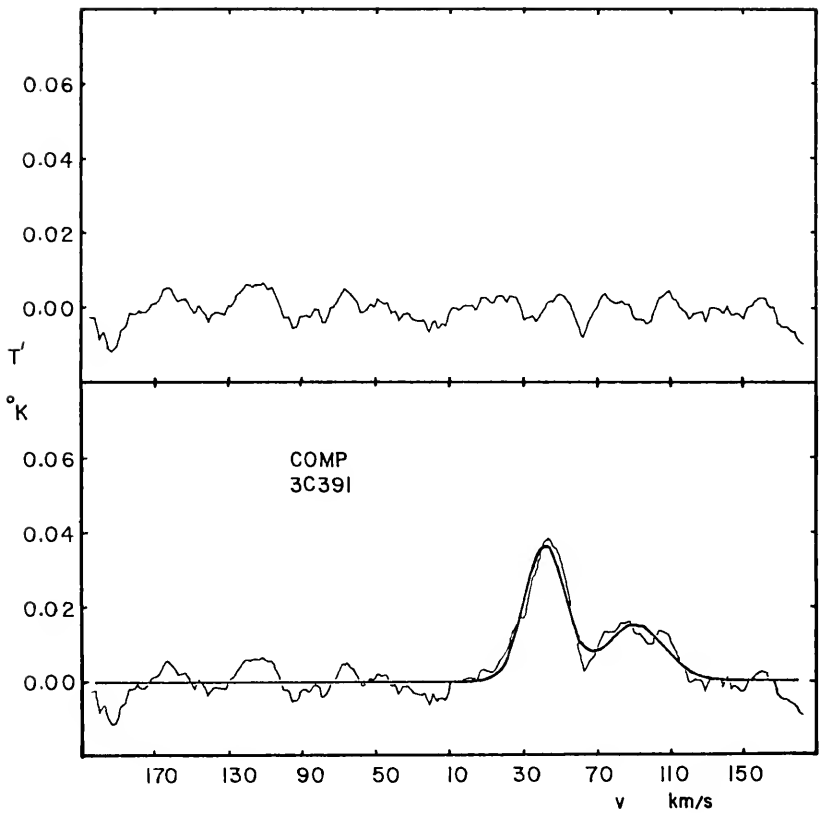
0.06
0.04
0.02
0.00
T'
°K
COMP
3C391
0.06
0.04
0.02
0.00
170
130
90
50
10
30
70
110
150
v km/s

Figure IV-8. Gaussian Profiles Fitted to the 3C391 COMP Spectrum with Two Gaussians Through the High-Velocity Feature. The lower curve is the fitted spectrum. The upper curve is that of the residuals.

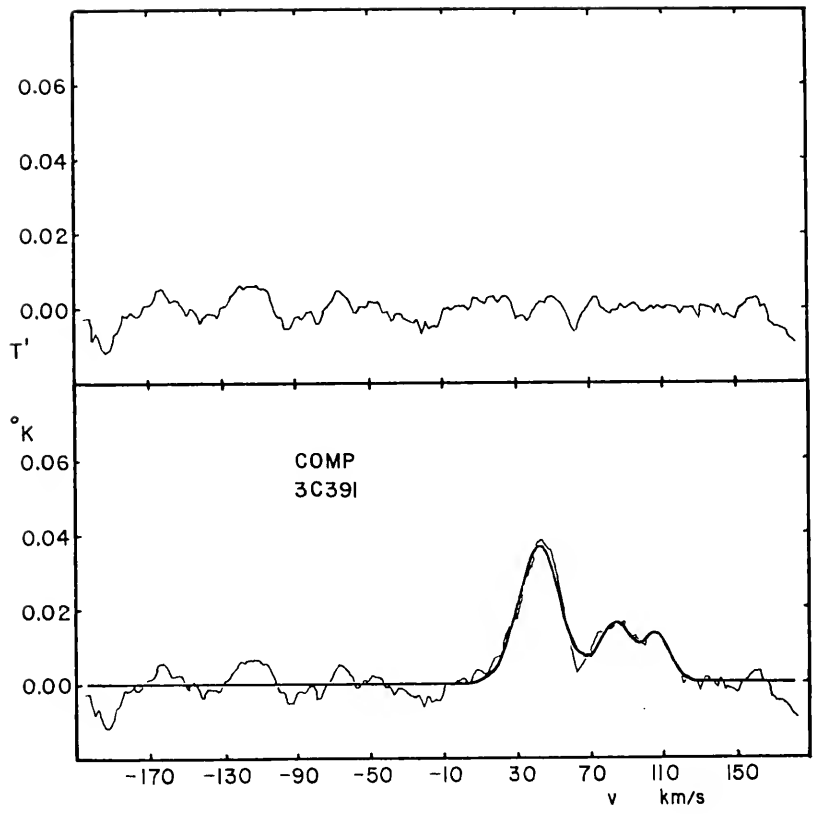
0.06
0.04
0.02
0.00
T'
°K
0.06
0.04
0.02
0.00
COMP
3C391
-170
-130
-90
-50
-10
30
70
110
150
v km/s

Figure IV-9. Gaussian Profiles Fitted to the 3C396 Spectrum. The lower curve is the fitted spectrum. The upper curve is that of the residuals.

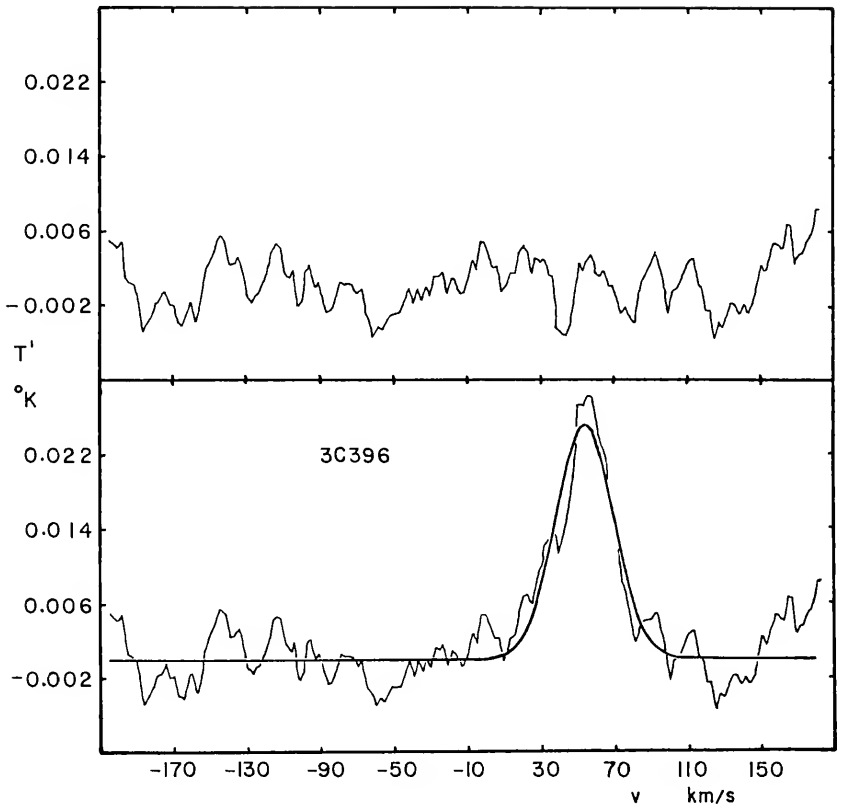
0.022
0.014
0.006
-0.002
T'
°K
3C396
0.022
0.014
0.006
-0.002
-170
-130
-90
-50
-10
30
70
110
150
v km/s

Figure IV-10. Two Gaussian Profiles Fitted to the Pulsar 1858+03 Spectrum. The lower curve is the fitted spectrum. The upper curve is that of the residuals.

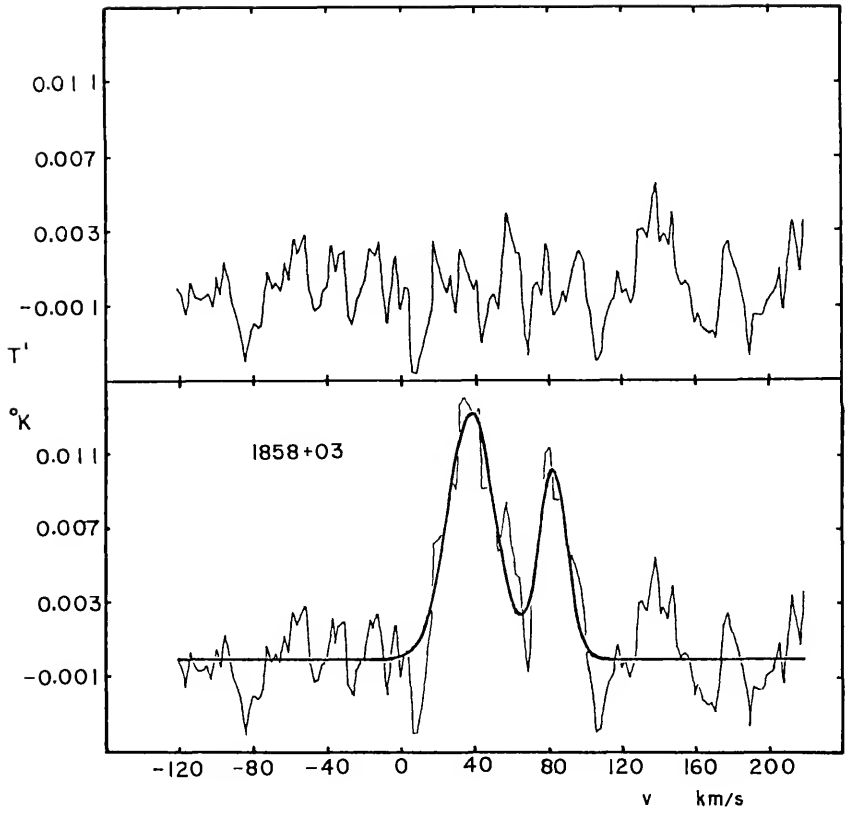
0.011
0.007
0.003
-0.001
T'
°K
1858+03
0.011
0.007
0.003
-0.001
-120
-80
-40
0
40
80
120
160
200
v km/s

Table IV-4
Parameters of the Spectral Features

v_c [km/s]	s_{vc} [km/s]	T_o' [°K]	$s_{T_o'}$ [°K]	$\Delta\nu$ [kHz]	$s_{\Delta\nu}$ [kHz]	P [°K kHz]	s_P [°K kHz]	Δv [km/s]	$s_{\Delta v}$ [km/s]
3C391									
41.86	0.69	0.021	0.0007	217.838	9.987	4.870	0.276	38.799	1.779
99.82	0.31	0.045	0.0007	200.611	4.372	9.610	0.257	35.729	0.779
41.90	0.52	0.021	0.0005	213.684	7.742	4.777	0.207	38.057	1.379
80.66	1.11	0.014	0.0022	103.398	12.874	1.540	0.309	18.415	2.293
COMP 3C391									
41.82	0.48	0.037	0.0012	146.237	6.486	5.756	0.316	26.045	1.155
90.47	1.35	0.015	0.0011	210.976	19.609	3.369	0.399	37.575	3.489
42.20	0.38	0.037	0.0010	149.427	5.383	5.885	0.265	26.613	0.959
83.39	1.26	0.016	0.0012	120.573	18.409	2.053	0.349	21.474	3.279
105.99	1.39	0.013	0.0015	87.317	16.219	1.208	0.264	15.551	2.888
3C396									
53.94	0.70	0.025	0.0010	203.398	9.185	5.413	0.326	36.225	1.636

Table IV-4 - continued

v_c [km/s]	s_{vc} [km/s]	T_o' [°K]	$s_{T_o'}$ [°K]	$\Delta\nu$ [kHz]	$s_{\Delta\nu}$ [kHz]	P [°K kHz]	s_P [°K kHz]	$\Delta\nu$ [km/s]	$s_{\Delta\nu}$ [km/s]
Pulsar 1858+03									
38.08	0.98	0.013	0.0009	169.363	13.420	2.344	0.247	30.165	2.390
82.48	1.00	0.010	0.0011	105.065	13.511	1.118	0.189	18.713	2.406

CHAPTER V

MODELS FOR THE INTERSTELLAR MEDIUM IN THE DIRECTION OF 3C391

3C391: A Summary of Previous Observations

The radio source 3C391 has the nonthermal spectrum of a supernova remnant (SNR). Caswell *et al.* (1971) give its spectral index between 750 MHz and 5 GHz to be -0.57. However, there is a turnover of the spectrum and the spectral index between 80 and 408 MHz is about 0.13. Low frequency optical depths derived from radio recombination lines and also the continuum spectrum itself strongly indicate that the low frequency decrease in the flux is due to absorption by the interstellar gas rather than due to a process within the SNR itself (Bridle and Kesteven, 1971; Gordon, 1972; Dulk and Slee, 1972).

Assuming that the absorption is due to the interstellar gas, the optical depth at 80 MHz may be determined by assuming that the flux from the SNR follows a power law in the frequency range between 80 MHz and 5 GHz. The spectral index is constant over this range and was found to be -0.50 using the fluxes measured at 408 MHz 5 GHz. The observed flux at 80 MHz, S(80) was compared to that expected

from the power law, $S_o(80)$. For 3C391,

$$\tau(80) = \ln \frac{S_o(80)}{S(80)} = 0.84\ (\pm 0.3).$$

The antenna beamwidth used was ($\alpha x \delta$) = 3.7 x 4.8 arc minutes which is the size of the angle subtended by 3C391.

Caswell et al. (1971) compute this optical depth to be 1.3 assuming a spectral index of -0.57 between 80 MHz and 5 GHz. Goss (1972) makes use of the H109α recombination line power and the 5 GHz brightness temperature computed by Jackson and Kerr (1971) to compute $\tau(80)$ for the direction $l = 31\overset{\circ}{.}2$, $b = 0°$. This position is $0\overset{\circ}{.}7$ away from 3C391, but the optical depth was assumed to be valid for the direction of 3C391. For an electron temperature range of 10^2 to 10^4, Goss finds that $\tau(80)$ is close to one.

From the observations tabulated by Caswell et al. (1971) it is evident that the size of 3C391 does not change appreciably with frequency. Their Mills Cross observations at 408 MHz give its size as ($\alpha x \delta$) = 3.2 x 3.4 arc minutes. Their drift scan map shows the source to be "an intense compact feature within a weaker more extended structure." Their angular resolution is ($\alpha x \delta$) = 2.06 x 3.47 arc minutes. Bridle and Kesteven (1971) detect the same

structure with a 10.63 GHz map. Goss (1972) determined the size at 31.4 GHz to be 3.2 arc minutes in diameter; his resolution was 2.8 arc minutes. A map made by Chaisson (1974a) at 15.5 GHz with a resolution of 2.1 arc minutes shows an arc of structure which is generally surrounded by the lowest intensity isophote of the 10.63 GHz map of Bridle and Kesteven (1971) which they claim to be of low reliability.

The distance to 3C391 can be estimated by two methods, from an empirical relation between radio surface brightness and from 21 cm absorption profiles. The 21 cm absorption profile obtained by Radhakrishnan et al. (1972) (shown in Figure V-1) has an absorption peak with a radial velocity of 107 km/s with respect to the local standard of rest (LSR). This is only slightly higher than the maximum velocity of 105 km/s predicted by the Schmidt rotation model for the galaxy (Schmidt, 1965) and observed by Burton (1970) at a galactic longitude of 31°.9. Assuming pure circular galactic rotation of the gas, the maximum velocity corresponds to emission from the tangent point where the line of sight at 31°.9 intersects the 5.3 kpc (radius) orbit. Also, it is assumed that the sun is 10 kpc from the galactic center. The distance from the sun to this point is 8.5 kpc. Since the 21 cm line is seen in absorption against the SNR at this velocity, it can be concluded that the SNR

lies no nearer than 8.5 kpc. Because of the distance ambiguity of the radial velocity-distance relation (cf. Mihalas and Routly, 1968, p. 126), it cannot be determined with certainty whether the other absorption features lie in front of the tangent point or behind it. Therefore, all that can be said is that the distance to 3C391 is greater than 8.5 kpc and may be as close as 13.4 kpc. Ilovaisky and Lequeux (1972) derive a distance-luminosity function for galactic supernova remnants. They use 3C391 as a calibrator for which the distance was assumed to be 11 ± 2 kpc.

There is considerable disagreement as to the nature of the interstellar medium in the direction of 3C391. The intent of this study is to provide another data point which can be used with previous studies to generate a consistent model. Of particular interest are the recombination line observations of Cesarsky and Cesarsky (1973a,b) who observed wide ($\sim$30 km/s) H92α, H157α, and H166α lines in the direction of 3C391. Using their H92α line and τ(80) measured by Dulk and Slee (1972), they employ a unique technique to derive an electron temperature of 20°K with the gas in non-LTE. Chaisson (1974a) takes issue with this solution and presents an argument in support of the low frequency absorption resulting mainly from an H II region imbedded in the two-phase medium and the remaining absorption from the partially ionized cool component of the medium.

The wide recombination lines are indicative of thermal broadening of a hot emitter. For that reason Chaisson suggests that the recombination lines are emitted by the H II regions from which most of the absorption results. Downes and Wilson (1974) also conclude that the line emission can come from H II regions rather than from H I regions. The structure seen in Chaisson's map could possibly be evidence for there being one or more H II regions in the intervening medium. However, it is not certain that the arc of sources which surrounds the east, south, and west of 3C391 exist in the medium. Since they are included within an isophote of Bridle and Kesteven's (1971) map, the sources form a structure within 3C391 itself. Also, both Chaisson (1974a) and Bridle and Kesteven (1971) find an increase in the continuum flux at high frequencies above 10 GHz over that expected from the spectral index at lower frequencies. This excess flux, they suggest, could be due to at least one H II region imbedded in the intervening medium. Goss (1972) does not, however, see any evidence for an excess at 31.4 GHz and suggests that the low frequency absorption and radio recombination lines are both due to a diffuse medium with a temperature ranging from 10^2 to 10^4 °K.

Figure V-1 shows the 21 cm absorption and emission spectra obtained by Radhakrishnan et al. (1972) placed

Figure V-1. Comparison of This Study's 3C391 Spectrum with 21 cm Spectra. The 21 cm spectra are obtained from Radhakrishnan, *et al.* (1972). The bar —C— indicates the range where carbon lines would appear if they are related to the hydrogen features. The location of CO features observed by Dickel and Dickel (1974) are indicated with arrows.

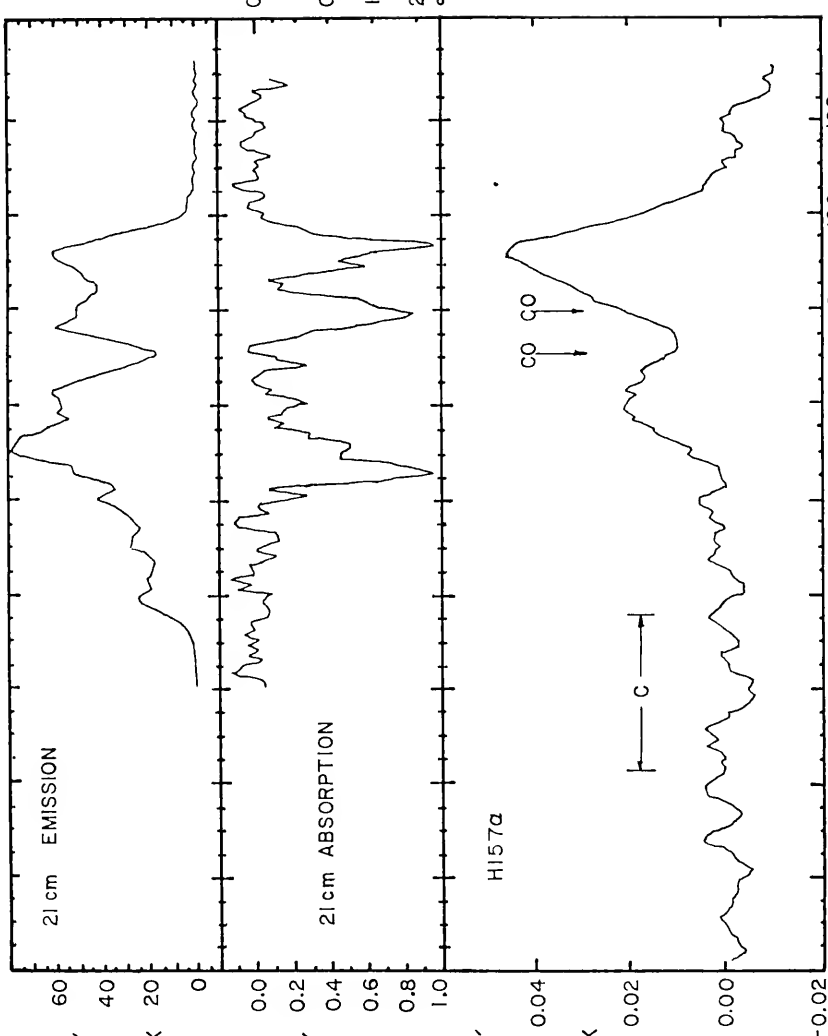
21 cm EMISSION
T'
°K
60
40
20
0
21 cm ABSORPTION
RELATIVE INTENSITY
0.0
0.2
0.4
0.6
0.8
1.0
OPTICAL DEPTH
0.0
0.5
1.0
2.0
∞
H157α
T'
°K
0.04
0.02
0.00
-0.02
CO
CO
C
-160
-120
-80
-40
0
40
80
120
160
v km/s

above this study's H157α spectrum. Figure V-2 shows the recombination line spectra which the Cesarskys (1973a,b) observe placed above that of this study's. The Cesarskys' H147α and H166α spectra show a possible feature at a velocity of -45 km/s which they suggest may be real and may be the C157α line. The velocities in both figures are with respect to the local standard of rest. On this study's spectrum, the horizontal bar labeled with a C indicates the range of velocities in which the C157α line would be if observed, assuming that it is colocated with one or more of the hydrogen line emission regions. The vertical arrows labeled with CO indicate where the CO features, seen by the Dickels (1974), are located.

Downes and Wilson (1974) looked for but did not detect H134α and C134α recombination lines. Their signal-to-noise ratio is such that the H134α peak temperature is less than 0.02 °K and that of the C134α is less than 0.03 °K. Since $T_L \propto 1/n$, these limits are close to the expected H134α peak temperature and probably above the expected C134α peak temperature.

The work which has been discussed is summarized in Table V-1. The conclusion which one might draw from this discussion is that there are three possible models of the interstellar medium—at least in the direction of 3C391—which must be considered: a group of cold, partially ionized H I regions, one or more H II nebulae, or an

Figure V-2. Comparison of Radio Recombination Line Spectra from the Direction of 3C391. The upper two spectra, H166α and H157α, are from Cesarsky and Cesarsky (1973a). The H92α spectrum is from Cesarsky and Cesarsky (1973b). The bottom spectrum is the H157α spectrum of the present study. All velocities are with respect to the local standard of rest.

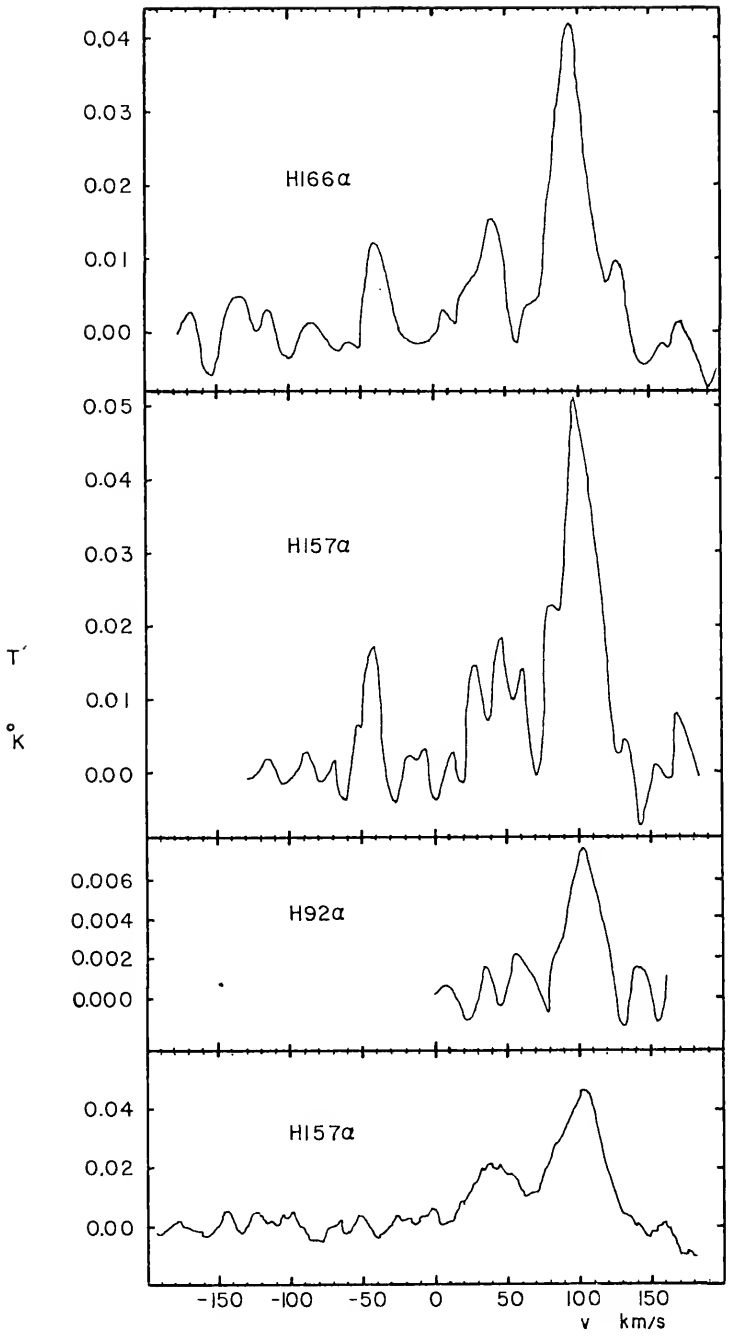
0.04
0.03
0.02
0.01
0.00
H166α
0.05
0.04
0.03
0.02
0.01
0.00
H157α
T'
°K
0.006
0.004
0.002
0.000
H92α
0.04
0.02
0.00
H157α
-150
-100
-50
0
50
100
150
v km/s

Table V-1

Summary of Observations in the Direction of 3C391

Reference	Type of Observation	Antenna Resolution ($\alpha x \delta$)	Results
Caswell *et al.* (1971)	Continuum 408 MHz	2!06x3!47	Derived spectral index of -0.57 and $\tau(80) = 1.3$
Bridle and Kesteven (1971)	Continuum 6.63 & 10.63 MHz	?	Flux excess at 10.63 GHz due to an H II region along the line-of-sight.
	21 cm emission & abs.	11'	
Gordon (1972)	----	----	From other observations concluded that low frequency absorption is from interstellar gas rather than SNR itself.
Dulk and Slee (1972)	Continuum 80 MHz	3!7x4!8	$\tau(80) = 0.84(\pm 0.3)$ which arises from low density H II region.
Goss (1972)	Continuum 31.4 GHz	2!8	No flux excess at 31.4 GHz.
Ilovaisky and Lequeux (1972)	----	----	Derived distance luminosity function for SNR's. Used distance to 3C391 of 11±2 kpc.

Table V-1 (continued)

Reference	Type of Observation	Antenna Resolution ($\alpha \times \delta$)	Results
Hughes, Thompson, and Colvin (1972)	21 cm emission & abs.	?	Survey of 21 cm spectra
Radhakrishnan et al. (1972)	21 cm emission & abs.	$\sim$6'	Survey of 21 cm spectra
Cesarsky and Cesarsky (1973a)	H157α and H166α	?	Observed possible C157α and C166α features
Cesarsky and Cesarsky (1973b)	H92α	2'.3	Concluded that emission is from cold ($\sim$20 °K) regions
Chaisson (1974a)	Continuum 15.5 GHz	2'.1	Flux excess at 15.5 GHz. Suggests that recombination lines are emitted by low density H II region.
Downes and Wilson (1974)	H134α and C134α	4'.8	Did not detect H134α or C134α from 3C391
Jackson and Kerr (1971, 1975)	H110α	6'	Emission from low density H II. (Beam was 7' from 3C391)
Pankonin (1975)	H248α	11'	Emission from low density H II region.

extended diffuse H II region. The remainder of this chapter will discuss this study's observations in terms of parameters consistent with these models.

The Models

The D-Method Models

This is the method used by the Cesarskys (1973b) in obtaining a model from their H92α recombination line spectrum. They began by assuming a transfer equation solution suitable for an H I region observed in front of a strong continuum source. From Equation II-43, which assumes that τ_L and $\tau_T << 1$, the line temperature is

$$T_L(\nu) = \tau_L^*(\nu)\ (b_m T_e - b_n \beta_{mn} T_R).$$

The radiation temperature is the sum of several terms:

$$T_R = T_T + T_N + T_{SNR} + 2.7.$$

T_{SNR} is the radiation temperature of 3C391 as experienced by the line-emitting region and T_T and T_R are the respective temperatures of the thermal and nonthermal ambient radiation fields excluding that of 3C391. The 2.7 °K term represents the universal thermal background radiation. The line power emitted along a unit pathlength, Δs, is

$$\Delta P(\nu) = \kappa_L^* (b_m T_e - b_n \beta_{nm} T_R) \Delta s. \qquad V\text{-}1$$

The line absorption coefficient (Equation II-34) is

$$\kappa^* = \int_{\text{Line}} \kappa^*(\nu) d\nu = \int_{\text{Line}} 1.071 \times 10^7 \phi(\nu) \frac{\Delta n}{n} f_{nm} T_e^{-2.5} \exp(\epsilon_n/kT) N_i N_e d\nu,$$

where N_i is the number density of the recombining ion (hydrogen). The thermal continuum absorption coefficient at 80 MHz along Δs is found by combining Equations II-7 with the defintion of optical depth;

$$\Delta\tau(80) = 4.710 T_e^{-1.5} \ln(0.6194\ T_e^{1.5}) \langle N_e \textstyle\sum_j Z_j^2\ N_j \rangle \Delta s. \qquad V\text{-}2$$

Dividing Equations II-28 and V-1 by $\tau(80)$ and $\Delta\tau(80)$ respectively provides two functions, D and D_o, defined as follows:

$$D_o \equiv \frac{\eta_B P_L}{\tau_T(80)} \quad ;$$

so,

$$D_o = 2.274 \times 10^4 \eta_B \frac{\Delta n}{n} f_{mn} \frac{(b_m T_e - b_n \beta_{mn} T_R) \exp(\epsilon_n/kT)}{\ln(0.6194\ T_e^{1.5})} \cdot \frac{E_L}{E_T} \qquad V\text{-}3$$

and

$$D \equiv \frac{\eta_B \Delta P_L}{\Delta\tau(80)} \quad ;$$

so,

$$D = 2.274\times10^4 \, \eta_B \, \frac{\Delta n}{n} \, f_{nm} \, \frac{(b_m T_e - b_n \beta_{mn} T_R) \exp(\varepsilon_n/kT)}{\ln(0.6194\, T_e^{1.5})} \cdot \frac{\langle N_e N_H \rangle \Delta s_L}{\langle N_e \Sigma_j Z_j^2 N_j \rangle \Delta s_T} \quad .V\text{-}4$$

The antenna main beam efficiency, η_B, is the ratio of main beam solid angle to total antenna solid angle (Kraus, 1966, p. 73). Neglecting the contribution of carbon to the electron pool, the Cesarskys use

$$\sum_j Z_j^2 \, N_j = H_{H+} + N_{He+} = 1.1 \, N_{H+} \quad ;$$

so, $E_T = 1.1\, E_L$ if the absorption and line emission media are colocated and their respective path lengths, L_T and L_L, are equal. If C^+ is present, the abundance is $N_C \simeq N_{C+} \simeq 4\times10^{-4}\, N_H$ (Spitzer, 1968, p. 122). Then $\Sigma Z_j^2\, N_j = 1.1 N_H$ is a good approximation only if the fractional ionization, $x \equiv N_e/N_H$, is high. N_H is the total hydrogen density; $N_H = N_{Ho} + N_{H+}$.

This technique computes D for models specified by choices of T_R, N_e, and T_e. For each model, curves of $D(T_e)$ for specific values of N_e and T_R will be computed and compared to the observed quantity, D_o, in such a way that

N_e and T_e can be specified. The estimate of T_R will remain the same for all models. There are two problems, however. First, there is one "known," D_o, and three "unknowns," T_R, N_e, and T_e. This is complicated by the fact that b_n and β_{mn} are functions of these variables and, particularly at low temperatures (T_e<100 °K), this functional relationship is not well known. There is controversy regarding the bound-bound collision cross-sections at these temperatures which correspond to kinetic energies near the reaction threshold (Percival and Seaton, 1972; Dupree, 1972b). N_e is not completely eliminated in Equation V-4 since b_n and β_{mn} are nonanalytic functions of it.

The second problem involves the relation between D_o and D. D_o is a ratio of integrated quantities; D is a ratio of differentials. The Cesarskys (1975b) show that, for the H92α line, two extreme conditions provide limits for D. D(H92α) will be largest for an LTE solution for which $T_e \simeq 20$ °K. Since for this case $b_n=\beta_{mn}=1$, N_e does not have to be specified and does not enter into the solution. The conditions for which D will be a minimum are a non-LTE situation where $T_e \simeq 10$ °K and $N_e<10^{-3}$ cm^{-3}. At these electron densities collisions need not be considered and the departure parameters are better known. These conditions dictate that $6<D_o(H92\alpha)<60$ °K kHz.

The Cesarskys' spectral line gives D_o=6.8 °K kHz from which they conclude that the most probable temperature of the emitter is 20 °K with a possible range of temperature of $0<T_e<1000$ °K due to the observational error of 70 percent. Substitution of T_e=20 °K into Equation II-51 gives $E_L=<N_e\ N_{H+}>L=4$ pc cm^{-6}.

There is another matter which should be considered. In a two-phase medium, the line emission from each phase must be considered. In an earlier paper, the Cesarskys (1971) showed that for a two-phase medium like those proposed by Field, Goldsmith, and Habing (1969) and Hjellming, Gordon, and Gordon (1969), the line emission will come predominantly from the cold regions. The fraction of the line power from the hot region increases as T_e decreases because $T_L \propto T_e^{-2.5}\ N_e^2$. However, emission from the hot component will generate a weak and wide ($\sim$80 km/s) line because of the temperature dependence and the fact that this gas is widely distributed so that there is line broadening resulting from differential galactic rotation along the line of sight. Consequently the hot region spectral feature will be difficult to identify because it will be immersed in the baseline noise or be hidden by one or more features from the cool regions. For these reasons, the Cesarskys (1975b) consider emission only from a cool region.

It should be noted that the antenna beam used to obtain this study's spectra is 18 arc minutes in diameter which is considerably larger than Cesarskys' beam (2.3 arc minutes) and 3C391 (3.5 arc minutes). It will be assumed that $\tau(80)$ is constant within the 18 arc minute beam and, therefore, the D-method can be used for this study. The comparison of the high-velocity features of the 3C391 and its COMP spectra (Figure IV-2) shows a variation of line power by a factor of 2.9 over a distance of 17 arc minutes. The 42 km/s feature varies oppositely by a factor of 1.2 and is not seen in the H92α beam which is 2.3 arc minutes wide.

Since a high-velocity feature appears on both the 3C391 and its COMP beams, it seems to originate from an extended region. Using this feature only, a solution consistent with the H92α observations may be possible using the D-method. However, considering that the solution is expected to yield a low temperature, it is relevant to consider the 21 cm high-velocity absorption features. There are two prominent features, one at about 80 km/s and another at 107 km/s. This raises the question as to whether the H157α high-velocity feature is single, centered on 99.82 km/s and having a half-power width of 35.7 km/s or is double with components at 80.66 km/s (Δv = 18.4 km/s) and 102.8 km/s (Δv = 29.2 km/s). It is not certain whether or

not this feature is double on the H92α spectrum. There may be a component at about 80 km/s, but its peak is no more than two times the RMS noise. The Cesarskys' (1973a) H166α and H157α spectra show some structure other than the 103 km/s feature which has an intensity roughly three times the RMS. Taking each spectrum by itself, it is not clear that there should be a feature around 80 km/s. Taken together, the spectra indicate a strong possibility of there being a feature there.

To see what effect the choice of situation has on the solution, both possibilities will be considered. Assuming that the feature is single and using $\tau(80)$ from Dulk and Slee (1972),

$$D_o(H157\alpha) = \frac{9.61\ (\pm 0.26)}{0.84\ (\pm 0.3)} = 11.44\ (\pm 2.89)\ ^\circ K\ kHz.$$

Taking only the 103 km/s feature if a double feature exists,

$$D_o(H157\alpha) = \frac{7.87\ (\pm 0.19)}{0.84\ (\pm 0.3)} = 9.37\ (\pm 2.37)\ ^\circ K\ kHz.$$

Assuming that the uncertainty quoted for $\tau(80)$ is one standard deviation, the standard deviation of D_o is computed by

$$s_D = \left[P^2 \, s_\tau^2 + \tau(80)^2 \quad s_P^2 \right]^{1/2}$$

(Parratt, 1961, p. 117).

For the H157α line, Equation V-4 becomes

$$D = \frac{3.83 \times 10^5 \, (b_m T_e - b_n \beta_{mn} T_R) \exp(6.4059/T_e)}{T_e \ln (0.6194 \, T_e^{1.5})} \cdot \frac{E_L}{E_T} \quad . \qquad \text{V-5}$$

T_e and T_R are brightness temperatures. D and D_o are in terms of antenna temperature; therefore, the constant multiplier in Equation V-5 contains the factor $\eta_B = 0.8$, the beam efficiency of the 43-meter NRAO telescope at the H157α frequency (Gottesman and Gordon, 1971).

T_R may be computed from the transfer equation solved for the situation shown in Figure V-3. If the gas between 3C391 and the line emitter has a kinetic temperature T_e and continuum optical depth τ_T, then

$$T_R = T_e \, (1 - e^{-\tau} T) + W \, T_{SNR} + T_N + 2.7 \, . \qquad \text{V-6}$$

The dilution factor, W, is given by

$$W = A(\nu) \, \frac{1}{4\pi} \, \frac{\pi}{4} \, \frac{d_s^2}{R_R^2} \exp(-\tau_T) \qquad \text{V-7}$$

(cf. Equation II-46).

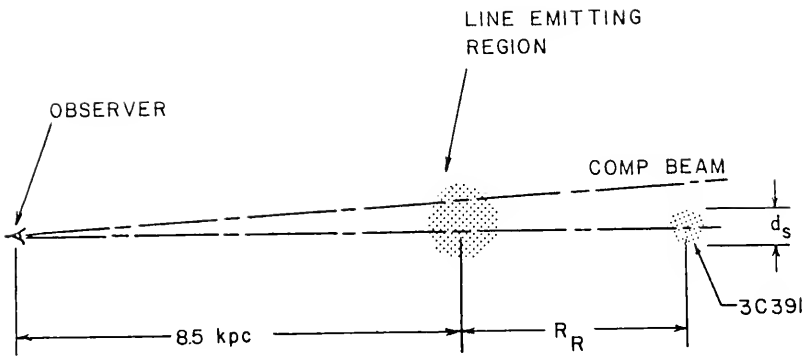

Figure V-3. Geometry for Determining T_R. This is a schematic drawing and is not to scale.

Ilovaisky and Lequeux (1972) determine the diameter of 3C391 to be 11 pc. For this discussion, it can be assumed that $T_{SNR} = 10^4$ °k and the gas between 3C391 and the line emitter has the characteristics of the intercloud medium of the Field, Goldsmith, and Habing (1969) two-phase model; then, $T_e = 7500$ °K and $N_e = 0.012$ cm^{-3}. Also it will be assumed that $N_e = N_{H+}$, $E_T = 1.1<N_e^2>R_R = 1.6\times10^{-4}\ R_R$. Since 3C391 is between 8.5 and 13.4 kpc from the sun (Caswell et al., 1971), the range on R_R is $0<R_R<4.9$ kpc.

W can be calculated directly from a flux measurement. The flux, S_S, measured at 1667 MHz is 16.4 (±1.5) Jy (Caswell et al., 1971). The COMP beam is in the ridge; so, subtracting its observed continuum temperature from that observed in the 3C391 beam should provide a good approximation to the radiation temperature of 3C391 itself. From Table IV-3, T_C'(3C391) = 10.7 °K and T_C'(COMP) = 6.1 °k. Their difference is 4.6 °K.

The flux measurements give

$$T_C' = \eta_B \frac{\Omega_S}{\Omega_M} \frac{c^2}{2k\nu^2} \cdot \frac{S_S}{\Omega_S} = 5.7\ °K,$$

where Ω_M and Ω_S are the respective solid angles of the antenna main beam and 3C391 as seen at the telescope. Therefore the flux at 1667 MHz provides a reasonable estimate of WT_{SNR} at 1683 MHz.

At the line emitter 3C391 subtends a solid angle of $\Omega_\star$ which is equal to $\pi d_S^2/4\ R_R^2$. Then

$$WT_{SNR} = \frac{c^2}{2k\nu^2} \frac{S_S}{\Omega_S} \frac{\Omega_\star}{4\pi} .$$

The following table shows that $T_R \approx T_N + 2.7$ except when the line emitter is adjacent to the SNR. The optical depth is computed from Equation II-8. Since the optical depth is so small, T_R is not attenuated and is equal to the observed

Table V-2

Calculation of Radiation Temperature

R_R [pc]	E_T [pc cm^{-6}]	τ_T	$W\ T_{SNR}$ [°K]	$T_R - T_N$ [°K]
5.5	0.009	2.9×10^{-10}	60	17.7
550	0.088	1.4×10^{-8}	6×10^{-3}	2.7

continuum brightness temperature and Equation V-6 reduces to

$$T_R = T_N + 2.7 = T_C. \qquad \text{V-8}$$

Then for 3C391, $T_R = 10.7/\eta_B = 13.4$ °K. This makes the thermal component 20 percent of the total continuum if only the 2.7 °K background is present. This is midway between the percentages computed by Gottesman and Gordon (1970) who argue for 10 percent and Matthews, Pedlar, and Davies (1973) who obtain 30 percent.

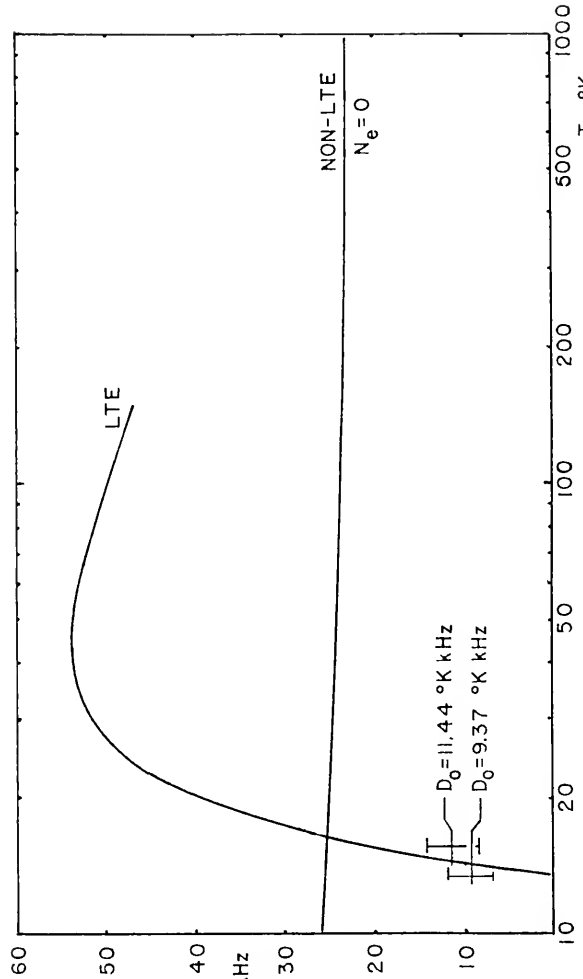

Figure V-4. D Plotted as a Function of Electron Temperature. T_R = 13.4°K. The solutions for D_0 = 11.44 (±2.89)°K kHz are shown with error bars.

Figure V-4 shows the plot of Equation V-5 with all of the parameters which have been drived in the discussion. Two extreme cases are plotted. The solid curve is the LTE function for which $b_n = b_m = \beta_{mn} = 1$. The dashed curve is the collisionless non-LTE case where $N_e \lesssim 10^{-4}$ cm^{-3}. The non-LTE departure parameters were computed by Dupree (1972). Their values are listed in Table V-3.

Table V-3

Non-LTE Departure Parameters with $N_e < 10^{-4}$
[from Dupree (1972)]

T_e [°K]	b_m	$b_n\beta_{mn}$
10	0.0583	-0.0438
20	0.1150	-0.1442
100	0.2720	-1.0414
1000	0.5350	-8.7328

The values of D_o, 9.37±2.37 and 11.44±2.89, are indicated on the plot by labeled horizontal lines with error bars. Considering both values of D_o, it is seen that the solution is an LTE gas with a temperature of 14.3±0.3 °K.

The solution disagrees markedly in one respect from that of the Cesarskys' (1973b) which is a non-LTE solution with a most-probable temperature of 20 °K. To obtain this solution for this study's spectrum, D_o would have to be 25.3 °K kHz, a value well outside of the error quoted. The value of D_o (H157α) which the Cesarskys predict is about 25 °K kHz.

If $\tau(80) = 1.3$, as derived by Caswell et al. (1971), the H157α solution would be closer to T_R, but the H92α solution would yield a temperature of less than 10 °K. This is evident from Cesarskys' (1973b) Figure 3. Recent unpublished observations suggest that $\tau(80)$ may be close to 0.4 (Chaisson, 1974b). If this is the correct value, D_o(H157α) will be about 24.2 °K kHz which will give a non-LTE solution with a temperature of about 60 °K if P is 7.87 °K kHz and an indeterminate solution if P is 9.61 °K kHz. However, with $\tau(80) = 0.4$, D_o(H92α) will be 14.2 °K kHz giving a non-LTE solution with a temperature of about 1000 °K.

Even though the surrounding hot medium will generate a wide, shallow line, it is necessary to determine what effect this component will have on the solution. For this purpose, Equation V-5 can be modified to

$$D = \frac{\Delta P(c) + \Delta P(h)}{\Delta\tau(80, c) + \Delta\tau(80, h)} , \qquad V\text{-}9$$

where, letting x equal to c for the cold component and h for the hot component,

$$\Delta P(x) = 1.84 \times 10^6 \, T_x^{-2.5} \exp(6.4049/T_x) \cdot (b_m T_x - b_n \beta_{mn} T_R) \Delta E_{Lx}$$

and

$$\Delta\tau(80,x) = 4.710 \, T_x^{-1.5} \ln(0.6194 \, T_x^{1.5}) \Delta E_{Tx}.$$

Because of the different number densities in, and vastly different path lengths through, the two regions, it cannot be assumed that their emission measures will be equal. Therefore, they will not cancel and at least two more variables are added to the solution.

To solve equation V-9, four combinations of emission measures will be chosen. For each combination $E_T = 1.1\ E_L$ for both components. The cold region non-LTE departure parameters are those computed by Dupree (1972) and listed in Table V-3. For the surrounding hot region, T_e will be 7500 °K and N_e is assumed to be near 0.01 cm^{-3} for the purpose of computing the departure parameters. The values of T_e and N_e correspond to those of the stable, hot phase of the two-phase model of Field, Goldsmith, and Habing (1969). Also, $N_e = 0.01\ cm^{-3}$ is analogous to the collisionless case for which Dupree (1972) computed the "$N_e = 0$" parameters. Sejnowski and Hjellming (1969) have computed departure parameters for $T_e = 7500$ °K, but in order to obtain them for $N_e = 0.01\ cm^{-3}$, they must be estimated by extrapolating the radiative asymptote through n = 157 (cf. Figure II-5). With this extrapolation, the departure parameters for the non-LTE hot medium are $b_m = 0.75$ and $\delta_{mn} = 10^{-3}$, which makes $b_n\beta_{mn} = -68.95$.

For each of the models examined, D(H157α, Te(c)) will be computed for each of the possibilities:

(a) cold region in LTE, hot region in non-LTE
(b) cold region in LTE, hot region in LTE
(c) cold region in non-LTE, hot region in non-LTE
(d) cold region in non-LTE, hot region in LTE.

In each of these cases, the continuum emission measure is assumed to be related to the electron density by $E_T(c) = N_e(c)^2\ \rho_L\ L$ and $E_T(h) = N_e(h)^2\ (1 - \rho_L)\ L$, where L is the total line-of-sight path length through both media and ρ_L is the line-of-sight filling factor of the cold regions. L will be assumed to be equal to the distance to 3C391 although this may not be a good assumption since the electron density may be appreciably different in the ridge gas than it is in the solar neighborhood. From Figure IV-2 it is seen that a portion of the line of sight does not lie within the ridge. It is not clear what the ridge boundary is like and how much N_e differs in and out of the ridge. Pulsar data seem to indicate that, in the solar neighborhood, $N_e = 0.03\ cm^{-3}$ (Guelin, 1974). The error in choosing L = 8.5 kpc should have little effect on the solution if it is shown that the hot region does not contribute much to the recombination line power.

Model 1 is essentially the same as that previously examined; it is based on the Cesarskys' (1973b) model for a cold region emitter: $E_L(c) = 4\ pc\ cm^{-6}$ and $T_e = 20\ °K$.

Model 2 is based on Model 1 but with $E_L(c)$ reduced by a factor of 10 to see what the effect of doing so would be. The electron density remains the same and the path

length through the cold region becomes 85 pc. If the region is spherical, it would subtend an angle of 34 arc minutes. This is a reasonable size because the line strength observed by the COMP beam is about one-third of that observed by the 3C391 beam. This suggests that the size of the emitting region may be about 34 arc minutes in diameter.

Model 3 is based entirely on the results of Field, Goldsmith, and Habing (1969). A filling factor of $\rho_L = 0.006$ is used for this analysis which falls into the range they suggest. The cold region emission measure is based on the information given in their Figures 1 and 2.

Model 4 was inspired by the results of Chaisson's (1972) recombination line observations in the direction of W3A, and H II region located at l = 134° and b = 0°. His spectrum indicates the presence of hydrogen, helium, carbon, and a blend of heavy element recombination lines. The residuals he obtains by removing Gaussian features from his spectrum suggest the possibility of an additional weak, narrow component of the prominent hydrogen feature. He concludes that the weak, narrow feature originates from a cold region where the heavy elements (Mg, Si, S, and Fe) are located. The prominent feature, then, originates from the H II region. Using the H I and carbon lines and assuming the abundances given by Spitzer (1968, p. 122), he obtains $T_e = 100$ °K, $N_H = 10$ cm^{-3}, $N_{H+} = 1.8\ (\pm 1.4) \times 10^{-4}$ cm^{-3} and $N_e = 7\ (\pm 5) \times 10^{-3}$ cm^{-3} for the cold region. This gives most

probable values of $N_e N_{H+} = 1.26 \times 10^{-5}$ cm^{-6} and $N_e \sum_j Z_j^2 N_j = 1.1 N_e N_{H+} = 1.39 \times 10^{-5}$ cm^{-6}. Chaisson does not suggest a value for ρ_L, but a value of 0.01 will be used here because of the argument used for Model 2.

Figures V-5, 6, 7, and 8 show the D-curves plotted for each model and combination of thermodynamic condition. The parameters used for these are summarized in Table V-4. D was computed with a WATFIVE computer program.

The LTE cold curves, labeled a and b in each figure, are asymptotic at $T_e = T_R = 13.4$ °K. As the plots show, neither $D_o = 9.37(\pm 2.37)$°K kHz nor $D_o = 11.44$ (±2.89) °K kHz is large enough to obtain a non-LTE solution for the cold region. The result, therefore, remains the same as that for Figure V-4. The hot region has no effect on the solution and the error in assuming that L = 8.5 kpc is of no consequence. The RMS electron densities shown in Table V-3 are computed from

$$\langle N_e(x)^2 \rangle^{1/2} = \left[E_T(x)/s_x \right]^{1/2} ,$$

where s_x is either $s_c = \rho_L L$ or $s_h = (1 - \rho_L)L$. Table V-3 also shows the fraction, in percent, of the line power which originates from each of the two phases. It is apparent that the hot medium has little effect on the line power except when $E(c) \ll E(h)$.

Table V-4

D-Method Model Summary

	Cold Region						Hot Region				
Model	T_e [°K]	$N_e^{2\ 1/2}$ (cm^{-3}]	Path Length [pc]	E_T [pc cm^{-6}]	E_L [pc cm^{-6}]	%	$N_e^{2\ 1/2}$ [cm^{-3}]	Path Length [pc]	E_T [pc cm^{-6}]	E_L [pc cm^{-6}]	%
1	14.5	0.07	850	4.40	4.00	100	0.015	7650	1.72	1.57	0
2	14.3	0.07	85	0.44	0.40	99.8	0.014	8415	1.72	1.89	0.2
3	14.5	0.05	51	0.15	0.14	99.5	0.016	8449	2.16	1.97	0.5
4a	13.7	0.007	85	1.18×10^{-3}	1.07×10^{-3}	60.2	0.014	8415	1.72	1.89	39.8
b	13.8	0.007	85	1.18×10^{-3}	1.07×10^{-3}	67.02	0.014	8415	1.72	1.89	32.8

Note for Model 4:
a values are for a non-LTE hot region

b values are for an LTE hot region

Figure V-5. D Plotted as a Function of the Cold Medium Temperature for Two Phase Model 1. The key is as follows:

a ——— LTE cold, non-LTE hot
b ····· LTE cold, LTE hot
c — — non-LTE cold, non-LTE hot
d ·-·- ·-·- non-LTE cold, LTE not

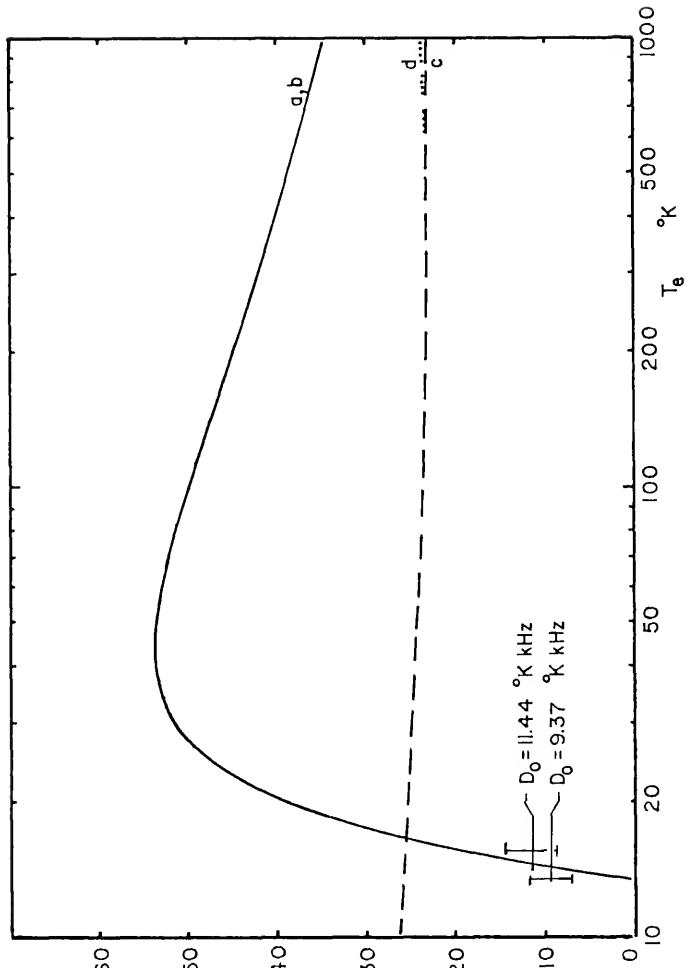
D
°K kHz
60
50
40
30
20
10
0
10
20
50
100
200
500
1000
T_e °K
a,b
c
d
D_0 = 11.44 °K kHz
D_0 = 9.37 °K kHz

Figure V-6. D Plotted as a Function of the Cold Medium Temperature for the Two Phase Model 2. The key is as follows:

a ——— LTE cold, non-LTE hot
b ····· LTE cold, LTE hot
c — — non-LTE cold, non-LTE hot
d ···· ···· non-LTE cold, LTE hot

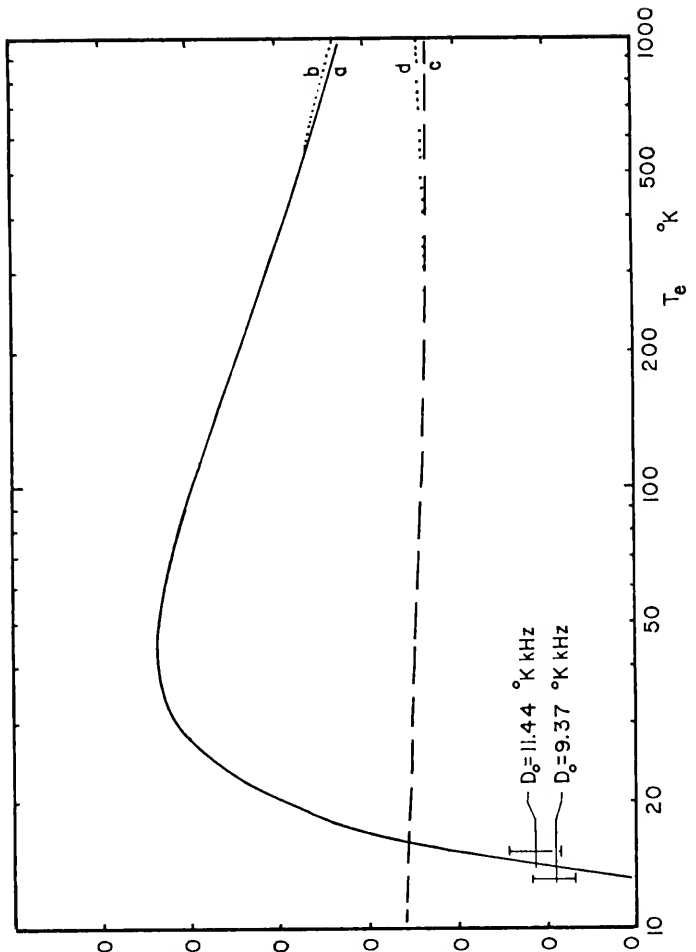
D
°K kHz
60
50
40
30
20
10
0
10
20
50
100
200
500
1000
T_e °K
a
b
c
d
d
D_o=11.44 °K kHz
D_o=9.37 °K kHz

Figure V-7. D Plotted as a Function of the Cold Medium Temperature for the Two Phase Model 3. The key is as follows:

a ——— LTE cold, non-LTE hot
b ····· LTE cold, LTE hot
c — — non-LTE cold, non-LTE hot
d ···· ···· non-LTE cold, LTE hot

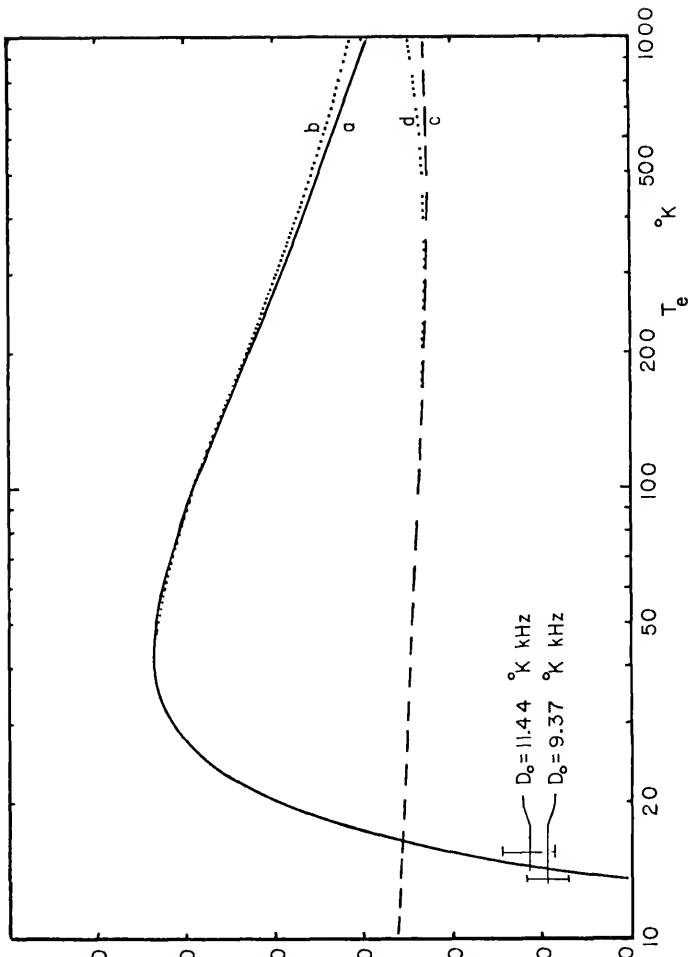
D
°K kHz
60
50
40
30
20
10
0
10
20
50
100
200
500
1000
T_e °K
a
b
c
d
D_o= 11.44 °K kHz
D_o= 9.37 °K kHz

Figure V-8. D Plotted as a Function of the Cold Medium Temperature for the Two Phase Model 4. The key is as follows:

a ——— LTE cold, non-LTE hot
b ····· LTE cold, LTE hot
c — — non-LTE cold, non-LTE hot
d ···· ···· non-LTE cold, LTE hot

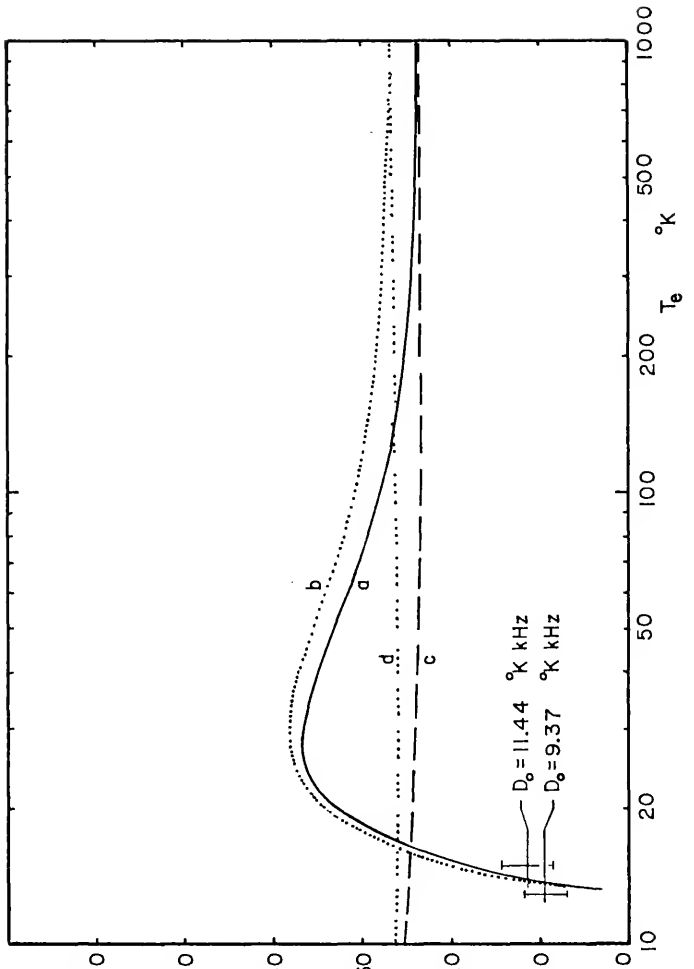
D
°K kHz
60
50
40
30
20
10
0
10
20
50
100
200
500
1000
T_e °K
a
b
c
d
D_o = 11.44 °K kHz
D_o = 9.37 °K kHz

Two matters must be considered. First, there is the question of the validity of the cold region departure parameters. They were chosen for the case where $N_e \lesssim 10^{-4}$. Because of the proximity of the neighboring curves, there is some tolerance; that is, N_e can be somewhat larger without affecting the departure from LTE. The amount of tolerance depends on n and T_e. At n = 157 and T_e = 10 °K, the electron density of the medium should not exceed 10^{-3} cm^{-3}. If T_e = 1000 °K, the electron density could be as large as 0.1 cm^{-3}. The error from using collisionless values for a medium where N_e is actually about 0.1 cm^{-3}—as was done for Models 1, 2, and 3—is probably not large. Percival and Seaton (1972) claim that there are large uncertainties in the bound-bound collision cross-sections. For that reason the Cesarskys (1973b) estimate that the collisionless condition may be valid at electron densities which are 60 times that expected from Dupree's (1972) curves. If the D-curve for N_e = 0.1 cm^{-3} were used, it would fall between curves a and c because collisions will be more frequent and bring the level populations closer to their LTE values. Consequently, the D_o-lines will not intersect the non-LTE curves and the solution is not affected.

Finally, there is the question as to the use of the D-method for the H157α spectrum since the antenna beam is much larger than 3C391. As mentioned before, Figure 1 of

Cesarsky and Cesarsky (1973b) predicts that D_o obtained with an antenna beam 2.3 arc minutes in diameter should be 25 °K kHz. The fact that the 18 arc minute beam yields a much smaller D_o may indicate clumping or small scale structure within the emitting region seen by the antenna beam. Because of beam dilution the antenna power is less than it would be if the line emitting region filled the beam. Since the D-method gives uncertain results, another approach will be taken.

Isolated Cold Region Models

Since the background radiation is quite small, a solution to the transfer equation can be used which is applicable to an isolated region. The solution will be left in terms of line power in order to avoid the use of a parameter with a large uncertainty such as $\tau(80)$. A solution which is consistent between the H92α and the H157α spectra will be found by adjusting emission measures until both observed line powers are duplicated. By doing this, both T_e and E_L can be determined if there is a consistent solution.

From Equation II-45, the peak line antenna temperature is

$$T_L'(v_c) = \rho_B \eta_B T_e \left[A(v_c) \left(1 - e^{-(\tau_L+\tau_T)}\right) - \left(1 - e^{-\tau_T}\right) \right]; \qquad V\text{-}10$$

where,

$$A(v_c) \equiv \frac{\tau_T + b_m \tau_L^*}{\tau_L + \tau_T} = \frac{1 + b_m \tau_L^*/\tau_T}{1 + b_n \beta_{mn} \tau_L^*/\tau_T} \quad .$$

Both optical depths are peak values (i.e., at $v = v_c$) and $\tau_L = b_n \beta_{mn} \tau_L^*$. The optical depths τ_L^* and τ_T are computed from Equations II-28 and II-8 respectively. Let Ω_L, Ω_M, and Ω_A be the solid angles of the line emitting region, antenna main beam, and total antenna beam respectively. Then $\rho_B = \Omega_L/\Omega_M$ and $\eta_B = \Omega_M/\Omega_A$. For these models it is assumed that the line emitting region fills the H157α and H92α beams. So, in both cases $\rho_B = 1$. It is also assumed that $E_T = 1.1\ E_L$. The integrated line power, P, in °k kHz, is computed by the use of Equation V-10 and Equation II-35;

$$P = 1.0645\ T_L'(v_c) \frac{\nu_o}{c} \Delta\nu_D \quad .$$

In computing the H157α line power, a single high-velocity Gaussian feature with full half-power width of 35.73 km/s ($\Delta\nu_D$ = 200.6 kHz) is used. The expected H157α and H92α line powers are computed for a range of emission measures. Both LTE and collisionless non-LTE functions are computed. The departure parameters used are those computed by Dupree (1972), the same as those used for the D-method and tabulated in Table V-3.

A consistent solution between this study's spectrum and the H92α spectrum is found graphically. Figure V-9 shows non-LTE curves and Figure V-10 shows the LTE curves. Each curve is the integrated line power, P, plotted as a function of electron temperature and is labeled by the value of the emission measure used in computing it. In both figures, the H157α curves are placed above those for H92α and the horizontal lines represent the respective observed line powers: $P_o(H92\alpha)$ = 5.7 (±2.4) °K kHz and $P_o(H157\alpha)$ = 9.61 (+0.26, -1.27) °K kHz. The error with $P_o(157\alpha)$ is determined by considering the possibility of the feature being double. The error bar for both P_o-lines is represented in the figures by shaded strips.

The intersection of the P_o-lines with each of the respective curves in Figures V-9 and 10 is plotted in Figure V-11. Each of the four curves in Figure V-11 is, then, the locus of points which relate the temperature and emission measure required to produce the observed line power. Error strips are not shown. An intersection of the respective LTE or non-LTE loci defines a consistent solution.

The LTE curves do not intersect; therefore, the emitting medium is not in LTE. The non-LTE loci do, however, intersect. The angle between them is small, making the solution difficult to identify. The most probable values are T_e = 53 (±6) °K and E_L = 9.9 (±0.6) pc cm^{-6}. This solution does not involve the errors in either locus. The

Figure V-9. Non-LTE Integrated Line Power as a Function of T_e for an Isolated Cold Region. The upper curves are for the H157α line; the lower curves are for the H92α line. Each curve is labeled with the emission measure (in pc cm^{-6}) used to compute it. The observed line power is represented by the line labeled with P_o and the shading represents the error bars.

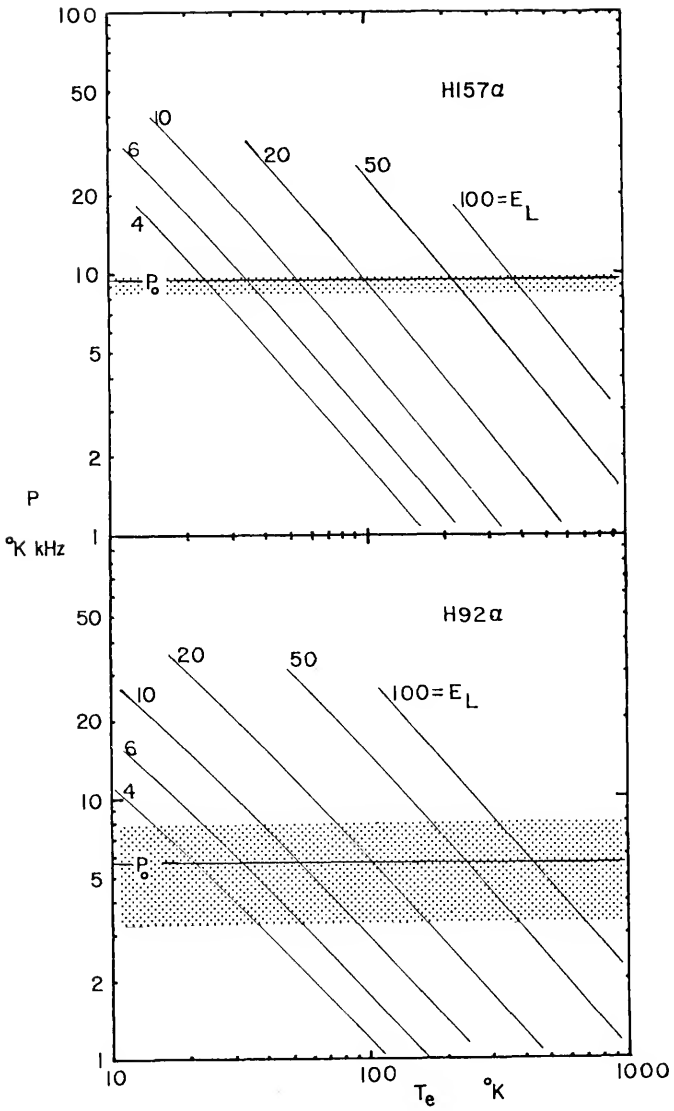
H157α
10
6
20
50
100=E_L
4
P_o
H92α
20
50
10
100=E_L
6
4
P_o
P
°K kHz
100
50
20
10
5
2
1
10
100
1000
T_e °K

Figure V-10. LTE Integrated Line Power as a Function of T_e for an Isolated Cold Region. The upper curves are for the H157α line; the lower curves are for the H92α line. Each curve is labeled with the emission measure (in pc cm-6) used to compute it. The observed line power is represented by the line labeled with P_o and the shading represents the error bars.

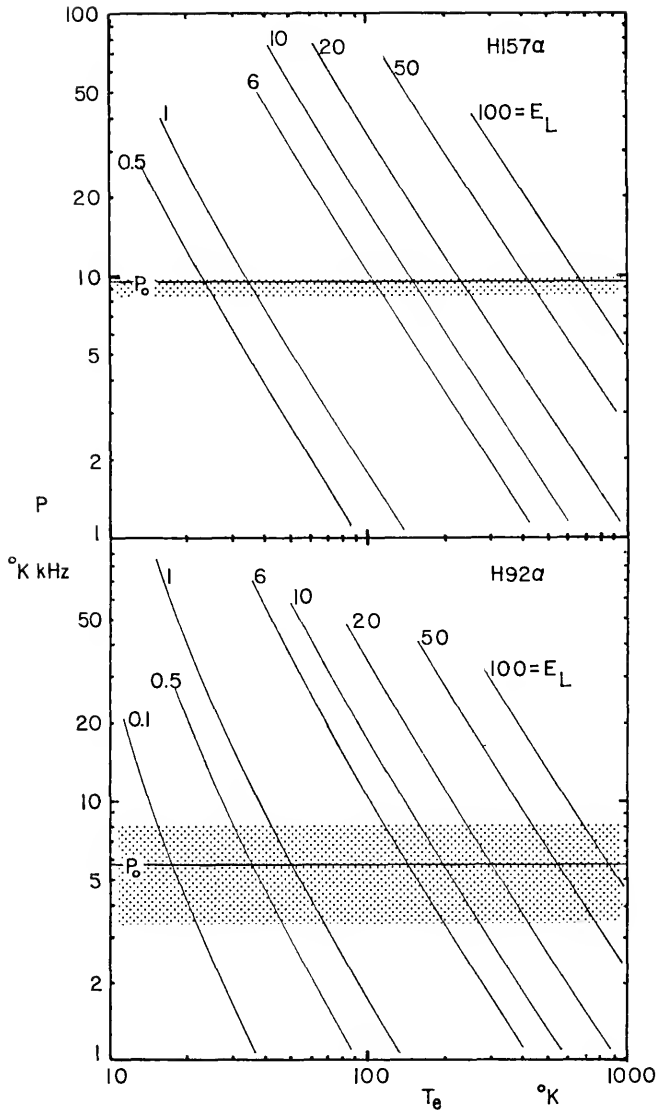
H157α
100=E_L
50
20
10
6
1
0.5
P_o
H92α
100=E_L
50
20
10
6
1
0.5
0.1
P_o
P
°K kHz
100
50
20
10
5
2
1
10
100
1000
T_e °K

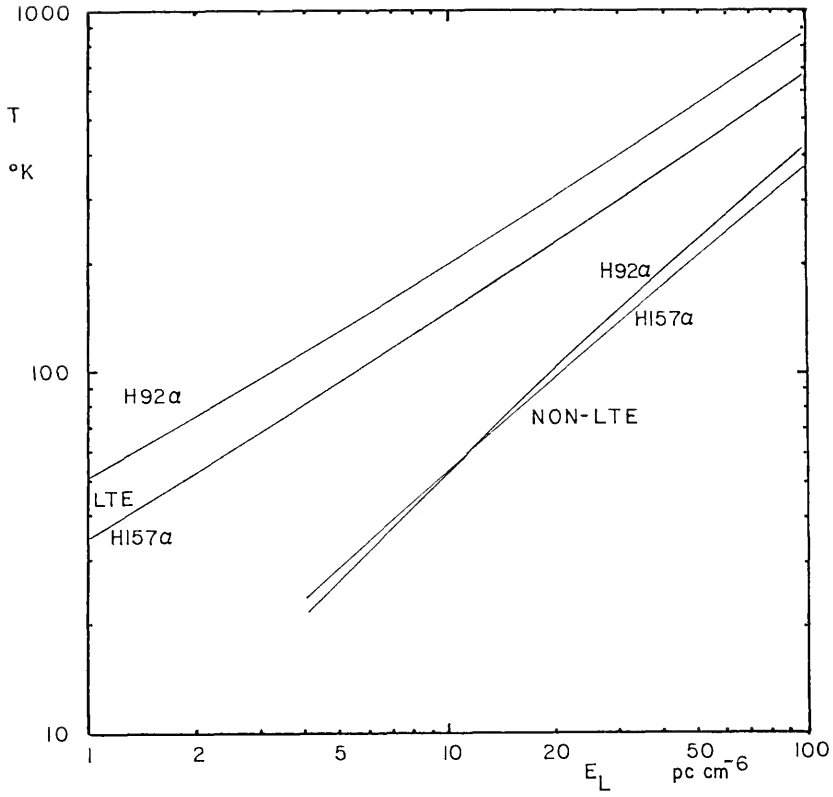

Figure V-11. Isolated Cold Region Model Solutions. The consistent solution is indicated by the intersection of the lines. There is no LTE solution. The non-LTE solution is T_e = 53°K and E_L = 9.9 pc cm^{-6}.

error strip for each locus would encompass both lines and render an uncertainty to the solution equal to the range of the loci. Hence the solution presented is only a best estimate.

This solution temperature does not seem to agree very well with the most probable temperature derived by the Cesarskys (1973b) but is closer to the 21 cm spin temperature of 60 °K derived by Radhakrishnan and Goss (1972). But considering the uncertainties, the agreement is all right. This result, along with the alignment of the high-velocity recombination line features with the 84 and 105 km/s 21 cm absorption features, tends to indicate that their regions of origin are spatially related.

The beam dilution was taken to be unity for both lines because the variation of the H157α line power between its two beams seems to indicate that the emitting region fills both of them. This suggests a H157α emission region size of about 85 pc. This, however, is quite a bit larger than the average size of the 21 cm absorption regions (5 pc) derived by Baker and Burton (1975). If 85 pc is equal to the total path length through the recombination line emission region, the emission measure of 9.9 pc cm^{-6} derived here results in an RMS electron density of 0.34 cm^{-3}. It is possible that the recombination lines may come from a cluster of 5 pc clouds. Since $N_H > 0.34$ cm^{-3}, Equation II-54 shows that the spin and electron kinetic temperatures are equal.

It is difficult to explain the width of the recombination line features if the emitter has a temperature of 53 °K. Since 53 °K is the gas kinetic temperature, the thermal line broadening should be 1.6 km/s (Equation II-34). This is obviously much smaller than the observed line width which is between 30 and 36 km/s. Turbulence within the cold emission region will cause some broadening, but the average total half-intensity width of 21 cm absorption features seen in the galactic plane is about 3 km/s; this includes all broadening effects (Radhakrishnan and Goss, 1972). The widths of the 80 and 107 km/s features observed in the direction of 3C391 are 10 and 3 km/s respectively. The 80 km/s feature may be a blend of two or more features (Radhakrishnan and Goss, 1972).

The discrepancy between the 21 cm absorption and radio recombination line widths suggests considering other models.

The Hot Spot Models

The observational results of Matthews, Pedlar, and Davies (1973), Gottesman and Gordon (1970), and Chaisson (1974a) suggest that the recombination line emission regions must be hotter than 1000 °K. One possibility is a distribution of very small, hot H II regions. Altenhoff *et al.* (1973) have observed 10 discrete continuum sources within 36 arc minutes of the position ($l = 24°$, $b = 0°$) at which

Gottesman and Gordon (1970) and Gordon and Gottesman (1971) observed recombination lines. This is a region in which Altenhoff et al. (1970) indicate there are no resolved continuum sources. The 10 discrete sources were observed at a wavelength of 11 cm and with a spatial resolution of 4.4 arc minutes. According to Guelin (1974), three or more of these sources produce 25 km/s-wide recombination lines. These are about as wide as those observed in the direction of 3C391. Weak and broad (Δv = 80 km/s) lines were observed between these sources.

Assuming that these "Hot Spot" sources are widely distributed throughout the galactic ridge, expected line powers will be calculated; the calculations will be based on as much evidence as is available. The expected line powers of H157α and H92α emission will be compared to those observed.

Guelin (1974) provides no more information on these sources than has been mentioned except that it was implied that they are separated by a minimum of 4.5 arc minutes. With this spacing, 13 of them can be distributed within the 18 arc minute H157α antenna beam. The maps of the region surrounding 3C391 made by Caswell et al. (1971), Dulk and Slee (1972), Bridle and Kesteven (1971), and Chaisson (1974a) show no collection of discrete sources within 18 arc minutes of 3C391. Since Guelin does not mention the intensity of the sources, one cannot be certain of their

absence since, in all cases, the maps were presented with the background removed. The structure seen by Chaisson (1974a) with a 2.1 arc minute beam at 15.5 GHz is enclosed by the weakest isophotes of all other maps and is probably, therefore, structure within the SNR rather than of the intervening medium.

Braes and Miley (1972) have produced an aperture synthesis map of a 1°x1° region in which Cygnus X-3 is located. This is in the Cygnus X region, a distribution of H II regions appearing roughly circular in shape with a diameter of about six degrees. There are about 100 known thermal continuum sources in this region (Wendker, 1970). Radio recombination lines have been observed in several places between these continuum sources (Gottesman and Gordon, 1970; Seacord and Gottesman, unpublished observations). The map of Braes and Miley (1972) does show some structure. There are a few extended sources, one of which coincides with an OB association (Cygnus OB2 or VI Cygni) and the others coincide with known H II regions. There are about 15 discrete sources having a flux density considerably less than that of Cyg X-3, 0.021 Jy. However, no more than five of these sources exist in any 18x18 arc minute area over the entire 1°x1° map and some of these sources are closer together than 4.5 arc minutes.

There are two cases for which discrete H II regions have been studied. Habing et al. (1973) have observed H II

regions which are related to Type I OH maser sources. One of these, ON-1, had previously been studied by Winnberg et al. (1973). ON-1 is located at l = 69°.5 and b = -1°.0 and has an emission measure of about 2.7×10^8 pc cm^{-6}, an electron density of about 10^5 cm^{-3}, and a diameter of 0.03 pc or less. Winnberg et al. scanned a field of 24x24 arc minutes around ON-1 with a resolution of 1.3 arc minutes and found no other sources. If the sources observed by Altenhoff et al. (1973) are like that associated with ON-1, it is apparent that they do not occur frequently out of the galactic ridge. This agrees with the finding that radio recombination lines are not observed in the general interstellar medium outside the ridge.

Another case on which to base hot spot models is the hot, dense condensations, or "knots," within emission nebulae. An example of this kind of H II region is in the core of M42. For the knots there, Hjellming and Davies (1970) find that the average temperature, electron density, and emission measure are 10^4 °K, 2×10^4 cm^{-3}, and 10^7 pc cm^{-6} respectively. These averages are made over an effective path length of 0.02 pc which is assumed to be the size of the sources.

A series of models for a distribution of 0.02 pc H II regions will be considered. They are assumed to be distributed across and along an 18 arc minute beam such that 13 of them are observed in

it and there is one of them in the 2.3 arc minute H92α beam. The distribution has a centroid located at a distance of 8.5 kpc from the sun. The angle subtended by one of these sources is about 0.48 arc seconds. Therefore, the beam dilution factor, ρ_B, is 1.65×10^{-6} for the H157α beam and 6.80×10^{-6} for the H92α beam.

The integrated line power, P, is computed with Equation V-10. LTE and non-LTE cases are computed for which N_e = 1, 10, 10^2, and 10^3 cm^{-3}. The temperatures and range of emission measures are based on the results of Hejllming and Davies (1970) and Habing et al. (1974); $T_e = 7.5 \times 10^3$ and 10^4 °K with $10^4 \leq E_L \leq 5 \times 10^8$ pc cm^{-6}. The non-LTE departure parameters were computed by Sejnowski and Hjellming (1969) and are tabulated in Table V-5. The slope of the b_n-curve, $\delta_{mn} = (b_m - b_n)/b_m$, is also shown.

Figures V-12 and 13 show P(H157α) and P(H92α) plotted as a function of emission measure. Figure V-12 is for T_e = 7500 °K and Figure V-13 is for T_e = 10000 °K. In both figures the H157α curves are plotted above those of H92α and the vertical line labeled with P_o represents the observed line power: P_o(H157α) = 9.61 (+0.26, -1.27) °K kHz and P_o(H92α) = 5.7 (±2.4) °K kHz. The shaded strip represents the error bars. The non-LTE curves are labeled with the electron density for which the departure parameters were computed. The H92α LTE curves are drawn dashed. For both temperatures, the H157α LTE line powers are less than

Table V-5

Departure Parameter Used in the Hot Spot Models
[Computed by Sejnowski and Hjellming (1969)]

	$N_e[cm^{-3}]$	b_m	δ_{mn}	β_{mn}
H157α $T_e = 10^4$ °K				
	10	0.9024	2.710×10^{-3}	-335.38
	10^2	0.9739	8.900×10^{-4}	-109.27
	10^3	0.9951	1.085×10^{-4}	- 12.433
	10^4	1.0000	3.550×10^{-5}	- 3.3947
H157α $T_e = 7.5\times10^3$ °K				
	10	0.8858	3.200×10^{-3}	-297.05
	10^2	0.9701	1.100×10^{-3}	-101.24
	10^3	0.9922	2.230×10^{-4}	- 19.708
	10^4	1.0000	4.31×10^{-5}	- 3.057
H92α $T_e = 10^4$				
	10	0.7340	1.428×10^{-3}	- 34.858
	10^2	0.8056	5.750×10^{-3}	-144.02
	10^3	0.9265	3.740×10^{-3}	- 93.133
	10^4	0.9810	1.000×10^{-3}	- 24.100
H92α $T_e = 7.5\times10^3$				
	10	0.6952	1.670×10^{-3}	- 30.459
	10^2	0.7743	6.850×10^{-3}	-128.71
	10^3	0.9138	4.170×10^{-3}	- 77.749
	10^4	0.9762	1.200×10^{-3}	- 21.594

Figure V-12. Integrated Line Power as a Function of Emission Measure for a 7500°K Hot Spot. The upper curves are for the H157α line. The lower curves are for the H92α line. Each non-LTE curve is labeled with the electron density for which it is calculated. The observed line power is represented by the line labeled with P_o and the shading represents the error bars.

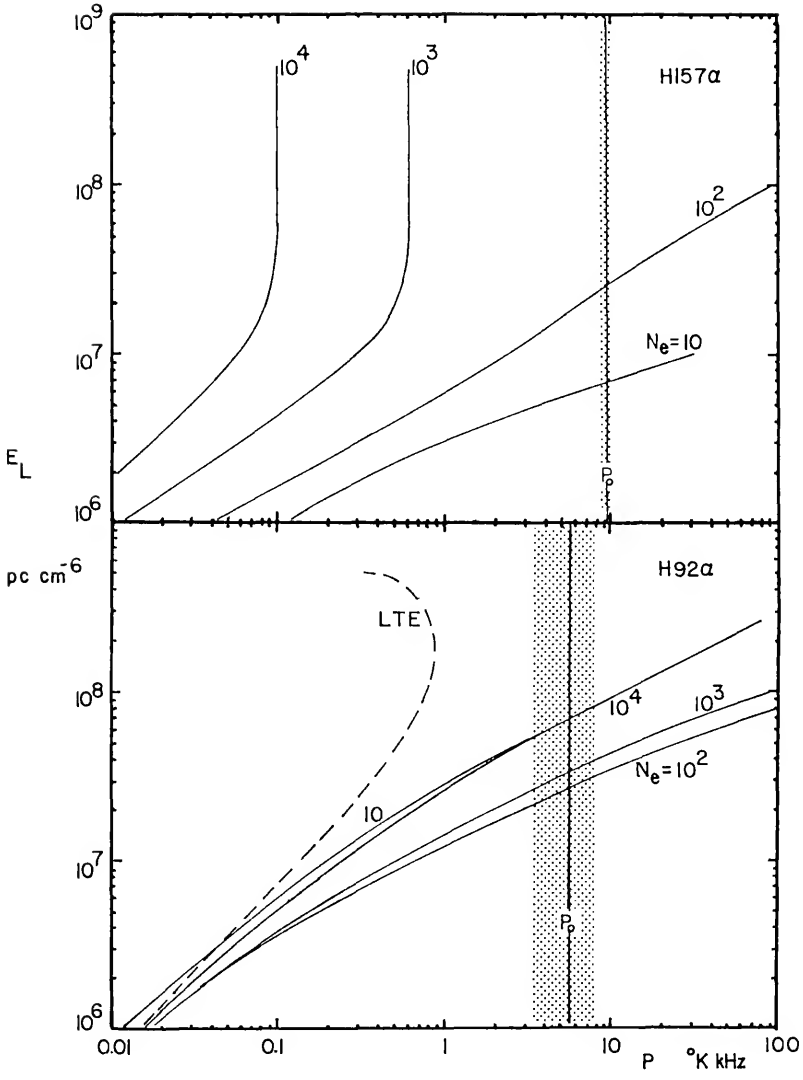
H157α
10^4
10^3
10^2
N_e=10
P_o
E_L
pc cm^{-6}
H92α
LTE
10^4
10^3
N_e=10^2
10
P_o
10^9
10^8
10^7
10^6
0.01
0.1
1
10
100
P °K kHz

Figure V-13. Integrated Line Power as a Function of Emission Measure for a 10 000°K Hot Spot. The upper curves are for the H157α line. The lower curves ar for the H92α line. Each non-LTE curve is labeled with the electron density for which it is calculated. The observed line power is represented by the line labeled with P_o and the shading represents the error bars.

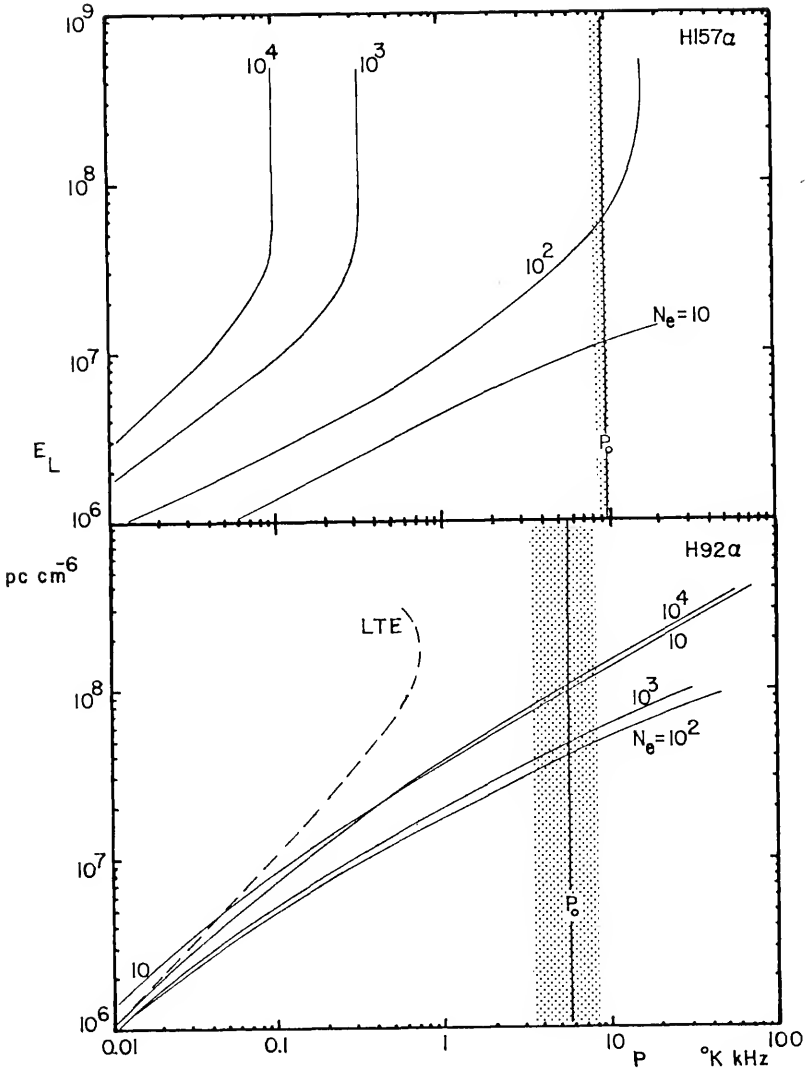
H157α
10^4
10^3
10^2
$N_e = 10$
P_o
E_L
pc cm^{-6}
H92α
LTE
10^4
10
10^3
$N_e = 10^2$
P_o
10
10^9
10^8
10^7
10^6
0.01
0.1
1
10
100
P °K kHz

0.01 °K kHz and, therefore, are not shown in the figures.

Figure V-12 indicates a consistent solution for T_e = 7500 °K because the $P_o(H157\alpha)$ and $P_o(H92\alpha)$ lines intersect the respective N_e = 100 cm^{-3} curve at $E_L \approx 2.6 \times 10^7$ pc cm^{-6}. The intersection is well within the error limits.

The situation for T_e = 10000 °K is not as simple. The solution occurs between the curves for N_e = 10 and 100 cm^{-3}. Simple interpolation is impossible because the dependence of the departure parameters on the electron density inverts the E_L-P relationship of the H157α and H92α curves between N_e = 10 and 100 cm^{-3}. Consequently, in order to obtain a consistent solution, the functions were replotted as P being a function of N_e, using E_L as a parameter. This is shown in Figure V-14. The locus of the points of intersection between the P_o lines and the constant E_L curves is shown in Figure V-15. The H157α and H92α loci intersect at the values $E_L = 4 \times 10^7$ and $\langle N_e \rangle = 81$ cm^{-3}. The intersection occurs within the range dictated by Figure V-13.

Table V-6 compares the derived models with the prototypes on which they were based. The agreement between the emission measures is not good and there is no agreement between the electron densities. $\langle N_e \rangle$, the electron density averaged over the path length L, is at least two orders of

Figure V-14. Integrated Line non-LTE Power as a Function of Electron Density for a 10 000°K Hot Spot. The upper curves are for the H157α line. The lower curves are for the H92α line. Each curve is labeled with the emission measure for which it was calculated. The observed line power is represented by the line labeled with a P_o and the shading represents the error bars.

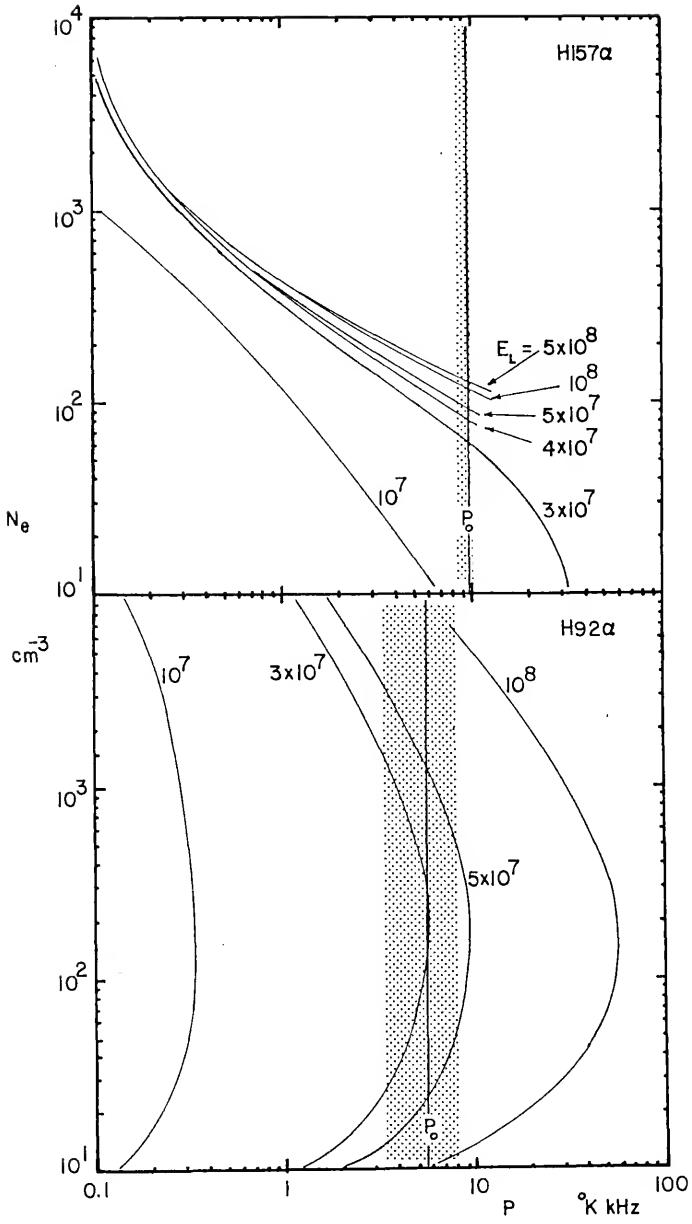
H157α
H92α
N_e
cm^{-3}
E_L = 5x10^8
10^8
5x10^7
4x10^7
3x10^7
10^7
P_o
P °K kHz
0.1
1
10
100

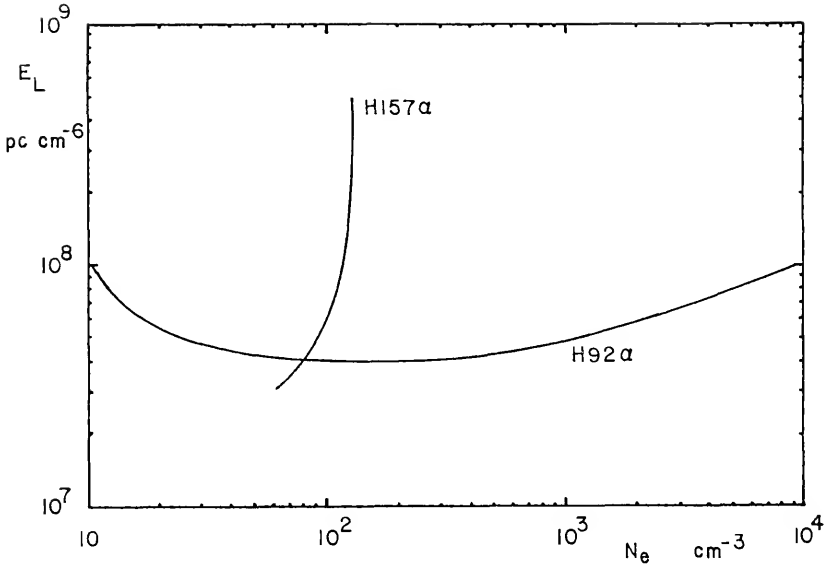

Figure V-15. Hot Spot Model Solution for T_e = 10 000°K. The solution is given by the intersection of the two curves; E_L = 4 x 10^7 pc cm^{-6} and $\langle N_e^2 \rangle^{1/2}$ = 81 cm^{-3}.

Table V-6

Comparison of Models with Their Prototypes

Emission Nebula Knots

	This Study	M42 (Hjellming and Davies, 1970)
T_e	10000 °K	10000 °k
E	4×10^7 pc cm^{-6}	1.26×10^7 pc cm^{-6}
$\langle N_e \rangle$	81 cm^{-3}	2.5×10^4 cm^{-3}
$\langle N_e^2 \rangle^{1/2}$	4.47×10^4 cm^{-3}	6×10^3 cm^{-3}
$\langle N_e \rangle / \langle N_e^2 \rangle^{1/2}$	0.16	$\sim$4.2
τ_T	4.8	>1*1

H II Region Associated with Type I OH Masers

	This Study	ON-1 (Winnberg et al., 1973)
T_e	7500 °K	8000 °K
E	2.6×10^7 pc cm^{-6}	2.7×10^8 pc cm^{-6}
$\langle N_e \rangle$	100 cm^{-3}	---
$\langle N_e^2 \rangle^{1/2}$	3.64×10^4 cm^{-3}	1.3×10^5 cm^{-3} *2
$\langle N_e \rangle / \langle N_e^2 \rangle^{1/2}$	0.28	---
τ_T	5.5	>1

Notes

*1 Gordon (1974)

*2 A diameter of 3660 au is assumed

magnitude too small for either type of region. $\langle N_e \rangle$ can be compared with the RMS electron density computed by dividing the emission measure by the path length, 0.02 pc.

Table V-6 also shows the ratio $\langle N_e \rangle / \langle N_e^2 \rangle^{1/2}$ and the 1.683 GHz continuum optical depth. The ratio would indicate the amount of clumping along the line of sight if $\langle N_e \rangle$ and $\langle N_e^2 \rangle^{1/2}$ were obtained by independent measurements. Winnberg et al. (1973) made no determination of $\langle N_e \rangle$. Hjellming and Davies (1970) solved Equation V-10 for several α-, β-, γ-, δ-, and ε-lines to obtain values of $\langle T_e \rangle$, $\langle N_e \rangle$, and $\langle E_L \rangle$. So, $\langle N_e \rangle$ and the RMS value of it should be independent except for the fact that they both were obtained from radio recombination line observations. This is true in the case of this study also. An independent determination of $\langle N_e \rangle$ would be through the measurement of a pulsar's dispersion measure (cf. Equation II-55). Since it is probable that there are more electrons along the line of sight than are responsible for the radio recombination line emission, the $\langle N_e \rangle$ does not represent an average over the line of sight and, therefore, $\langle N_e \rangle / \langle N_e^2 \rangle^{1/2}$ does not measure clumping.

However, it is apparent that the ratio should represent the same quantity in both the analysis in this study and in that of Hjellming and Davies (1970) and would, therefore, indicate agreement or disagreement with the type of source being considered. There is clearly a lack of agreement, not only with this ratio, but with all parameters derived.

The number of sources in the H157α beam was chosen to be the maximum number allowed with a minimum intersource spacing of 4.5 arc minutes. To determine what effect a smaller number of sources in the 18 arc minute beam would have on the solution, Figure V-16 shows the line power-emission measure curves for 13, 10, and 5 sources in the beam. The number of sources enters into the calculation by the beam dilution factor, ρ_B. Each curve in Figure V-16 is labeled by the number of sources. The upper set of curves is for T_e = 7500 °K; the lower curve is for T_e = 10000 °K. In both sets, the dashed curves are for N_e = 100 cm^{-3} and the solid curves are for N_e = 10 cm^{-3}.

Reducing the number of sources has the effect of reducing the electron density and increasing the emission measure. So, the size of the emitting region increases greatly. The recombination line emission seems to favor an electron density more like that of the more tenuous gas surrounding the dense knots of an emission nebula. This is in agreement with the conclusion of Brockelhurst and Seaton (1972). Consequently, the results of this analysis do not seem to support the possibility that radio recombination lines observed from the galactic ridge are emitted by a collection of small ($\tilde{\sim}$0.02 pc), dense, hot, H II regions like ON-1 or the condensations in emission nebulae.

Figure V-16. The Effects of the Number of Sources on the Hot Spot Model Curves. The non-LTE, H157α integrated line power is plotted as a function of emission measure for T_e = 7500°K (upper set of curves) and T_e = 10 000°K (lower set of curves). The dashed curves in both sets are for N_e = 100 cm^{-3}; the solid curves are for N_e = 10 cm^{-3}. Each curve is identified by the number of sources in the antenna beam. The observed line power is identified by P_o.

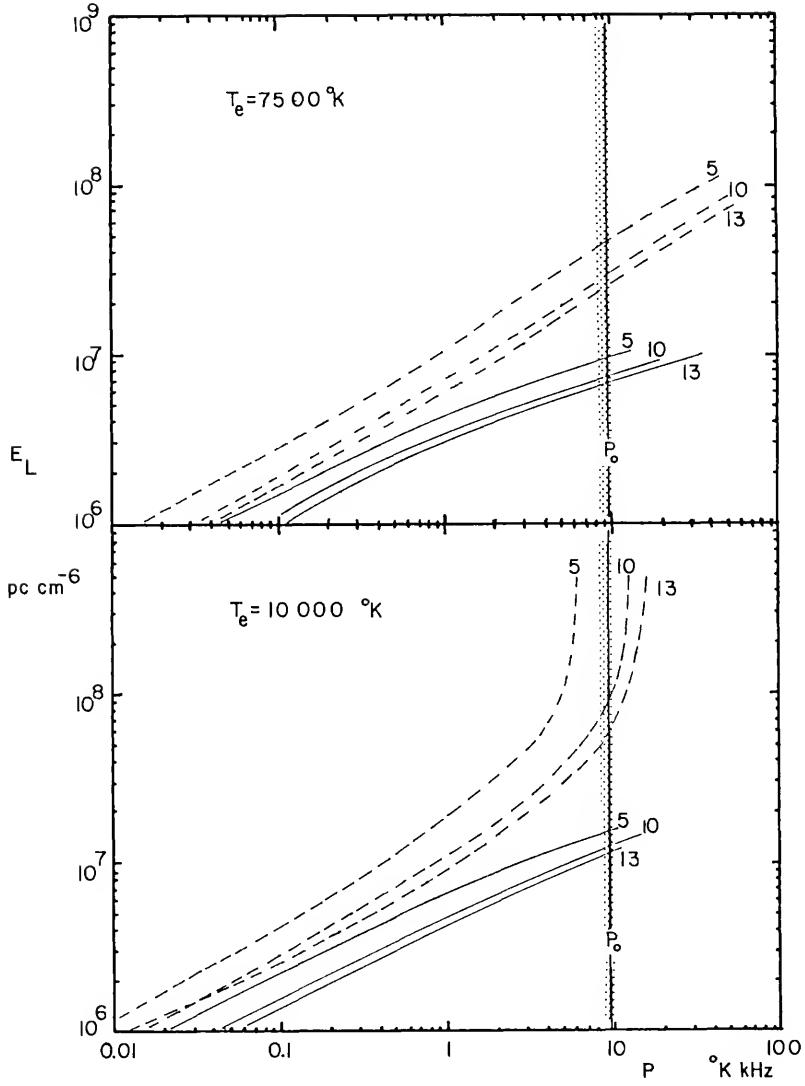
10^9
10^8
10^7
10^6
T_e=7500 °K
5
10
13
5
10
13
P_o
E_L
pc cm^{-6}
T_e= 10 000 °K
5
10
13
5
10
13
P_o
0.01
0.1
1
10
100
P °K kHz

H II Nebula Models

Chaisson (1974a) suggests that the H92α line observed by the Cesarskys (1973b) is emitted by a hot (7500 °K), low density (N_e = 22 cm^{-3}) H II region embedded in a two-phase medium rather than by the cold regions which the Cesarskys' results suggest. There are several arguments in favor of this which also apply to this study's spectra. The line widths ($\gtrsim$30 km/s) are like those observed from emission nebulae which are much larger than those of the corresponding 21 cm absorption features ($\lesssim$10 km/s). Also, the 80 MHz optical depth measured by Dulk and Slee (1972) can, in part, be caused by a partially ionized cool region with the remaining absorption caused by an H II nebula. In fact, recent unpublished observations indicate that $\tau(80)$ may be 0.4 (Chaisson, 1974b) which is the value it would be if the recombination lines were emitted only by the nebula (Chaisson, 1974a). He detects an excess continuum flux at 15.5 GHz which could result from the nebula. However, it should be noted that Goss (1972) points out that his 31.4 GHz observations do not indicate an excess flux. Finally, the Cesarskys (1973b) derive an ionization rate of $\zeta_H \gtrsim 10^{-12}$ sec^{-1} from their cold-region model. However, Hjellming, Gordon, and Gordon (1969) derive $\zeta_H \sim 10^{-15}$ sec^{-1} from pulsar dispersion measurements and Hughes, Thompson, and Colvin (1971) obtain a range of $1.9\times10^{-15} \leq \zeta_H \leq 4.0\times10^{-15}$ sec^{-1} from 21 cm absorption spectra.

These arguments suggest considering an H II nebula model. The model curves were computed with Equation V-10 for LTE and non-LTE cases. The temperature, T_e, was restricted to 7500 °K and the non-LTE models were computed for electron densities of 10 and 100 cm^{-3} using the departure parameters of Sejnowski and Hjellming (1969) given in Table V-5. Because of the variation of the line intensities between the 3C391 and its COMP beam, it was assumed that the nebula subtends an angle of about 34 arc minutes, giving it a diameter of 85 pc at a distance of 8.5 kpc. Therefore, since it completely fills the H157α and H92α beams, the beam dilution factor is unity for both.

Figure V-17 shows the integrated line power plotted as a function of emission measure. The H157α curves are drawn solid; those for the H92α line are drawn dashed. Each set consists of three curves, the LTE curve and the non-LTE curves labeled by the electron density used to compute it. The observed integrated line power for each line is indicated by the horizontal lines labeled with P_o(line). As for the previous models, P_o(H157α) = 9.61 (+0.26, -1.27) °K kHz and P_o(H92α)=5.7 (±2.4) °K kHz.

A constant solution is obtained when the lines of P_o(H157α) and P_o(H92α) intersect their respective LTE or non-LTE curve at a common value of E_L. Because of the large errors involved, it is difficult to ascertain exactly what

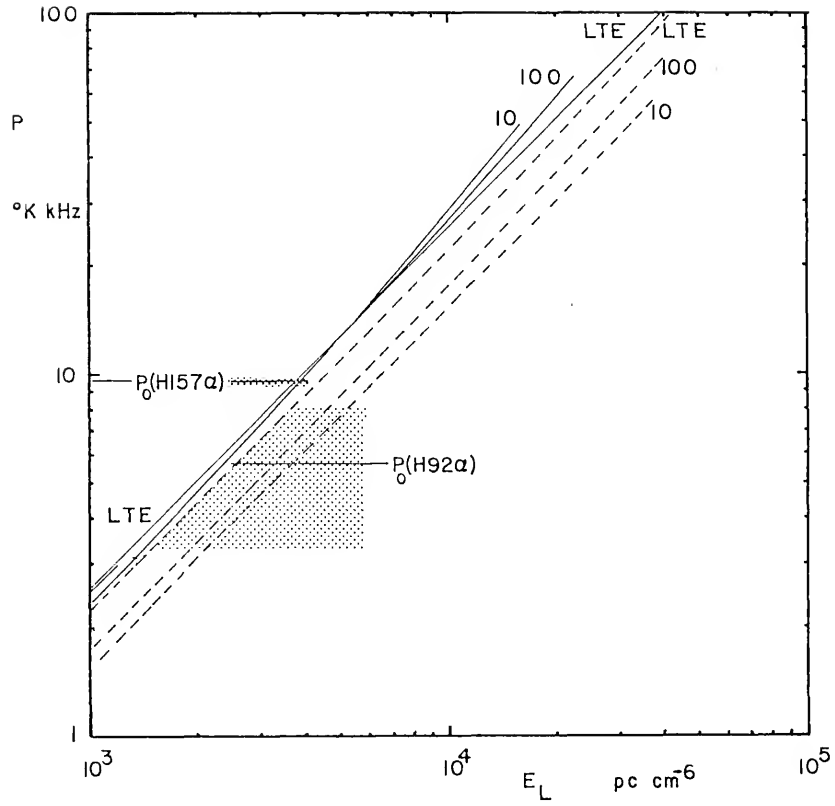

Figure V-17. H II Nebula Model Solution. The integrated line power is plotted as a function of the line emission measure. The H157α curves are drawn solid; those for the H92α line are drawn dashed. The non-LTE curves are labeled with the electron density used in their computation. The observed line powers are identified by P_0 (line) and the error bars are indicated by the shaded strip.

values apply to the solution. Perusal of the areas of intersection in Figure V-17 is easier with a table. Thus, Table V-7 indicates the value of emission measure where the lower error limit, P_o(line), and upper error limit intersect each of the curves. From the figure and table, it appears likely that the solution is close to $E_L = 3.8 \times 10^3$ pc cm^{-6} with N_e = 10 cm^{-3}. Since $P_o(H157\alpha) = 9.6$ °K kHz is closer to the upper error limit, the solution $E_L = 3.3 \times 10^3$ pc cm^{-6} with N_e = 100 cm^{-3} is not unlikely. The table and figure indicate that an LTE solution is unlikely since a common intersection is so close to both error limits. There is astrophysical evidence which also suggests this.

The likely range of parameter values agrees well with those Chaisson (1974a) obtains by an independent method: $\langle N_e \rangle = 22$ cm^{-3} and $E_T \approx 4 \times 10^3$ pc cm^{-6}, giving $E_L = E_T/1.1 \approx 3.6 \times 10^3$ pc cm^{-6}. This solution also compares favorably with the parameters applicable to visible H II nebulae. For example, the North American nebula complex (W80) has a diameter of about 50 pc and $\langle N_e \rangle \approx 10$ cm^{-3} (Kaplan and Pikelner, 1970, p. 153) which gives $E_T \approx 5 \times 10^3$ pc cm^{-6}.

Finally, it should be noted that, in a very recent paper, Jackson and Kerr (1975) conclude that radio recombination lines originate from small, low-density H II nebulae like this study's H II nebula model except that the electron temperature they derive is close to 4400 °K. Their results

Table V-7

The Emission Measure of the Intersections in Figure V-7

Curve	H157α			H92α		
	Lower Limit	P_o(H157α)	Upper Limit	Lower Limit	P_o(H92α)	Upper Limit
N_e=10	3.4	3.9	3.9	2.1	3.7	5.3
N_e=100	3.3	3.8	4.0	1.9	3.3	4.7
LTE	3.3	3.8	4.0	1.5	2.6	3.7

All emission measures are given in units of 10^{-3} cm pc^{-6}.

will be discussed in more detail in Chapter VI where the ridge as an entity will be discussed. Also, as this was being written, Pankonin (1975) reported on his H248α recombination line observation of 3C391. His line indicates nothing which has not been observed before and he favors a low density H II region as the source of the line.

Table V-8 summarizes the models derived in this chapter. The discussions made during the derivation of these models suggest that the most likely models are the Isolated Cold Region and the H II Nebula models. In the following chapter, additional arguments will be considered from which a most probable model, including the distribution of the emission sources, will be considered.

Table V-8

Summary of Model Solutions

Model	Thermo-dynamic State	T_e [°K]	E_L [pc cm^{-6}]	$\langle N_e \rangle$ [cm^{-3}]	Assumed Path Length [pc]	$\langle N_e^2 \rangle^{1/2}$ [cm^{-3}]
D-Method*						
1	LTE	14.3	4.00	.07	850	--
2	LTE	14.3	0.40	.07	85	--
3	LTE	14.3	0.14	.05	51	--
4	LTE	13.7	1.07×10^{-3}	.007	85	--
Isolated Cold Region	non-LTE	53	9.9	$\leq 10^{-3}$	85	0.34
Hot Spot	non-LTE	7500 10000	2.65×10^{7} 4×10^{7}	100 81	0.02 0.02	3.64×10^{4} 4.47×10^{4}
H II Nebula	non-LTE	7500	3.8×10^{3}	~ 10	85	6.69

*Values given are for cold region since it is the predominate emitter.

CHAPTER VI

FURTHER CONSIDERATIONS AND APPLICATIONS OF THE MODELS

Discussion of the Models

This discussion pertaining to the models suggests that the most plausible condition is that the recombination line-emitting region is either an isolated cold ($T_e \simeq 53$ °K) region or a low density emission nebula similar to W80. In order to decide on a final model, several more parameters will be calculated and compared to the results of other work. Three of these parameters are the 1683 and 80 MHz optical depths and the continum antenna temperature at 1683 MHz, which are expected to be observed from each of the models.

The D-Method models involve a two-component medium which will be considered to be a cold region surrounded by hot gas. The continuum antenna temperature, $T_T^{\prime}$, is given by

$$T_T^{\prime} = \eta_B\{T_e(h)[1-\exp(-\tau_f(h))] + \frac{\Omega_c}{\Omega_M} T_e(c)\exp(-\tau_f(h))[1-$$

$$\exp(-\tau(c))] + T_e(h)\exp(-\tau(c)-\tau_f(h))[1-\exp(\tau_b(h)]\}.$$

In this equation, Ω_c is the solid angle subtended by the cold region. For these models it is greater than the antenna main beam solid angle, Ω_M; so, $\Omega_c/\Omega_M = 1$. All optical depths are for the thermal continuum. That of the hot gas in front of the cold region is $\tau_f(h)$ and that of the hot gas behind the cold region is $\tau_b(h)$. It will be assumed that the hot gas is distributed equally in front of and behind the cold region; so, $\tau_f(h) = \tau_b(h)$. For a single component recombination line emitter with a continuum optical depth τ_T and observed through an optically thin gas ($\tau \sim 3 \times 10^{-7}$), Equation VI-1 reduces to

$$T_T' = \eta_B \frac{\Omega_L}{\Omega_M} T_e[1-\exp(-\tau_T)],$$

where Ω_L is the solid angle subtended by the line-emitting region. For all except the Hot Spot models, $\Omega_L/\Omega_M = 1$. For the Hot Spot models $\Omega_L/\Omega_M = 1.65 \times 10^{-6}$.

The continuum optical depths at 1683 and 80 MHz and the 1683 MHz continuum antenna temperature for each of the models are listed in Table VI-1. If the isolated cold region were surrounded by a hot gas, the situation would be similar to that of the two-component model. From the table it is evident that this hot region would contribute a neglibible amount to the antenna temperature. If the Hot Spots are surrounded by a low density HII nebula, the observed contribution to the continuum temperature would be about 4 °K.

Gordon and Gottesman (1971) observed H197β recombination lines in Cygnus X and at two positions in the ridge, at longitudes of 23°.9 and 25°.1. The ratio of H157α to H197β integrated line powers are 3.21, 3.95, and 4.56 for longitudes 23°.9 and 25°.1 and Cygnus X respectively. The H197β line powers expected in the direction of 3C391 are calculated for each model using the parameters of Table V-7 and Equation V-10 except for the D-Method models where the integrated line power is given by

$$P(H197\beta) = 1.0645\Delta\nu_D[0.8\tau_L^*(H197\beta)\ (T_e - T_R)].$$

The power ratio, P(H157α)/P(H197β), for each model is listed in the fifth column of Table VI-1. The velocity half-power width of the line used to calculate line power was taken to be same as that observed for the H157α line, 35.7 km/s or 201.8 kHz. A comparison of the power ratios in Table VI-1 with those found by Gordon and Gottesman is made with the assumption that a radical change from region to region within the ridge is not to be expected. Acutally, their ratios did not change much between the ridge regions and that in Cygnus X.

Another parameter which will be used to evaluate the models is the hydrogen ionization rate, $\zeta_H = H_e N_H + \alpha_2(T)/N_H$ (Equation II-48). The partial recombination coefficient, $\alpha_2(T)$, is computed from Equation II-22. Then

$$\alpha_2(T) = 2.065 \times 10^{-11}\ T^{-1/2} \zeta_2(T)$$

and $\zeta_2(T)$ is obtained from Figure II-3. Because radiative recombination directly into the ground state generates a photon which immediately ionizes a neighboring hydrogen atom, the ionization rate from outside sources is related to recombination into all levels expect the ground level. Therefore, the partial recombination coefficient is used rather than the total coefficient (Dalgarno and McCray 1972).

In calculations of ζ_H for the Hot Spot and HII Nebula models, total ionization in the regions is assumed. Then $N_H = N_H{}^+$. Also, $N_e = 1.1 N_H{}^+$ to account for electrons contributed by helium. Then $\langle N_e\ N_H{}^+ \rangle / N_H$ reduces to $\langle N_e \rangle$.

For the D-Method and Isolated Cold Region models, $N_e H_H{}^+$ is assumed to be equal to N_e^2. The total hydrogen density is nearly equal to the neutral hydrogen density, N_{H° which is related to the 21 cm line integrated optical depth by means of Equation II-52;

$$\int_{\text{line}} \tau_{21}(\nu) d\nu = 2.58 \times 10^{-15} \int_0^L \frac{N_{H^\circ}(s)}{T_s}\, ds.$$

$\int \tau_{21}(\nu)\, d\nu$ is obtained from Table 2 of Radhakrishnan *et al.* (1972b). There are three high-velocity features in the absorption spectrum which are located at 80, 101, and 107 km/s. In calculating N_H for the cool models, is assumed that

Table VI-1

Additional Model Parameters

Model	$\tau_T(1683)$	$\tau_T(80)$	T_T' [°K]	$\frac{P(H157\alpha)}{P(H197\beta)}$	N_H [cm^{-3}]	$\frac{N_e}{N_H}$	ζ_H [sec^{-1}]
D1	c: 4.02×10^{-4} h: 2.77×10^{-7}	1.34	0.0078	2.75	0.269	2.19×10^{-1}	3.57×10^{-13}
D2	c: 4.02×10^{-5} h: 2.78×10^{-7}	0.134	0.0027	27.46	2.69	2.19×10^{-2}	3.57×10^{-14}
D3	c: 1.41×10^{-5} h: 3.49×10^{-7}	4.71×10^{-2}	0.0028	78.13	4.49	9.04×10^{-3}	1.39×10^{-14}
D4	c: 1.08×10^{-7} h: 2.78×10^{-7}	3.78×10^{-4}	0.0021	3.84×10^{4}	2.58	2.29×10^{-3}	3.82×10^{-16}
Isolated Cold	7.30×10^{-4}	0.729	0.0309	5.04	9.98	8.47×10^{-5}	8.77×10^{-19}
Hot Spot 7500	4.618	2.73×10^{3}	0.0098	56.16	90.9	1.0	3.27×10^{-11}
10000	4.817	2.76×10^{3}	0.0131	49.21	73.6	1.0	2.07×10^{-12}
H II Nebula	6.75×10^{-4}	0.393	4.05	3.62	9.1	1.0	3.27×10^{-12}

$N_H \simeq N_{H^\circ}$ and, since the effective beam width of the 21 cm measurements is no greater than the 18 arc minute beam used in this study, all three features are assumed to be represented by a blend in the H157α spectrum. N_H is, therefore, computed using all of them. Then

$$<N_H> = 3.876\times10^{14}\frac{<T_K>}{L}\int\tau_{21}(\nu)\,d\nu$$

$$= 3.876\times10^{14}\frac{<T_K>}{L}[1.0645\ \Sigma_i \tau_{21}(i)\Delta\nu_{Di}]$$

$$= 18.97\frac{<T_K>}{L}\ .$$

The path length, L, is in pc. $<N_H>$ is listed in the sixth column of Table VI-1. The fractional ionization, $x \equiv N_e/N_H$, is listed in the seventh column.

A perusal of this table indicates problems with most of the models. For all cases except the H II Nebula, the recombination line emission region contributes a negligible fraction to the observed continuum temperature. In these cases the thermal portion of the total continuum is the 2.7 °K universal background radiation.

The 80 MHz continuum optical depth computed on the basis of model parameters shows considerable disagreement with measured values. The value of $\tau(80)$ for D-1 is equal to that obtained by Caswell et al. (1970). That for the Isolated Cold Region model is a bit lower than the value of 0.83 derived by Dulk

and Slee (1972). $\tau(80)$ for the H II Nebula model is equal to that which Chaisson (1974a) suggests.

Of the eight models considered here, only three produce H157α/H197β ratios which are reasonably close to those obtained by Gordon and Gottesman (1971), model D-1 and the Isolated Cold Region and H II Nebula models. The extremely high ratio for model D-4 results from $P(H197\beta) \propto \tau_L^* \propto E_L = 1.07 \times 10^{-3}$ pc cm^{-6}.

If the recombination lines arise from a cold region, one would expect to find a hydrogen density between 10 and 100 cm^{-3} and an ionization rate near 10^{-15} sec^{-1}. These values are in agreement with the two-component model of Field, Goldsmith, and Habing (1969) for which the ionization rate is 4×10^{-16} sec^{-1} as expected from 2 Mev cosmic ray protons. The ionization fraction of their model is about 5.5×10^{-4}. None of the D-models agree very well with their model. For a temperature near 14.3 °K, their model would require that $N_H \sim 100$ cm^{-3}. Lockman and Gordon (1973) obtain a low temperature ($T \lesssim 100$ °K) solution from H159α recombination lines observed in the galactic plane in regions near the center. They did not detect the H200β line. So, P(H159α)/P(H200β) was greater than would be expected from a gas in LTE. This result, the results of Cesarsky and Cesarsky (1973b), Table VI-1, and the discussion immediately following the derivation of the D-Method models suggest that a 14.3 °K, LTE solution is not valid.

The Isolated Cold Region model fares only a little better with respect to N_H, x, and ζ_H. The Field, Goldsmith, and Habing (1969) model suggests that $N_H \simeq 30$ cm^{-3} and $x = 1.3 \times 10^{-3}$ if $T_e = 53$ °K and the carbon abundance is a factor of ten less than what is usually assumed (Spitzer, 1968, p. 122). The depletion of carbon (due to accretion on negatively-charged grains) is supported by preliminary analysis of ultraviolet observations with satellites (Dupree, 1974) and, perhaps, by the fact that the C157α line was not observed in this study. Nevertheless the number densities and fractional ionization of the model derived here are too small. The agreement is not improved by introducing a time-dependent source of ionization as suggested by Gerola *et al.* (1974).

The hydrogen densities derived for the Hot Spot models are much too small since the prototypes require that $N_e > 10^3$ cm^{-3}. It is difficult to imagine how such an electron density can be obtained in the Hot Spot models where $N_H \sim 100$ cm^{-3}. Evaluation of these models by means of the ionization rates is not possible since the source of energy is not known.

Of all models studied, the H II nebula produces the most promising set of parameters. The value of N_H derived is reasonable when compared to that of W80 (Kaplan and Pikelner 1970, p. 153). If the region is ionized by a hot star, total ionization is to be expected. The ionization

rate due to a star with a flux S_u at frequencies greater than that of the Lyman limit is (Equation II-50)

$$\zeta_H = \frac{3S_u}{4\pi r_s^3 N_H} .$$

S_u is tabulated by Spitzer (1968, p.116). The Stromgren radius, r_s, for this model is 42.5 pc. Then, for an O5 star, $\zeta_H = 3.61 \times 10^{-13}$ sec^{-1}. If r_s is decreased to 25 pc, the size of W80, $\zeta_H = 1.77 \times 10^{-12}$ sec^{-1}. In either case, a cooler star provides a smaller ionization rate. In order to obtain the variation of line strength between the 3C391 and COMP beams, the size of the nebula cannot be very much less than 85 pc. So, in order to exist with an ionization rate of 3.27×10^{-12} sec^{-1} or less, the nebula must be a small cluster of nebulas together occupying a region 85 pc in diameter.

The arguments favoring and rejecting the models studied here are summarized in Table VI-2. It is apparent that the best model for the source of radio recombination lines from the galactic ridge, at least in the direction of 3C391, is a low-density H II region. Other aspects of this model—particularly the relation of H I absorption spectra to it—will now be discussed.

A recent paper by Jackson and Kerr (1975) supports this conclusion except that for their model they derive a temperature of 440 ($\pm$600) °K. Also, they claim that

Table VI-2

Criteria for Acceptance or Elimination of Models

For	Against
D-Models	
1. The temperature agrees with Cesarsky and Cesarsky (1973).	1. The solution is LTE which is unlikely if the gas is cold.
2. There is a 21cm absorption feature which lines up with the highest velocity H157α feature.	2. The use of the D-Method may not be valid since the H157α beam is much larger than the angular size of 3C391 and the solution to the transfer equation is based on a neighboring strong continuum source.
3. The D-1 Model gives a reasonable value for P(H157α)/P(H197β) as compared to that observed by Gordon and Gottesman (1971).	3. P(H157α)/P(H197β) disagress with Gordon and Gottesman (1971) by a considered amount except Model D-1.
	4. The line widths are too large for T_K = 14 °K.
	5. Models D-1, -2, and -3 require ζ much greater than that provided by a plausible mechanism.
	6. N_H is too small.
	7. Except for D-1, τ(80) is not in agreement with measured values

Table VI-2 - continued

For	Against
Isolated Cold Region	
1. The temperature (53 °K) is close to T_s of 60 °K from Radhakrishnan and Goss (1972) or 71 (±9) °K from Hughes, Thompson and Colvin (1971).	1. The line widths are too large for T_K=53°.
2. H157α features are aligned with 21 cm emission features.	2. N_e, N_H, and the fractional ionization are too small.
3. The caluclated value of τ(80) is reasonable.	
Hot Spot Models	
1. Hot spots have been observed in the ridge (Altenhoff et al. 1973) where no continuum sources had been known to exist.	1. Existence of hot spots in region around 3C391 is not certain.
	2. There is disagreement between derived values of E. N_e, and N_H and those of prototypes.
	3. Lines should show noticeable pressure broadening but they do not.
	4. Derived balue if τ(80) disagrees markedly from observed values.

Table VI-2 - continued

For	Against
H II Nebula Model	
1. Chaison (1974a) and Bridle and Kesteven (1971) find continuum flux excess at ν>10GHz which could be explained by an H II nebula.	1. Does not directly explain the alignment of H 157α features with those of the 21 cm absorption spectrum. However, as in the case with M42 (Balick, Gammon and Hjellming, 1974), H II nebulae may, in general, have cold H I regions adjacent to them.
2. The derived parameters agree with those of known nebulae (e.g., W42 and W80).	
3. The galactic ridge as the part of the galaxy where H II regions are most likely to found (Hodge, 1974).	
4. These nebulae are warm enough and are likely to have enough turbulence to produce the line widths.	
5. The derived value of τ(80) is equal to that which Chaisson (1973a) suggests.	
6. The thermal continuum temperature agrees with that of Altenhoff *et al.* (1970).	

consideration of non-LTE will not affect their results significantly. Their argument for assuming LTE was discussed in an earlier paper (Jackson and Kerr, 1971) where they show that the ratio of the line temperature, T_L, expected from a non-LTE gas to the line temperature, T_L^*, expected from an LTE gas is roughly equal to b_m. They assume that $b_m \simeq 1$ for the H110α line (ν = 4874 MHz). However, consulting Figure II-4, it is seen that $b_{111} < 0.7$. The best way of determining how much the kinetic temperature is above 4400 °K, is to observe higher order lines with rest frequencies close to that of the H110α line. The line strength depends on β_{mn} as well as b_m. The gas in these nebulae may not be far out of LTE because the solution shown in Figure V-7 indicates only a small difference between the non-LTE solutions for N_e = 10 and 100 cm^{-3} if $E_L \simeq 3 \times 10^3$ pc cm^{-6}. In this case there is no appreciable difference between the 100 cm^{-3} non-LTE and the LTE solutions.

Hjellming and Davies (1970) determine that the recombination line emission regions in nebulae such as M42 and M17 are in non-LTE even though they are denser and hotter than is the model derived by Jackson and Kerr (1975). It has been pointed out, however, that the recombination lines arise from the more tenuous gas which surrounds the dense knots. It is difficult to explain why such knots would be out of LTE since, with their temperature and electron density, collisional excitation must dominate for

large n. So, the recombination lines must come from the low density, non-LTE gas surrounding them.

It is interesing to note that the model developed in this study is not very much different than the model developed by Matthews, Pedlar, and Davies (1973). The average temperature and emission measure which they compute from H166α lines are 6.2×10^3 °K and 2.7×10^3 pc cm^{-6} respectively as compared to 7.5×10^3 °K and 3.8×10^3 pc cm^{-6} derived by this study. Like Jackson and Kerr, they assume a condition of LTE. Another difference between their model and that of this study is the size of the region. The positions which they observed were spaced 5° to 10° apart and they could not observe the change in the spectrum over a distance as small as that observed here. From their observations they conclude that the emission regions are extended 3° to 5° in the galactic plane which is equivalent to a size in order to 0.5 to 10 kpc. This study suggests that the structure is much smaller, being in the order of 85 pc or smaller. This is in agreement with the conclusions of Jackson and Kerr (1975).

It has been mentioned that high spatial resolution maps of the region surrounding 3C391 (cf. Chaisson 1974a) do not indicate the presence of discrete sources like the ten such sources reportedly observed by Altenhoff *et al.* (1973) near the direction l = 23°.92, b = -0°.32. But, the possibility of their existence in the direction of 3C391

cannot be discounted completely. If they do exist, it is not completely clear how they fit into the model proposed by this study. Without knowing more about the size, distribution, continuum flux density, and recombination line spectra of these sources, it can only be assumed that they form a small-scale structure within the H II nebulae. Perhaps they are dense condensations associated with star formation. If that is so, it is not clear why they are not seen in Chaisson's (1974a) map. The structure seen in his map is included within the isophotes of the map of Bridle and Kesteven (1971) and it appears to be structure within 3C391 and not of the intervening medium.

There must be an explanation for the alignment of the 21 cm absorption features, which are associated with cold gas, with the H II nebulae. This can be explained by cool cloud-like regions which lie close to the nebulae. Being close to each other, they will both have the same central velocities. This arrangement is similar to the structure of the Orion nebula described by Balick, Gammon, and Hjellming (1974).

The distribution of the H II nebulae must explain the observed central velocities and relative intensities of the recombination line features from the region around 3C391 including the COMP beam. If circular galactic rotation can be assumed, the Schmidt rotation model (Schmidt, 1965) can position the emission regions along the line of sight. In

the region inside the sun's orbit, there is a twofold ambiguity between velocity and radial distance. Figures VI-1 and 2 show the positions of the emission regions. Figure VI-1 is for the case where the high-velocity feature is single; Figure VI-2 is for the case where it is double. In both figures, an outer boundary with a radius of 8 kpc is drawn in to encompass the low-velocity feature.

The outer boundary of the ridge has been generally thought to be a circular disc or an annulus with an outer radius of 7 kpc (Matthews, Pedlar, and Davies, 1973). If the ridge is a disc-shaped distribution of H II nebulae with a nebular density which drops off rapidly beyond 7 kpc, the boundary may not be well defined. At longitudes progressively near the tangent to the boundary, the lines of sight will pass through fewer nebulae and recombination line emission will become patchy. So, even though recombination lines have not been detected in the direction of the tangent to the 8 kpc circle ($l = 53°$)(Gordon and Cato, 1972), it is reasonable to expect that some nebulae lie this far from the galactic nucleus.

The Hughes, Thompson, and Colvin (1971) 21 cm absorption spectrum shows an absorption feature at 42 km/s. There is a weak feature at this velocity in the Radhakrishnan et al. (1972b) spectrum. From this it can be assumed that either 3C391 is beyond 14 kpc or the H II nebula and its neighboring cold cloud responsible for the 42 km/s features are located at a distance of about 3.1 kpc from the sun.

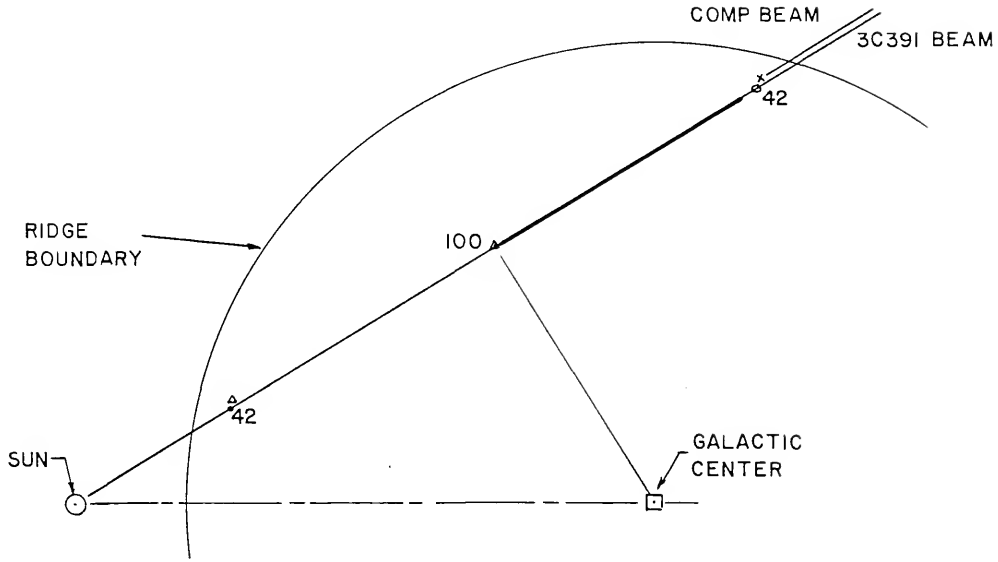

Figure VI-1. H II Nebula Positions Assuming a Single High-Velocity Component. For 3C391, the near positions are shown with a solid dot, the far position by an open circle. For the COMP beam, the near positions are shown with a Δ, the far position with an x. The approximate center velocity of the region is shown next to it. The heavy solid line shows the most probable range of distance to 3C391. The sun is 10 kpc from the galactic center.

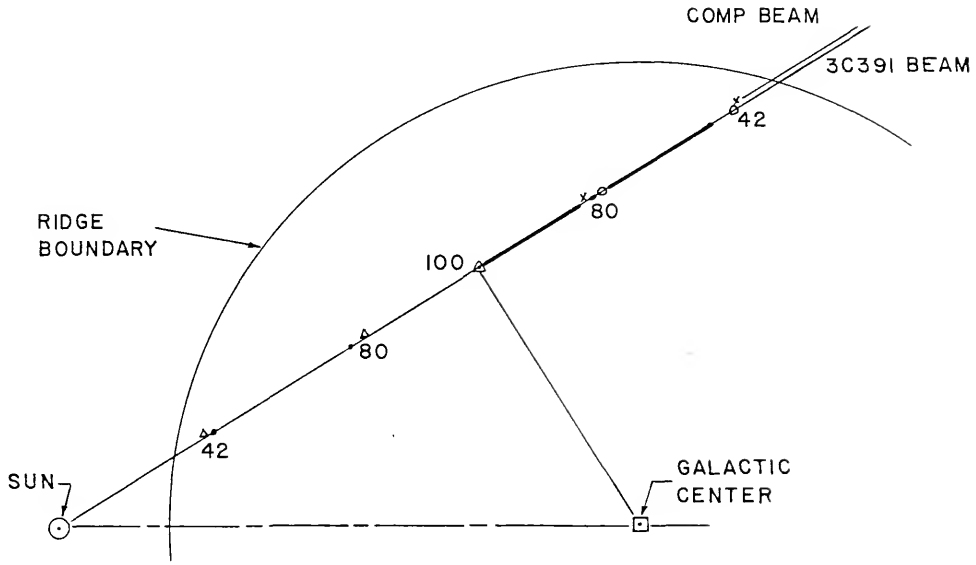

Figure VI-2. H II Nebula Positions Assuming a Double High-Velocity Component. The symbols are identical to those used in Figure VI-1.

If these H II nebulae are to explain the spectra of other galactic ridge surveys, it must be hypothesized that the ridge phenomena are caused by a distribution of H II nebulae. It is confined to a disk- or ring-shaped region extending about 70 pc above and below the plane (Gordon, Brown, and Gottesman, 1972) and limited to a galactocentric radius of about 8 kpc. In order to test this hypothesis, the spectra from the directions of the pulsar, 3C396, and its COMP beam will be examined. Following this, the results of this study will again be compared with other surveys of the plane.

The Pulsar 1858+03

Determining the distance to a pulsar is not a trivial task. The distance to the stronger pulsars can sometimes be determined from the 21 cm absorption spectrum which is obtained by subtracting the pulse-off spectrum from the pulse-on spectrum (Gordon *et al.* 1969). An estimate of the distance can be calculated from the dispersion measure,

$$DM \equiv \int_0^L N_e \, ds = \langle N_e \rangle L,$$

if the mean electron density can be determined independently. The determination of $\langle N_e \rangle$ is particularly difficult in the galactic plane. A recent survey of interstellar

medium research (Guelin, 1974) indicates that the average electron density within about 2 kpc of the sun is 0.03 cm^{-3}. $\langle N_e \rangle$ is much larger in the ridge.

The reason for choosing the pulsar 1858+03 as a direction in which to observe radio recombination lines is that it appears to lie in the ridge. Its dispersion measure is 402 ($\pm$2) pc cm^{-3} (Manchester and Taylor, 1972) which is, by far, the largest dispersion measure known as of late 1971.

The H157α spectrum from the direction of 1858+03 is shown in Figure IV-5. The center-velocity, peak temperature, half-power width, and the integrated line power of each feature are brought from Table IV-3 and shown in Table VI-3. In addition to these parameters, the Doppler temperature of each feature, computed from Equation II-37, is shown in the last column of this table. The Doppler temperature is the kinetic temperature of the gas if the line broadening were entirely thermal.

Table VI-3

Spectral Parameters for 1858+03

v_c km/s	$T(v_c)$ °K	v km/s	P °K kHz	T_D °K
38.08	0.013	30.16	2.34	19 890
82.48	0.010	18.71	1.12	7 654

Figure VI-3 shows the possible positions along the line of sight of the other two features as determined by the Schmidt rotation model. The near positions are indicated by dots and labeled A and B. The far positions are indicated by x's and labeled A' and B' respectively. A boundary with an 8 kpc radius is shown.

The technique to determine the distance to the pulsar will be to compute the expected dispersion measure at points along the line of sight. The distance at which the computed dispersion measure equals 402 pc cm^{-3} will be the distance to the pulsar. The line of sight passes through four different types of region, each with its own electron density and path length. They are the region outside the ridge, cold H I regions, the diffuse hot gas, and the H II nebula. The arrangement with one H II nebula is shown schematically in Figure VI-4. The parameters of the regions used to computed the distance, R, to the Pulsar 1858+03 are listed in Table VI-4.

Up to the ridge boundary, the accumulated dispersion measure is 78 pc cm^{-3}. If a nebula is encountered, the dispersion measure will rise sharply. If the path length through the nebula is 32.4 pc, the dispersion measure on the far side of it will be 402 pc cm^{-3}. The diagram in Figure VI-4 purposely shows the line of sight not passing through the center of the nebula to illustrate that the path length through it may be less than its diameter. If the line of

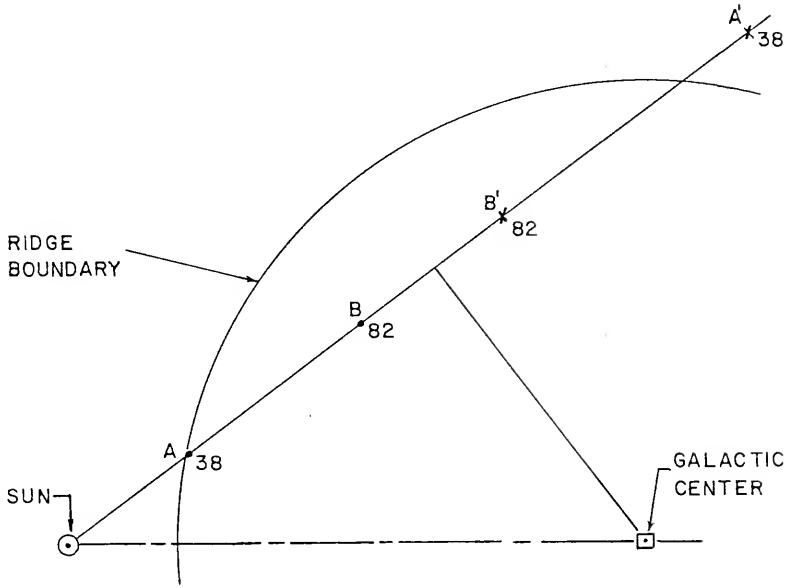

Figure VI-3. H II Nebula Positions in the Direction of the Pulsar 1858+03. The near positions are shown by dots, the far positions by x's. The center velocity of each region is shown next to it. Two possible ridge boundaries are shown. The sun is 10 kpc from the galactic center.

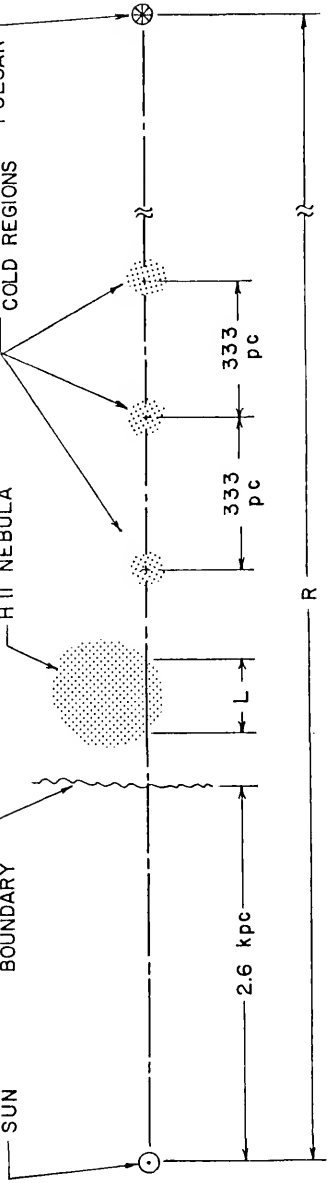

Figure VI-4. Schematic Diagram of the Regions Along the Line of Sight to the Pulsar 1858+03. This is not drawn to scale.

Table VI-4

Parameters of the Regions Shown in Figure IV-4

Parameter	Value	Reference
Path Length, Sun to Ridge Boundary	2.6 kpc	Figure VI-4
$\langle N_e \rangle$ Outside Ridge	0.03 cm^{-3}	Guelin (1974)
Diameter of Cold H I Region	5 pc	Baker and Burton (1975)
Ne in H I Regions	0.055 cm^{-3}	Field, Goldsmith, and Habing (1969)
Average Distance Between H I Region	333 pc	Radhakrishnan and Goss (1972)
<Ne> in Surrounding Hot Region (b=0)	0.17 cm^{-3}	Baker and Burton (1975)
Path Length through H II Nebula	adjustable	Figure VI-4
$\langle N_e \rangle$ in H II Nebula	10 cm^{-3}	This work

sight misses the nebula entirely, the distance to the pulsar must be 15.9 kpc, which is beyond A'. This distance is based on a path length through a two-phase medium for which the dispersion measure increases 30.17 pc cm^{-3} for each kpc of path length. The distance of 15.9 kpc is also considerably larger than that derived for other pulsars, particularly those for which their lines of sight encounter H II regions (Terzian, 1972; Prentice and ter Haar, 1969).

Although it is possible that the line of sight encounters neither nebula, it seems more likely that it passes through part of one since, otherwise, the pulsar would lie beyond the solar orbit. Hence, a distance of 2.6 kpc to 1858+03 appears most reasonable.

The 3C396 and COMP Spectra

These spectra will be used as a final check on the model which has been developed. The spectra are shown in Figure IV-3. The results of Gaussian profile fitting for the 3C396 spectrum are shown in Figure IV-9 and the parameters of the fit are given in Table IV-4. The reliability of what may be features at velocities of 58 and -119 km/s is relatively poor since the peak temperatures are only about four times the RMS noise. Nevertheless, by comparing the 3C396 with its COMP spectrum in Figure IV-3, it is seen that the peak temperature of the 54 km/s feature decreases by more than a factor of two in the distance between the two antenna beam centers which, is 30 arc minutes.

The absorption spectrum in the direction of 3C396 observed by Hughes, Thompson, and Colvin (1971) consists of a wide envelope extending from -10 to 98 km/s and appears to be a blend of many features. There is no structure at 53 or 58 km/s. The 21 cm emission spectrum is flat and extends over the same range as does the absorption spectrum.

A means of checking the model with the 3C396 spectrum is to compute the optical depth at 80 MHz and compare it with that measured by Dulk and Slee (1972). The line emission measure is computed from Equations V-10 and II-41 graphically by using Figure V-17. Using the graph sets T_e = 7500 °K. If a non-LTE gas with N_e = 10cm^{-3} is considered, E_L = 2.30x10^3 pc cm^{-6}. A gas with $N_e \geq 100$ cm^{-3} is in LTE; then, E_L = 2.15x10^3 pc cm^{-6}. It will be assumed that the recombination line emission region is similar to that in the direction of 3C391 (ie. non-LTE with N_e = 10 cm^{-3}). Therefore it will be assumed that $E_T = 1.1E_L$ = 2.53x10^3 pc cm^{-3} in the direction of 3C396. By the use of Equation V-2, $\tau(80)$ = 0.237. Dulk and Slee obtain $\tau(80)$ = 0.49 ($\pm$0.3). The values differ by a factor of two, but are in agreement within the errors quoted. The dissagreement is about the same as it is between Dulk and Slee's value for the line of sight to 3C391 and that derived from the H II Nebula model as shown in Table VI-1. In this case, however, the agreement with Chaisson (1974a, b) is good. It is possible that Dulk and Slee's values for $\tau(80)$ may be consistently large by a factor of two.

Distribution of the Recombination Line Sources Within the Ridge

The major objective of this study has been to determine what kind of region is responsible for radio recombination line emission observed from the galactic plane. The best model is a distribution of small, low-density H II nebulae. The last property of the model to be considered in this study is the distribution of these nebulae within the ridge. The recombination line surveys which have been mentioned can be used to obtain a rough picture of this distribution. The accuracy of this picture is severely limited by the resolution of the spectra—which prevents the separation of blended line features—and non-circular orbital motion (e.g. streaming) of the interstellar gas. Even if circular motion is assumed, placement of the nebulae along their lines of sight is confused by the two-fold ambiguity of the radial velocity-distance relation.

In spite of these limitations, a "first order" approximation to the distribution can be drawn from the radio recombination line observations in the ridge from longitudes between 5° and 130°. The surveys not included in this summary are those from regions closer than 5° from the galactic center made by Lockman and Gordon (1973) and Matthews, Davies, and Pedlar (1973). They are excluded because there is no radial velocity from which a position can be obtained. All Doppler shifts are due to streaming of the gas. Both

surveys show considerable variation of the line profile over a distance of a few tenths of a degree.

Table VI-5 lists the observations made in the range $5° \leq l \leq 130°$. If at some longitude no line was observed, "none" is entered in the last comumn. For several longitudes, it is apparent that a wide feature is a blend of unresolved features. For these cases, the central velocity of the end features has been estimated by using the turnover points of the blend. At the bottom of the table is the list of references—each with the spectral line observed—indicated in the third column. The possible locations, based on the Schmidt circular rotation model, are shown in Figure VI-5. The near and far positions are indicated by a dot and an x respectively. The blended features are shown as bars to indicate the range in which the features are located. Since Cygnus X has been observed to be a region of extensive radio recombination line emission (e.g., Gottesman and Gordon, 1970; Seacord and Gottesman, unpublished observations) its angular extent is shown. It lies along the local spiral arm or spur.

In Figure VI-5 the ridge boundaries, defined by the extent of the nebula positions, are drawn. It is seen that the radio recombination line ridge is an annulus with an inner radius of 4 kpc and an outer radius of 8.7 kpc. The distribution shown in the figure is quite similar to that of the giant H II region as shown by Mezger (1970). He

Table VI-5

Radio Recombination Line Sources in the Ridge

l	b	Reference	Velocity Features [km/s]
5.0	0	MPD	10
7.5	0	MPD	5 to 36
9.4	0.4	GC	12 to 22
13.5	0	MPD	15 to 40
15.8	0	GC	20 to 60
17.5	0	MPD	18 and 41
21.0	0	MPD	None
21.4	0	GC	80
23.92	-0.32	GG and JK	75
25.07	+0.01	GG	50 and 100
25.07	0.01	GC and JK	70
25.1	0.0	MPD	50 and 110
27.64	0.14	JK	None
29.18	0	JK	58
29.5	0	MPD	95
30.27	0	MK	30, 100
31.2	0	JK	25, 100
31.9	0	S, CC, P	41.9, 80.7, 102.8
32.1	-0.2	S	42.2, 83.4, 106.0
32.3	0	GC and JK	None
33	0	GBG	100
36.5	0	MPD	None?
37.2	-0.6	S	38.0, 82.5
38.9	0	S	58.2
39.2	-0.3	S	53.9
40.0	0	MPD	None
40.5	0	GC	None

Table VI-5 - continued

l	b	Reference	Velocity Features [km/s]
44.2	0	GC, P	40 to 87
47.5	0	MPD	None
52.2	0	GC	None
70.0	0	GC	-4
90	0	GC	None
110	0	GC	None
130	0	GC	None

Key to References and Spectral Line

MPD	Matthews, Pedlar, and Davies (1973); H166α
GC	Gordon and Cato (1972); H157α
JK	Jackson and Kerr (1975); H110α
GG	Gottesman and Gordon (1970); H157α
S	This study; H157α
GBG	Gordon, Brown, and Gottesman (1972); H157α
CC	Cesarsky and Cesarsky (1973a); H166α and H157α Cesarsky and Cesarsky (1973b); H92α
P	Pankonin (1975); H248α

Figure VI-5. Radio Recombination Line Sources in the Galactic Ridge. The dots represent the near positions; the x's represent the far positions. The symbol cross-with-dot represents maximum velocity positions. The heavy lines indicate blended features, solid for near positions and dashed for far positions. The sun is 10 kpc from the galactic center. Also shown are the boundaries to the ridge. The inner boundary if 4 kpc and the outer boundary is 8.7 kpc.

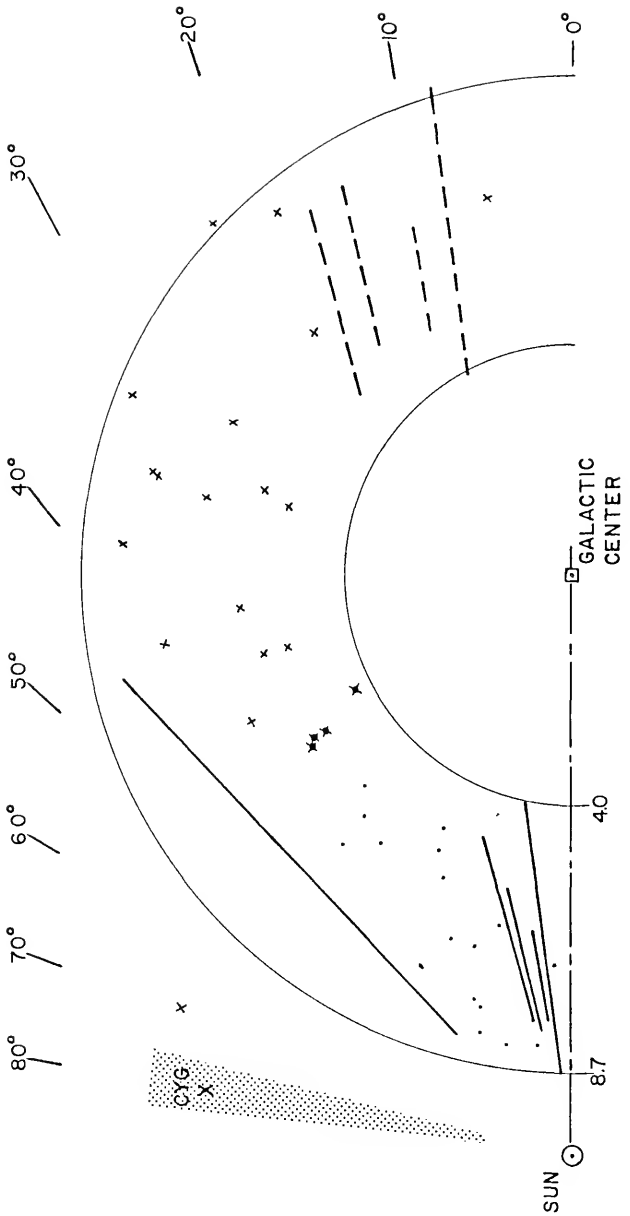
20°
10°
0°
30°
40°
50°
60°
70°
80°
GALACTIC CENTER
4.0
8.7
SUN
CYG X

defines the "giant" H II regions as those which satisfy the criterion $S(5\ GHz) \cdot D_n^2 \geq 400$; S(5 GHz) is the 6 GHz continuum flux and D_n is the nearer of the two kinematic distances.

Relevant to the distribution of the H II nebulae is their relation to H I gas. Comparing the 21 cm absorption and emission spectra and the H157α spectra of 3C391 (Figure V-1) and those of 3C396 indicated that the 21 cm spectra show more features and are extended over a greater velocity range than is so for the recombination line spectra. However, it should be noted that there is an H I emission peak close to each recombination line peak. A comparison of the radial velocities of H I and H II in the galactic plane within 60° of either side of the galactic center shows that it is generally true that H II features coincide with H I emission peaks (Mezger et al., 1970). One or more H I regions may be physically related to an H II nebula in a way that has been suggested for the Orion Nebula (Balick, Gammon, and Hjellming, 1974).

When relating radial velocities to distance, it must be noted that Burton (1971) has shown that the Schmidt model does not adequately explain the observed H I velocity-longitude maps. Gas streaming causes the rate of change of velocity along the line of sight, dv/ds, to change across a spiral arm. The velocity-distance relation is, therefore, very complicated. Consequently, Figure VI-5 does not represent

the actual nebular distribution well enough to relate the nebulae to spiral arm structure. The only conclusion that can be drawn from the figure is that, except for Cygnus X, these nebulae are restricted to an annulus with an outer radius of about 8.7 kpc and an inner radius of 4 kpc. It is possible that the wide spectrum from the longitude of 44°.2 may be a blend of features from a string of H II regions along the inner edge of the Sagittarius spiral arm. If this is correct, this string of nebulae and the Cygnus X complex do indicate a possible relationship between the radio recombination line ridge and galactic spiral structure.

CHAPTER VII

SUGGESTIONS FOR FURTHER RESEARCH

The results of this study do not conclusively determine a model for the radio recombination emission regions. However a distribution of low density (Ne = 10 cm^{-3}) H II nebulae seems to fit the data of this and previous studies most consistently. There are a number of aspects of the problem which need further study. These will be considered in this final chapter.

Assuming the conclusion that recombination line emission arises from low density nebulae is correct, the aspects of the general model which remain in question are as follows:

1. Size of the nebulae
2. Radial and z-direction distribution of the nebulae
3. Thermodynamic conditions in the nebulae; LTE vs. non-LTE
4. Energy source within the nebulae
5. Relation between nebulae and low frequency absorption

6. Relation of nebulae to H I gas, both hot and cold; and galactic structure in general
7. General relation with discrete sources seen by Altenhoff et al., 1973

The size of the nebulae can best be found by high resolution radio recombination line observations. The Altenhoff et al. (1970) continuum maps show considerable structure in the plane. To avoid confusion with recombination line emission from large H II complexes like W51, W49, or M42, observations should be confined to the regions like those observed by Matthews, Pedlar, and Davies (1973), Gottesman and Gordon (1970), Jackson and Kerr (1975) and Gordon and Cato (1972) which are between the continuum sources.

An approach taken in making the observations would be to use a large single aperture telescope to observe a high frequency line; say the H 92α at 8.3 GHz. The observations could be made in a rectangular pattern of contiguous beams. The extent of the grid should be thirty minutes of arc in longitude if possible and about thirty minutes above and below the plane. Several of these grids should be observed along the plane. One of the grids should encompass the region observed by Gordon and Gottesman (1970) and Altenhoff et al. (1973). One grid should be placed at the outer boundary of the ridge and at least one placed at an intermediate longitude. The outer boundary

of the ridge is not expected to be discrete; rather, as the longitude increases the number of nebulae decreases until the line of sight density drops to zero. This longitude, which is expected to be between 40 and 45°, can be estimated by observing individual regions between the continuum sources in this longitude range. At the ridge boundary there will be a minimum number of nebulae along the line of sight; thus, there is a better chance that one nebula can be identified individually.

This technique should provide a better estimate of size and distribution—radially and normal to the plane—of the nebulae. It would also provide a comparison between the ridge in general and the region in which Altenhoff et al. (1973) have observed recombination lines from discrete sources and the hot H I gas. Unfortunately the recombination line power decreases as the line frequency becomes large. For that reason each beam position would require at least 7 hours of integration time in order to get a ΔT of 0.002°K if the 43-meter NRAO telescope is used, making the entire program a large undertaking. It would have to be broken up into units in order to fit in with telescope scheduling.

More information on the thermodynamic condition of the gas in the nebulae can be obtained by observing several higher order ($\Delta n>1$) lines all with frequencies within a small range. A set of α-, β-, γ- and higher order lines should be observed from several regions between continuum

sources along the plane to ascertain if the thermodynamic state varies within the ridge. From each line the temperature of the gas is determined using the assumption that LTE applies. As Δn increases, the excited states of the atom are more apt to be collisionally excited and the measured excitation temperature approaches the electron kinetic temperature of the gas. The amount by which the measured temperature is less than the kinetic temperature is a measure of the departure from LTE. This technique was applied to denser nebulae by Hjellming and Davies (1970) from which the line powers are considerably larger than they are from the nebulae under consideration in this model. Consequently, the highest order of line observed will be smaller and the kinetic temperature may have to be estimated by extrapolation. The results of this experiment should be compared to the work of Matthews, Pedlar, and Davies (1973) and Jackson and Kerr (1971, 1975) who find the radio recombination line emission regions to be close to LTE. The results should also be compared to those of Brown and Balick (1973) who determine that this region should be considerably out of LTE.

Once the size, kinetic temperature and thermodynamic condition within the nebulae are better understood, it is hoped that a source of energy can be confirmed. A possibility which has been suggested in Chapters V and VI is that the energy source is one or more OB stars. Perhaps

if the distribution of these nebulae within the ridge disc can be determined, it will provide some confirmation of this. However, the distribution in the galaxy of OB stars at distances greater than 2 kpc is not known.

Obtaining a better understanding of the relation between the radio recombination nebulae and cold H I regions may come from observing with a matrix of beams at a high frequency line with the matrix centered on a source for which Radhakrishnan et al. (1972b) or Hughes, Thompson, and Colvin (1971) have published a 21 cm absorption spectrum. The velocity resolution of the observation must be as good as the absorption spectrum.

Confirming or rejecting a relation between low frequency absorption and radio recombination line emission in the ridge will require collaborative observations at low frequencies. Presently the 80 MHz optical depths of Dulk and Slee (1972) are open to question (cf. Chapter VI).

As mentioned in Chapter VI, the distributions of these nebulae can not be reliably determined using circular galactocentric orbits. A density wave model like that developed by Burton (1971) or Burton and Shane (1970) would produce a more correct distribution, but the nebulae must be positionally related to 21 cm emission regions. Such a relationship will be difficult to develop. If the energy source of the nebulae can be determined—for example if it is an OB association—the type of source may suggest a distribution.

The purpose of this study, as stated in Chapter I, has been to determine how the intersteller medium in the ridge differs from that in other regions of the galaxy such that it is a well-defined source of radio recombination lines. Although considerable uncertainty still exists, there is a trend—which this study supports—toward the acceptance of a distribution of distinct low density H II regions. As this chapter shows, there is much work that can be done to reduce the uncertainty. The location and proposed model of the ridge suggest that it is an extreme population I region. The relation between galactic structure and star formation has been shown; cf. Shu (1973) and Biermann (1973). It follows that the ridge may well prove to be an important component of spiral galaxies.

APPENDIX

The following are details of Equation II-7 and the derivation of Equation II-16.

The Thermal Continuum Absorption Coefficient

The general form of the thermal continuum absorption coefficient (Equation II-7) in terms of fundamental constants is

$$\kappa_T(\nu) = \frac{1}{4\pi^2\nu^2} \cdot \frac{32\pi^2 e^6}{3\sqrt{2\pi}\, M^3 c} \left(\frac{M}{kT_k}\right)^{1.5} \ln\left[\left(\frac{2k}{\gamma M}\right)^{2.5} \left(\frac{M}{\pi\gamma Ze^2}\right) T^{2.5}\nu^{-1}\right]$$

$$N_e \sum_i Z^2 N_i \qquad \text{A-1}$$

where Z is the effective nuclear charge number; e is the electron charge; M is the mass of the electron; k is Boltzmann's constant and γ is Euler's constant.

Population of Excited Levels

This is the derivation of Equation II-16. If N_i^* is the total number of ions in the i^{th} ionization state (e.g., number of hydrogen ions, N_{H^+}), then, taking Equation II-15

and summing over all levels,

$$N_i^* = \sum_{n=o}^{\infty} N_{ni}^* = \sum_{n=o}^{\infty} N_{oi}^* \frac{g_n}{g_o} \exp(-\chi_{in}/k\ T_{ex}) = \frac{N_{oi}^*}{g_o} u_i(T).$$

The partition function is

$$u_i(T) = \sum_{n=o}^{\infty} g_n \exp(-\chi_{in}/k\ T_{ex}). \qquad \text{A-2}$$

Therefore,

$$\frac{N_{ni}^*}{N_i^*} = \frac{g_n}{u_i(T)} \exp(-\chi_{in}/k\ T_{ex}). \qquad \text{A-3}$$

N_i^* can be found from the ionization, or Saha, equation;

$$\frac{N_i^*\ N_e}{N_o^*} = \left(\frac{2\pi M\ k\ T_K}{h^2}\right)^{1.5} \frac{2u_i(T)}{u_o(T)} \exp(-\chi_i/k\ T_K)\ .$$

N_o is the neutral atom number density and $u_o(T)$ is the partition function for the neutral atom. The ionization energy, χ_i, is the energy required to remove the last electron to form the i^{th} state of ionization. Setting $i = 0$ in Equation A-3 and dividing the Saha equation by it gives

$$\frac{N_i^*\ N_e/N_o^*}{N_{no}^*/N_o^*} = \frac{N_i^*\ N_e}{N_{no}^*} \frac{(2\pi\ M\ k\ T_K)^{-1.5}}{h^2} \cdot \frac{2u_i(T)}{g_n} \exp-(\chi_i - \chi_{in})/k\ T_{ex}. \qquad \text{A-4}$$

N^*_{no} is the quantity desired; so, the LTE number density of n-level excited atoms is

$$N^*_n = 4.143\text{x}10^{-16}\, N^*_i\, N_e\, T^{-1.5}\, \frac{g_n}{2u_i(T)}\, \exp(\varepsilon_{in}/k\, T_{ex}). \qquad \text{A-5}$$

All number densities are in units of cm^{-3}.

$\varepsilon_{in} \equiv -(\chi_i - \chi_{in})$ is the threshold energy which is the total energy of the electron in its orbit and equal to the sum of the kinetic and potential energies, $\varepsilon_K + V_n$. For hydrogenic ions, electron shielding of the nucleus can be ignored. If a_n is the Bohr radius of the n^{th} level,

$$V_n = \int_{\infty}^{a_n} F\, dr = \int_{\infty}^{a_n} \frac{Z\, e^2}{r^2}\, dr = -\frac{Z\, e^2}{a_n}\,.$$

The orbital kinetic energy is $\varepsilon_K = 1/2M\, a_n^2\omega^2$; ω is the orbital angular frequency. Then

$$\varepsilon_K = 1/2M\, a^2 \left(\frac{Z\, e^2}{a_n^3\, M}\right)^2 = \frac{Z\, e^2}{2\, a_n}$$

and $\varepsilon_{in} = -Z\, e^2/2\, a_n$. Since

$$\frac{Z\, e^2}{a_n^2} = M\, a_n\omega^2 = M\, a_n \left(\frac{Z\, e^2}{a_n^3\, M}\right)^2,$$

$$a_n = \frac{n^2(h/2\pi)^2}{M\ Z\ a^2}\,.$$

Finally

$$\varepsilon_{in} = \frac{-M\ Z^2\ e^4}{2\ n^2\ (h/2\pi)^2} .$$

Also, $\varepsilon_{in}/k = 157890\ Z^2/n^2$ from substitution of the values of the fundamental constants.

BIBLIOGRAPHY

Aller, L. H. 1963, Astrophysics: The Atmospheres of the Sun and Stars. 2nd edition. New York: The Ronald Press Co.

Altenhoff, W., Mezger, P. G., Wendker, H., and Westerhout, G. 1960, Veröffentlichungen der Universitäts Sternwarte zu Bonn, No. 59, 48.

Altenhoff, W. J., Downes, D., Goad, L., Maxwell, A., and Rinehart, R. 1970, A. and Ap. Supplement, 1, 319.

Altenhoff, W., Churchwell, E. B., Mebold, U., and Walmsley, M. 1973, personal communication, cited by Guelin (1973).

Andrews, M. H., Hjellming, R. M., and Churchwell, E. 1971, Ap. J., 167, 245.

Baker, P. L. and Burton, W. B. 1975, Ap. J., 198, 281.

Baker, P. L. and Diadiuk, V. 1973, Ap. Letters, 13, 199.

Balick, B., Gammon, R. H., and Hjellming, R. M. 1974, P.A.S.P., 86, 616.

Ball, J. A. 1972, "Measurements with Radio Frequency Spectrometers," in Methods of Experimental Physics, Volume II, M. L. Meeks, ed. New York: Academic Press (Preprint 1972).

Banks, D., Percival, I. C., and Richards, D. 1973, Ap. Letters, 14, 161.

Biermann, P. 1973, A. and Ap., 22, 407.

Blaauw, A., Gum, C. S., Pawsey, J. L., Westerhout, G. 1960, M.N.R.A.S., 121, 123.

Braes, L. L. E. and Miley, G. K. 1972, Nature, 237, 506.

Bridle, A. H. and Kesteven, M. J. L. 1971, A. J., 76, 958.

Bridle, A. H. and Venugopal, V. R. 1969, Nature, 224, 545.

Brockelhurst, M. 1970, M.N.R.A.S., 148, 417.

Brown, R. L. and Balick, B. 1973, Ap. J., 185, 843.

Burgess, A. and Percival, I. C. 1968, Advances in Atomic and Molecular Physics, 4, 109.

Burns, W. R. and Yao, S. S. 1969, Radio Sci., 4, 431.

Burton, W. B. 1970, A. and Ap. Supplement, 2, 261.

Burton, W. B. 1971, A. and Ap., 10, 76.

Burton, W. B. and Shane, W. W. 1970, "Neutral Hydrogen in the Sagittarius and Scutum Spiral Arms," p. 397 in The Spiral Structure of Our Galaxy, IAU Symposium 38, W. Becker and G. Contopoulos eds, Dordrecht: D. Reidel.

Caswell, J. L., Dulk, G. A., Goss, W. M., Radhakrishnan, V. and Green, A. J. 1971, A. and Ap., 12, 271.

Cesarsky, C. J. and Cesarsky, D. A. 1971, Ap. J., 169, 293.

Cesarsky, D. A. and Cesarsky, C. J. 1973a, Ap. J. (Letters), 183, L143.

Cesarsky, D. A. and Cesarsky, C. J. 1973b, Ap. J. 184, 83.

Chaisson, E. J. 1972, Nature Phys. Sci., 239, 83.

Chaisson, E. J. 1974a, Ap. J., 189, 69.

Chaisson, E. J. 1974b, personal communication.

Cram, T. R. 1973, TPOWER and SPOWER User's Manual, NRAO Computer Div. Internal Report No. 10.

Dalgarno, A. and McCray, R. A. 1972, Ann. Rev. A. and Ap., 10, 375.

Dickel, H. and Dickel, J. 1974, Personal communication.

Downes, D. and Wilson, T. L. 1974, A. and Ap., 34, 133.

Dulk, G. A. and Slee, O. B. 1972, Austral. J. Phys., 25, 429.

Dupree, A. K. 1969, Ap. J., 158, 491.

Dupree, A. K. 1972a, Ap. J., 173, 293.

Dupree, A. K. 1972b, Ap. Letters, 12, 125.

Dupree, A. K. 1974, Personal communication.

Dupree, A. K. and Goldberg, L. 1970, Ann. Rev. A. and Ap., 8, 231.

Dyson, J. E. 1969, Ap. J., 155, 47.

Encrenaz, P. and Guelin, M. 1970, Nature, 227, 476.

Field, G. B., Goldsmith, D. W., and Habing, J. J. 1969, Ap. J. (Letters), 155, L149.

Flannery, M. R. 1970, J. Phys. B: Atom. Molec. Phys., 3. 1610.

Gerola, H., Kafatos, M., and McCray, R. 1974, Ap. J., 189, 55.

Goldstein, S. J. 1962, A. J., 67, 171.

Goldwire, H. C. Jr. 1968, Ap. J. Supplement, 17, 445.

Gordon, M. A. 1971, Ap. J., 167, 21.

Gordon, M. A. 1972, Ap. J., 174, 361.

Gordon, M. A. 1974, "The Radio Characteristics of H II Regions and the Diffuse Thermal Background," Chapt. 3 in Galactic and Extragalactic Radio Astronomy, G. L. Verschuur and K. I. Kellerman eds., New York: Springer-Verlag.

Gordon, M. A., Brown, R. L. and Gottesman, S. T. 1972, Ap. J., 178, 119.

Gordon, M. A. and Cato, T. 1972, Ap. J., 176, 587.

Gordon, C. P., Gordon, K. J., and Shalloway, A. M. 1969, Nature, 222, 129.

Gordon, K. J. and Gordon, C. P. 1970, Ap. Letters, 5, 153.

Gordon, M. A. and Gottesman, S. T. 1971, Ap. J., 168, 361.

Goss, W. M. 1972, A. and Ap., 18, 484.

Gottesman, S. T. and Gordon, M. A. 1970, Ap. J. (Letters), 162, L93.

Guelin, M. 1974, Galactic Radio Astronomy, IAU Symposium No. 60, p. 51, Dordrecht: Reidel.

Guelin, M., Guibert, J. Huchtmeir, W., and Weliachew, L. 1969, Nature, 221, 249.

Habing, H. J. 1970, personal communication cited by Hughes, Thompson, and Colvin (1971).

Habing, H. J., Goss, W. M., Matthews, H. E., and Winnberg, A. 1974, A. and Ap., 35, 1.

Hagen, J. P., Lilley, A. E., McClain, E. F. 1955, Ap. J., 122, 361.

Hill, E. R., Slee, O. B., and Mills, B. Y. 1958, Austral. J. Phys., 11, 530.

Hjellming, R. M. 1972, "Interstellar Cloud Properties Revealed by Pulsars," p. 69 in The Physics of Pulsars, A. M. Lenchek ed., New York: Gordon and Breach.

Hjellming, R. M. and Davies, R. D. 1970, A. and Ap., 5, 53.

Hjellming, R. M. and Gordon, M. A. 1971, Ap. J., 164, 47.

Hjellming, R. M., Gordon, C. P., and Gordon, K. J. 1969, A. and Ap., 2, 202.

Hoang-Binh, D. and Walmsley, C. M. 1974, A. and Ap., 35, 49.

Hodge, P. W. 1974, P.A.S.P., 86, 845.

Holden, D. J. and Caswell, J. L. 1969, M.N.R.A.S., 143, 407.

Hughes, M. P., Thompson, A. R., and Colvin, R. S. 1971, Ap. J. Supplement, 23, 323.

Ilovaisky, S. A. and Lequeux, J. 1972, A. and Ap., 18, 169.

Jackson, P. D. and Kerr, F. J. 1971, Ap. J., 168, 29.

Jackson, P. D. and Kerr, F. J. 1975, Ap. J., 196, 723.

Kaplan, S. A. and Pikelner, S. B. 1970, The Interstellar Medium, Cambridge, Mass.: Harvard University Press.

Kellermann, K. I., Pauliny-Toth, I. I. K., and Williams, P. J. S. 1969, Ap. J., 157, 1.

Komesaroff, M. M. 1961, Austral. J. Phys., 14, 515.

Kraus, J. D. 1966, Radio Astronomy, New York: McGraw-Hill.

Kuhn, H. G. 1962, Atomic Spectra, New York: Academic Press.

Large, M. I., Mathewson, D. S., and Haslam, C. G. T. 1961, M.N.R.A.S., 123, 123.

Lilley, A. E. and Palmer, P. 1968, Ap. J. Supplement, 16, 143.

Lin, C. C., Yuan, C., Shu, F. H. 1969, Ap. J., 155, 721.

Lockman, F. J. and Gordon, M. A. 1973, Ap. J., 182, 25.

Manchester, R. N., Murray, J. D., and Radhakrishman, V. 1969, Ap. Letters, 4, 229.

Manchester, R. N. and Taylor, J. H. 1972, Ap. Letters, 10, 67.

Mathewson, D. S., Healy, J. R., and Rome, J. M. 1962a, Austral. J. Phys., 15, 354.

Mathewson, D. S., Healy, J. R., and Rome, J. M. 1962b, Austral. J. Phys., 15, 369.

Matthews, H. E., Davies, R. D., and Pedlar, A. 1973, M.N.R.A.S., 165, 173.

Matthews, H. E., Pedlar, A., and Davies, R. D. 1973, M.N.R.A.S., 165, 149.

Mauzy, R. 1968, Autocrrelation Receiver, Model II: IF Filter System, NRAO Electronics Division Internal Report No. 77.

McDaniel, E. W. 1964, Collision Phenomena in Ionized Gases. New York: John Wiley and Sons, Inc.

Menzel, D. H. 1969, Ap. J. Supplement, 18, 221.

Mezger, P. G. 1970, "The Distribution of H II Regions," in The Spiral Structure of Our Galaxy, IAU Symposium 38, Dordrecht: D. Reidel.

Mezger, P. G. and Henderson, A. P. 1967, Ap. J., 147, 471.

Mezger, P. G., Wilson, T. L., Gardner, F. F., and Milne, D. K. 1970, A. and Ap., 4, 96.

Mihalas, D. 1970, Stellar Atmospheres. San Francisco: W. H. Freeman and Co.

Mihalas, D. and Routly, P. M. 1968, Galactic Structure. San Francisco: W. H. Freeman and Company.

Mitchell, A. C. G. and Zemansky, M. W. 1934, Resonance Radiation and Excital Atoms. New York: The Macmillan Company.

Oster, L. 1961, Rev. Mod. Phys., 33, 525.

Pankonin, V. 1975, A. and Ap., 38, 445.

Parratt, L. G. 1961, Probability and Experimental Errors in Science. New York: John Wiley and Sons.

Peach, G. 1972, Ap. Letters, 10, 29.

Pedlar, A. and Hart, L. 1974. M.N.R.A.S., 168, 577.

Pengelly, R. M. and Seaton, M.J. 1964, M.N.R.A.S., 127, 165.

Percival, I. C. and Richards, D. 1970a, J. Phys. B: Atom. Molec. Phys., 3, 315.

Percival, I. C. and Richards, D. 1970b, J. Phys. B: Atom. Molec. Phys., 3, 1035.

Percival, I. C. and Richards, D. 1970c, Ap. Letters, 4, 235.

Percival, I. C. and Seaton, M. J. 1972, Ap. Letters, 11, 31.

Posener, D. W. 1959, Austral. J. Phys., 12, 184.

Prentice, A. J. R. and ter Haar, D. 1969, M.N.R.A.S., 146, 423.

Radhakrishnan, V., Brooks, J. W., Goss, W. M., Murray, J. D., and Schwarz, U. J. 1972a, Ap. J. Supplement, 24, 1.

Radhakrishnan, V. and Goss, W. M. 1972, Ap. J. Supplement, 24, 161.

Radhakrishnan, V., Goss, W. M.. Murray, J. D., and Brooks, J. W. 1972b, Ap. J. Supplement, 24, 49.

Saraph, H. E. 1964, Proc. Phys. Soc., 83, 763.

Schmidt, M. 1965, "Rotation Parameters and Distribution of Mass in the Galaxy," Chapt 22 in Galactic Structure, A. Blaauw and M. Schmidt eds., Chicago: Univ. of Chicago Press.

Seaton, M. J. 1959, M.N.R.A.S., 119, 81.

Seaton, M. J. 1962, Proc. Phys. Soc., 79, 1105.

Seaton, M. J. 1964, M.N.R.A.S., 127, 177.

Sejnowski, T. J. and Hjellming, R. M. 1969. Ap. J., 156, 915.

Shain, C. A., Komesaroff, M. M., and Higgins, C. G. 1961, Austral. J. Phys., 14, 508.

Shalloway, A. M., Mauzy, R., Greenhalgh, J., and Weinreb, S. 1968, Autocorrelation Receiver Model II: Operational Description, NRAO Electronics Division Internal Report No. 75.

Shore, B. W. and Menzel, D. H. 1968, Principles of Atomic Spectra. New York: John Wiley and Sons, Inc.

Shu, F. H. 1973, Amer. Scientist, 61, 524.

Sorochenko, R. L. and Berulis, J. J. 1969, Ap. Letters, 4, 173.

Sorochenko, R. L. and Berulis, J. J. 1971, Soviet Astron-A. J., 14, 683.

Spitzer, L. Jr. 1968, Diffuse Matter in Space. New York: John Wiley and Sons (Interscience).

Sullivan, W. T. III, 1973, Ap. J. Suppl. Series, 25, 393.

Terzian, Y. 1972, "Dispersion Measures and Distances to Pulsars," p. 85 in Physics of Pulsars, A. M. Lenchek ed., New York: Gordon and Breach.

Turner, B. E. 1973, Personal communication.

Weinreb, S. 1963, A Digital Spectral Analysis Technique and its Application to Radio Astronomy, M.I.T. Research Laboratory of Electronics, Technical Report 412.

Wendker, H. J. 1970, A. and Ap., 4, 378.

Westerhout, G. 1958, B.A.N., 14, 215.

Westerhout, G. 1969, Maryland-Green Bank Galactic 21 cm Line Survey, 2nd Ed, College Park, Md.: Univ. of Maryland.

Whiteoak, J. B. and Gardner, F. F. 1974, A. and Ap., 37, 389.

Wilson, T. L. 1972, A. and Ap., 19, 354.

Winnberg, A., Habing, H. J., and Goss, W. M. 1973, Nature Phys. Sci., 243, 78.

BIOGRAPHICAL SKETCH

Andrew Wilkin Seacord, II was born on 19 September, 1941 in Milwaukee, Wisconsin. His family moved to LaGrange, Illinois in 1942, to Evansville, Indiana in 1946, and to Western Springs, Illinois in 1952. He graduated from Lyons Township High School in June, 1959. He attended the University of Illinois from September, 1959 to February, 1964, and graduated with a Bachelor of Science in Electrical Engineering.

His graduate work began at the Pennsylvania State University in March, 1964, where he worked in the Ionosphere Research Laboratory and the Radio Astronomy Observatory. The thesis work for his Master of Science degree in Electrical Engineering was done under Dr. John P. Hagen. The degree was conferred in September, 1966.

Shortly before his thesis was completed, he began working for the National Aeronautics and Space Administration, at the Goddard Space Flight Center. There he served as an engineer with solar flares patrol instrumentation for the Apollo program.

On 9 March, 1968, he married Penelope Lee Connors. They presently have two children, Rebecca Louise and William Wilkin.

In June, 1970, he began work toward the doctorate at the University of Florida. During the first two years, he worked with Dr. T. D. Carr on the 26.3 MHz array telescope. However, for several years, he had been interested in galactic structure and the interstellar medium. So, when Dr. S. T. Gottesman joined the faculty, Mr. Seacord began studying under him. The Doctor of Philosophy is expected to be conferred in August, 1975.

I certify that I have read this study and that in my opinion it conforms to acceptable standards of scholarly presentation and is fully adequate, in scope and quality, as a dissertation for the degree of Doctor of Philosophy.

Stephen T. Gottesman, Chairman
Assistant Professor of Astronomy

I certify that I have read this study and that in my opinion it conforms to acceptable standards of scholarly presentation and is fully adequate, in scope and quality, as a dissertation for the degree of Doctor of Philosophy.

Thomas D. Carr
Professor of Physics and Astronomy

I certify that I have read this study and that in my opinion it conforms to acceptable standards of scholarly presentation and is fully adequate, in scope and quality, as a dissertation for the degree of Doctor of Philosophy.

Alexander G. Smith
Professor of Physics and Astronomy

I certify that I have read this study and that in my opinion it conforms to acceptable standards of scholarly presentation and is fully adequate, in scope and quality, as a dissertation for the degree of Doctor of Philosophy.

Michael T. Parkinson
Associate Professor of Physics

I certify that I have read this study and that in my opinion it conforms to acceptable standards of scholarly presentation and is fully adequate, in scope and quality, as a dissertation for the degree of Doctor of Philosophy.

Thomas L. Bailey
Professor of Physics and
Electrical Engineering

This dissertation was submitted to the Graduate Faculty of the Department of Physics and Astronomy in the College of Arts and Sciences and to the Graduate Council, and was accepted as partial fulfillment of the requirements for the degree of Doctor of Philosophy.

August, 1975

Dean, Graduate School

UNIVERSITY OF FLORIDA
3 1262 08666 220 1